Universidade Estadual de Londrina

LUCAS DOS SANTOS ARAUJO CLAUDINO

COGNITIVE RADIO:

SPECTRUM SENSING AND OPTIMAL RESOURCE ALLOCATION

Londrina
2018

LUCAS DOS SANTOS ARAUJO CLAUDINO

COGNITIVE RADIO:

SPECTRUM SENSING AND OPTIMAL RESOURCE ALLOCATION

Dissertação apresentada ao Programa de Pós-Graduação em Engenharia Elétrica da Universidade Estadual de Londrina como parte dos requisitos necessários para a obtenção do título de Mestre em Engenharia Elétrica.

Orientador: Prof. Dr. Taufik Abrão

Londrina
2018

Ficha Catalográfica

Claudino, Lucas

Cognitive Radio: Spectrum Sensing and Optimal Resource Allocation. Londrina, PR, 2018. 117 p.

Dissertação (Mestrado) – Universidade Estadual de Londrina, PR. Departamento de Engenharia Elétrica .

1. Sistemas de Telecomunicações. 2. Rádio Cognitivo. 3. Sensoriamento Spectral. 4. Precoding. I. Universidade Estadual de Londrina. Departamento de Engenharia Elétrica. Departamento de Engenharia Elétrica . II. Título.

LUCAS DOS SANTOS ARAUJO CLAUDINO

COGNITIVE RADIO:

SPECTRUM SENSING AND OPTIMAL RESOURCE ALLOCATION

Dissertação apresentada ao Programa de Pós-Graduação em Engenharia Elétrica da Universidade Estadual de Londrina como parte dos requisitos necessários para a obtenção do título de Mestre em Engenharia Elétrica.

BANCA EXAMINADORA

Orientador: Prof. Dr. Taufik Abrão
Universidade Estadual de Londrina – UEL

Prof. Dr. Fábio Renan Durand
Universidade Teconológica Federal do Paraná-UTFPR

Prof. Dr. Glauber Gomes de Oliveira Brante
Universidade Teconológica Federal do Paraná-UTFPR

Londrina, 09 de março de 2018.

"Nós somos aquilo que fazemos repetidamente. Excelência, então, não é um modo de agir, mas um hábito."

Aristóteles

Agradecimentos

Agradeço primeiramente a Deus pelas oportunidades e desafios e à minha família pelo apoio durante todo esse tempo. Agradeço especialmente à minha mãe Sandra Claudino e à minha noiva Nathalia Favaro pelas forças dadas durante a caminhada. Agradeço também ao meu avô Wilson Claudino, por ter ajudado em minha educação e também pela participação na fundação da Universidade Estadual de Londrina.

Gostaria de agradecer também aos colegas e professores do Departamento de Engenharia Elétrica da Universidade Estadual de Londrina, principalmente ao meu orientador Prof. Dr. Taufik Abrão pela orientação e paciência. Especiais agradecimentos aos meus colegas de mestrado Aislan Hernandes, Edno Gentili, João Lucas Negrão e Ricardo Tadashi Kobayashi.

Resumo

Redes de Rádio Cognitivo constituem uma tecnologia recente que busca fazer o uso otimizado do espectro de frequências, que jáestá super-utilizado. Essa tecnologia oferece meios para portadores de licensa compartilhar sua banda de frequências com outros usuários para possibilitar o uso eficiente e também recerber certos benefícios em troca, como descontos ou aumento do tempo de validade da licensa. Dado que essa tecnologia é relativamente recente, os seus estudos estão ainda incompletos e precisam de uma pesquisa mais aprofundada. A fim de contribuir com a literatura, este trabalho trás importantes contrubuições para diferentes áreas do Rádio Cognitivo.

Primeiramente, várias técnicas de sensoriamento espectral como Filtro Casado, Sensor de Energia, Sensor de Razão de Hadamard ou Sensor de Valor Absoluto de Covariância são analisados. Todos esses detectores são estudados e comparados de modo a oferecer ao leitor uma ampla visão sobre todas suas características, fraquezas e pontos fortes. Após esse estudo, o sensor mais promissor é escolhido para ser aplicado em um cenário realístico de transmissão sem fio. Escolheu-se o sensor de Razão de Hadamard, dado sua capacidade de prover altas taxas de detecção, baixa detecção errada ou alarme falso com um número necessário de amostras relativamente baixo.

A segunda parte desta Dissertação é baseada em técnicas de otimização não linear que buscam maximizar a soma das capacidades de uma rede de rádio cognitivo. Uma MISO-CRN (*Multiple-Input Multiple-Output Cognitive Radio Network*) foi escolhida como arquitetura de aplicação e sua otimização foi divida em duas partes: cancelamento de interferência e alocação de potência. Essa técnica é conhecida como Zero Forcing-Water Filing, e alcança a capacidade máxima de transmissão sob certas configurações de sistema e canal. Além disso, esta pesquisa desenvolveu também uma aproximação prática para encontrar o número ótimo de usuários secundários ativos que proporcione a máxima capacidade da rede. Essa é uma ferramenta muito útil, uma vez que pode prover uma maneira simples de escolha do número permitido de usuários secundários para um certo cenário.

Finalmente, técnicas de estimativa de canal aplicadas a redes de rádio cognitivo são estudadas. A transmissão completa em banda-base equivalente é descrita, a qual inclui a transmissão de sequência piloto, a estimativa da matriz de canal e uso dessa estimativa para gerar a matriz ótima de precodificação. Além disso, analisou-se o efeito da estimativa imperfeita do canal no sistema de transmissão com precodificação, na tentativa de se encontrar técnicas para superar esses problemas e melhorar o desempenho do sistema de comunicação com múltiplas antenas.

Palavras-Chave: sensoriamento espectral, rede de rádio cognitivo, maximização da capacidade, estimativa de canal, erro em estimativa de canal MIMO.

Abstract

Cognitive Radio Network is a recent and emerging technology that aims to optimally use the already overcrowded frequency spectrum. This technology offers means for license-holders to share their spectrum bandwidth with other users, in order to make an efficient use of it and also receive some benefits, like payback or increase in license time. Once this is a recent technology, many studies are still incomplete and need furthers research. Ir order to contribute with the literature, this work brings some important research of a few different parts of Cognitive Radio.

Firstly, various spectrum sensing techniques, such as Matched Filter, Energy Sensing, Hadamard Ratio Sensor or Covariance Absolute Value Detector are analyzed. All those sensors are studied and compared, in order to give a broad overview about its characteristics, strengths and weaknesses. After this study, the most promising detector is chosen to be applied into realistic wireless channels. The Hadamard Ratio Sonsor has been chosen, given its capacity of providing high detection rates, low miss detection or false alarm with a relatively low number of samples.

The second part is based on non-linear optimization techniques and aims to maximize the sum capacity of a cognitive radio network. A MISO-CRN was chosen as target architecture, and the optimization was divided into two parts: power allocation and interference nulling. This technique is known as Zero Forcing-Water Filing strategy, which achieves maximum sum capacity under certain system and channel configurations. Also, this research came up with a practical approximation to find out the optimum number of active secondary users to achieve maximum capacity. This is a very useful tool, once it can provide an easy way of choosing the allowed number of SUs for a given configuration of number of antennas at the base station and link quality (related to signal to interference plus noise ratio).

Finally, channel estimation techniques applied to cognitive radio networks are analyzed. A complete base-band transmission is described, which includes pilot sequence transmission, channel matrix estimation and optimal precoder matrix generation based on channel estimative. Also, the effect of imperfect channel estimation has been studied to provide means of developing techniques to overcome possible problems and enhance the MIMO communication performance

Keywords: spectrum sensing, cognitive radio networks, spectrum sensing, precoding, sum rate maximization, channel estimation, MIMO channel estimation error.

Contents

List of Figures

List of Tables

List of Acronyms

AWGN Additive White Gaussian Noise

CAV Covariance Absolute Value

BER Bit Error Rate

BS Base Station

CDF Cumulative Density Function

CS Coherent Sensing

CSI Channel State Information

CSIT Channel State Information at Transmitter

CsS Cyclo Stationary Sensor

CR Cognitive Radio

CRNs Cognitive Radio Networks

EnS Energy Sensor

FC Fusion Center

FCC Federal Communications Commission

GLRT Generalized Likelihood Ratio Test

HrS Hadamard Ratio Sensor

IID Independent Identically Distributed

IT Interference Temperature

KKT Karush-Kuhn-Tucker

LOS Line of Sight

M2M Machine-to-Machine

MB Multi-Band

MfS Matched Filter Sensor

MIMO Multiple Input and Multiple Output

MISO Multiple Input and Single Output

ML Maximum Likelihood

MMSE Minimum Mean Square Error

MRT Maximum Ratio Combining

MU Multi-User

OFDM Orthogonal Frequency Division Multiplexing

PSD Power Spectrum Density

PU Primary User

QoS Quality of Service

ROC Receiver Operating Characteristics

Rx Receiver

SB Single Band

SDR Software Defined Radio

SIMO Single Input and Multiple Output

SINR Signal-to-Interference plus Noise Ratio

SISO Single Input and Single Output

SNR Signal-to-Noise Ratio

SS Spectrum Sensing

SU Secondary User

Tx Transmitter

WF Watter Filing

ZF Zero Forcing

Notation

- Capital bold letters denote matrices: $\mathbf{H}$ and $\mathbf{Y}$;
- Small bold letters are vectors $\mathbf{s}$ and $\mathbf{y}$;
- Small italic letters represent scalars: s and x;
- $|\mathbf{X}|$ is the determinant of matrix $\mathbf{X}$;
- $||\cdot||$ is the Euclidean norm;
- $(\cdot)^H$ is the hermitian operator (transposed conjugate);
- $\nabla\mathbf{f}$ is the gradient of $\mathbf{f}$;
- $\nabla^2\mathbf{f}$ is Hessian matrix;
- $\mathbf{R}_y$ is the covariance matrix of variable y
- $\widehat{\mathbf{R}}_y$ is the sample covariance matrix of variable y
- $\mathcal{N}(m, \sigma^2)$ is a Gaussian Random process with mean m and variance σ^2;
- $\mathbb{E}[\cdot]$ is the statistic expectation;
- $\mathrm{tr}(\cdot)$ is the matrix trace operator;
- $Q(\cdot)$ is a Gaussian tail function (Q-function);
- $\mathbf{B}(\cdot,\cdot)$ is the Beta function;
- $\mathbf{B}_x(\cdot,\cdot)$ is a Incomplete Beta function;
- $\Gamma(\cdot)$ is the Gamma function;
- $\mathbb{L}(\cdot)$ is a Likelihood function;
- $\mathcal{L}(\cdot)$ is a log-Likelihood function;
- $P(x|y)$ is the conditional probability of x given y;

Symbols

Chapter 2	
Symbol	Description
T	Total period of time;
τ	Sensing period;
N	Number of samples;
P_t	Transmitted power;
P_m	Maximum transmitted power;
K	Number of SU antennas;
M	Number of PU antennas;
P_I	Average Interfering power;
P_{noise}	Noise power;
d	Distance between transmitter and receiver;
ψ	Path-loss exponent;
v	User's velocity;
f_d	Doppler shift;
f_c	Carrier frequency;
c	Light velocity;
T_L	Limit of interference temperature;
κ	Boltzmann's constant;
W	Bandwidth;
C_p	Primary user's Shannon capacity;
C_s	Secondary user's Shannon capacity;
R_p	Rate region for primary users;
R_s	Rate region for secondary users;
ξ_Z	Decision metric for spectrum sensor Z;
P_f^Z	False Alarm probability for spectrum sensor Z;
P_d^Z	Detection probability for spectrum sensor Z;
λ_Z	Decision threshold for spectrum sensor Z;
H_0	Hypothesis of absence of signal;
H_1	Hypothesis of presence of signal;
$s(k)$, $\mathbf{s}(k)$	Transmitted signal;

$n(k)$, $\mathbf{n}(k)$	Additive noise;
h	Multiplicative channel state constant;
$\mathbf{H}$	Channel matrix;
$y(k)$, $\mathbf{y}$, $\mathbf{Y}$	Received signal;
σ_x^2	Variance of variable x;
γ	Signal to Noise Ratio;
$\mathcal{M}_i$	i-th moment of a variable;
$\mathcal{M}_{-i}$	i-th negative moment of a variable;
Υ_L	Correlation strength;
$\widehat{\Upsilon}_L$	Normalized correlation coefficient;
$\boldsymbol{\Sigma}^{(i)}$	Covariance matrix under hypothesis i;
$\widehat{\boldsymbol{\Sigma}}^{(i)}$	Sample covariance matrix under hypothesis i;

Chapter 3

Symbol	Description
K:	Number of secondary users;
$\mathcal{K}$:	Set of secondary users;
M:	Number of primary users;
$\mathcal{M}$:	Set of primary users;
$\mathcal{S}$:	Set of active secondary users;
n_{BS}:	Base station's number of antennas;
I_m:	Interference limit to m-th PU;
I_p:	Interference from PUs to SUs;
P_{BS}	SU-BS's power constraint;
$\mathcal{C}_k$	Capacity of user k;
y_k :	Received signal;
η_k	AGWN noise;
γ	Signal to Interference plus Noise Ratio;
x_k:	Transmitted symbol;
$\mathbf{x}$:	Transmitted signal;
$\mathbf{h}_k$:	BS-SU link's channel vector;
$\mathbf{g}_m$:	BS-PU link's channel vector;
$\mathbf{q}_{m,k}$	PU-SU link's channel vector;
$\mathbf{w}_k$:	Precoding vector;
$\mathbf{t}_k$:	ZF precoding vector;
$\mathbf{p}$	Power allocation vector;

$\mathbf{H}$:	Collection of all SU channel vectors;
$\mathbf{G}$:	Collection of all PU channel vectors;
$\mathbf{W}$:	Collection of all precoding vectors;
$\mathbf{F}_{-k}$:	Collection of all channel vectors, except of user k;

Chapter 4

Symbol	Description
K:	Number of secondary users;
$\mathcal{K}$:	Set of secondary users;
$\mathcal{S}$:	Set of active secondary users;
M:	Number of primary users;
$\mathcal{M}$:	Set of primary users;
N:	Training realizations;
n_{BS}:	Base station's number of antennas;
I_m:	Interference limit to m-th PU;
I_p:	Interference from PUs to SUs;
P_{BS}	SU-BS's power constraint;
$\mathbf{y}$, $\mathbf{Y}$,:	Received signal;
p, $\mathbf{p}$, $\mathbf{P}$:	Transmitted pilot sequence;
x_k, $\mathbf{x}$:	Transmitted signal;
$\mathbf{h}_k$, $\mathbf{H}$:	SU channel vector and matrix;
$\mathbf{g}_k$, $\mathbf{G}$:	PU channel vector and matrix;
$\widehat{\mathbf{U}}$:	Estimated form of matrix $\mathbf{U}$;
n, $\mathbf{n}$, $\mathbf{N}$:	AGWN noise;
γ	Signal to Interference plus Noise Ratio;
$\mathbf{w}_k$:	Precoding vector;
$\mathbf{t}_k$:	ZF precoding vector;
$\mathbf{p}$	Power allocation vector;
$\mathbf{W}$:	Collection of all precoding vectors;
J:	Error between real and estimated;
$\mathcal{C}$	System capacity;
$\widehat{\mathcal{C}}$	System capacity with use of estimated channel matrix;
$\mathbf{R}_{AB}$:	Correlation matrix between variables A and B;

1 Introduction

Spectrum is a limited resource that has to be strictly regulated and correctly managed in order to provide means for high speed/quality transmissions. Until nowadays, each sub-band of the total spectrum bandwidth was assigned to one specific owner (PU, Primary User) who has payed rights to transmit over this frequencies; this means that no other user was allowed to exploit such pre-allocated spectrum, regardless if PU is using it or not. The problem is that, in the past decades, wireless technologies have been significantly developed and fixed available frequency bandwidths are becoming overcrowded and scarce. In recent studies, regulatory commissions, i.e. Federal Communications Commission (FCC), have discovered that spectrum is underutilized (FCC, 2002; DATLA; WYGLINSKI; MINDEN, 2009).

These studies reveal the need for new schemes of spectrum allocation. Hence, researchers are looking for strategies to enhance spectrum utilization efficiency. A recent technology known as cognitive radio (CR) aims to solve this spectrum scarcity problem via proposing a wireless transceiver able to interact with the environment and change its transmission parameters in order to achieve a better performance (FCC, 2003).

The concept of cognitive radio has been firstly introduced in (MITOLA; MAGUIRE, 1999), where the authors stated that CR may be interpreted as an evolution of Software Defined Radios (SDR), where various SDRs present a high level of computational intelligence. Such intelligence makes them able to mimic some human cognitive behavior like observation, orientation, planning, decision and action, in order to derivate a broad view about a wireless scenario and provide appropriate communication services.

Cognitive radio is basically a system with high environmental awareness able to dynamically access available bandwidths. Therefore, a CR is an special radio system with two main abilities: cognition and reconfigurability (KHATTAB DMITRI PERKINS, 2013). The cognition of a CR is basically an ability to sense the environment and observe spectral opportunities so the radio is able to iden-

tify available spectrum bands. The reconfigurability is related to the fact that a CR, after estimating the bandwidth usage, is able to interactively adapt its transmissions values and plans in terms of power, bandwidth and time.

A typical CR network (CRN) layout consists of a series of PUs coexisting harmoniously with CR devices (SU, Secondary User). PUs are also known as licensed users, which are the ones who own the license to transmit over some specific bandwidth. The idea of a CR proposes that SUs operate over a bandwidth, even though they do not hold a license. In order to do so, a series of constraints must be followed, i.e. the SU may only operate when PUs are not transmitting or the SU must not overcome an energy threshold in order not to affect PU's transmission (KHATTAB DMITRI PERKINS, 2013). According to the FCC (FCC, 2003), there are two main markets for CRN: rural market and general secondary market spectrum leasing. The CRNs in rural market plays an important role in terms of providing greater signal coverage for both PU and SU. The spectrum leasing allows licensees to freely offer their idle spectrum (either just a white space or the whole bandwidth) to secondary transmissions. This transaction benefits SUs because they will be able to seek for a bandwidth without buying a proper license and PUs might receive discount in their license or get payed by SUs for the leasing.

1.1 Basic Architectures of Cognitive Radio

A CRN can be divided in three different categories: Underlay, Overlay and Hybrid spectrum access strategies.

The **underlay** strategy allows spectrum sharing between PUs and SUs in respect to the whole authorized spectrum. Both users are able to transmit simultaneously at all frequencies; however, SUs are seen as noise at the PUs, what imposes that SUs do not create harmful interference and keep its transmitting power below a certain limit. Hence, when measuring primary's signal-to-interference plus noise ratio (SINR), the interference level must stay below a pre-determined value. This interference constraint means that the total power of any secondary signal must respect a spectral mask bounded by the power spectral density (PSD) interference over all frequencies under the sensing band. Alternatively, for low variant interference constraints scenarios, the threshold might be simply set according to an average value of the PSD interference taken across all the licensed frequencies (BIGLIERI et al., 2013).

The **overlay** strategy, also known as opportunistic spectrum access, proposes that all SUs must sense the spectrum and detect unused (idle) bandwidths for a certain period of time and at a certain geographic location. These idle bandwidths are known as white spaces, and SUs are always seeking to detect them, so they can transmit over these space with the maximum allowed power (SAYRAC HRISHIKESH VENKATARAMAN, 2012). When operating as overlay CRN, the SU must dedicate a period of time to sense the environment in order to identify not only idle bandwidths, but also PUs request to re-establish the transmission. Hence, there is a tradeoff between sensing time and transmission time.

A third strategy, the **hybrid** access, mixes both techniques. SUs also have to dedicate a period of time for the spectrum sensing; however, the device does not need to transmit only if a white space is detected. In case where a primary transmission is identified, SUs can use a reduced power and follow underlay power limit constraints. In case where there is an idle bandwidth, the SU adapt its transmission as an overlay spectrum access.

Figure 1.1 depicts all three access strategies. 1.1.a) shows the underlay method, where a SU device is allowed to transmit over all bandwidths (BW) with reduced transmission power in order to avoid any possible interference on primary transmissions. Figure 1.1.b) is the overlay method, where SU has to firstly sense the spectrum over a period of time t and, only if detected an idle band, adapt its power levels to transmit over that frequency. Figure 1.1.c) is the hybrid strategy, where SU also has to sense the spectrum; however, if detected a primary signal, the device transmits with reduced power (according to underlay constraints), otherwise it transmits with nominal power.

1.2 Applications of Cognitive Radio

The CR is a very promising idea, and researchers have been studying many different applications for this technology. However, these technologies are not much developed and ruled. The FCC has broadly stated a few possible areas for CRN, but did not specified strict regulations for them (FCC, 2003). Majority of CR studies are on TV bands, where intelligent CR devices opportunistically find many available bandwidths and use them to different applications. Additionally, (BIGLIERI et al., 2013) explain four typical scenarios for CRN: dynamic spectrum access in cellular systems, cellular data boost, machine-to-machine (M2M) communications and distribution and backhaul networks.

Figure 1.1: Access modes for cognitive radio.

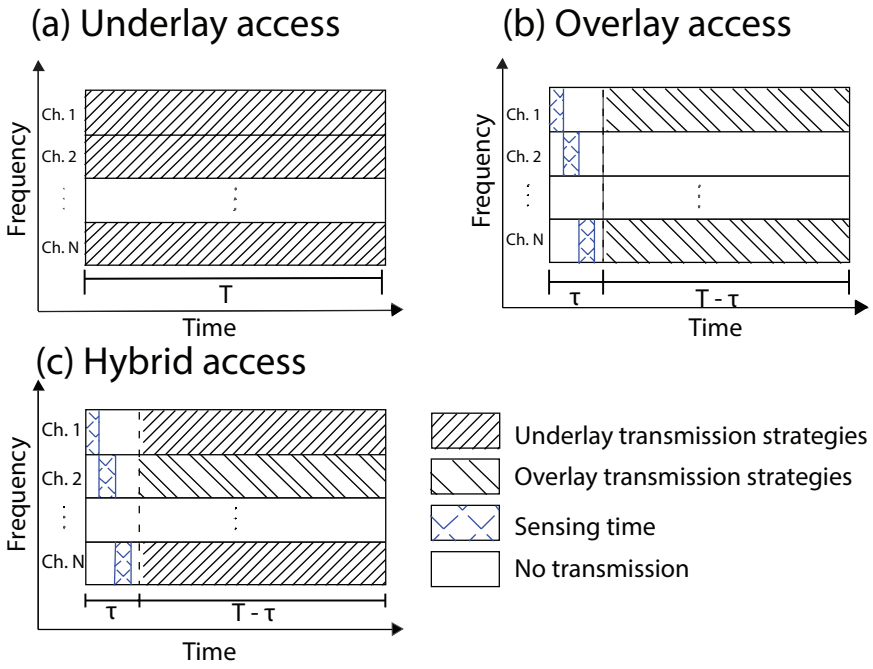

Next-generation cellular systems are relying on a much greater number of smart phones, portable devices and smart sensors to create networks with small cells embedded into large macrocells (AKYILDIZ et al., 2006). These small cells (femtocells or picocells) are a miniaturized version of a traditional base station transmitting with low power for small areas (ie. a shopping center transmission). The **dynamic spectrum access** (DSA) is an important resource for this new generation networks, because it provides a way to exploit idle spectrum and achieve higher spectral/power efficiency. CR implementation in this scenario targets to estimate wireless traffic's characteristics, mainly in peak demands, in terms of space and time usage of all available bandwidth.

Additionally, CRs are very useful to offload traffic of crowded wireless networks (**cellular boost**). This means that, during peak time, a CR can possibly detect white spaces and direct part of the traffic for these unused bandwidths and consequently alleviate the transmission of fully loaded networks. As an example, figure 1.2 shows a mesh network (AKYILDIZ; WANG; WANG, 2005) working in peak time. The hot-spots have non-real-time messages like mail, files, etc and also have the cognition to detect white spaces and follow this messages for end-users. By doing so, the hot-spots free some traffic so the base station (BS) is then able to deal with real-time communication like voice calls or video streaming. This architecture leads to capacity boost (BIGLIERI et al., 2013) and the only requirement is that end-users must be able to transmit in both white spaces and cellular band.

Another next-generation technology is the **machine-to-machine** communi-

Figure 1.2: Example of CR spectrum access in a mesh network.

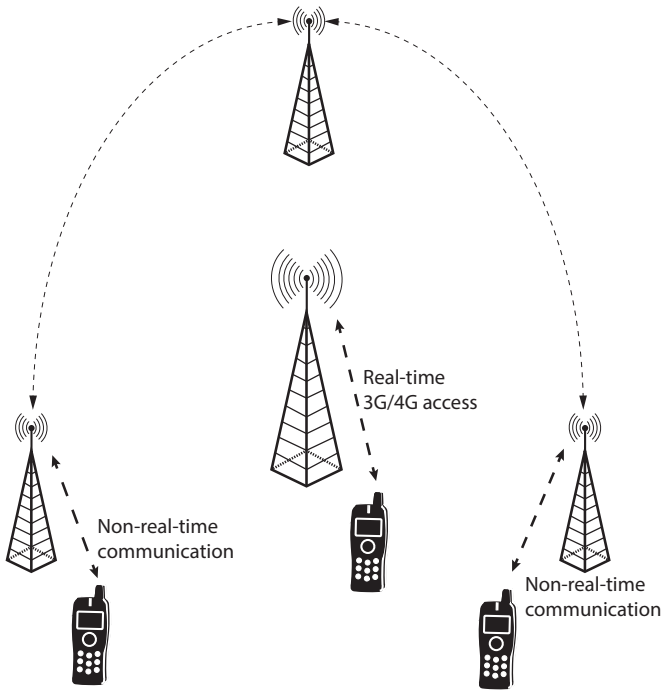

cation, which contributes to fully automation of entire sensors network (FADLULLAH et al., 2011). Cognitive radio may be useful in this context in terms of allowing a design of wireless M2M communication networks. The communication can be between a central decision making device and multiple sensors spread over the plant or even a full-duplex talk between sensors. Consequently, implementation of a CRN in this scenario will allow multiple devices to transmit over the available band, without necessity of buying license for more transmission bandwidth.

A CR can also enhance the **distribution and backhaul** of wireless networks. It will be useful not only for rural areas, but also for end-users who are at the edge of a coverage area. Figure 1.3 illustrates a typical problem of this situation. The end-users are out of range to communicate with BS1; however, BS3 has a white space available that can be used to establish a connection between users and BS1. The only update needed for this situation is the change for multi-band devices, once the users must be able to work in different bands, according to available white spaces.

The advance in technology has made architectures, designers and engineers start to design electronic devices to be used at home, ie. wireless video streaming, wireless printers, smart fridges, smart sensors etc. Design of fully automated homes is another very promising scenario for CRN. This is known as **cognitive digital homes** (BIGLIERI et al., 2013; LI; MANDAYAM; REZNIK, 2010). Figure 1.4 shows an example of a cognitive digital home, where many different devices and sensors are connected to a central node responsible for managing all connexions.

Figure 1.3: Example of a distribution and backhaul scenario.

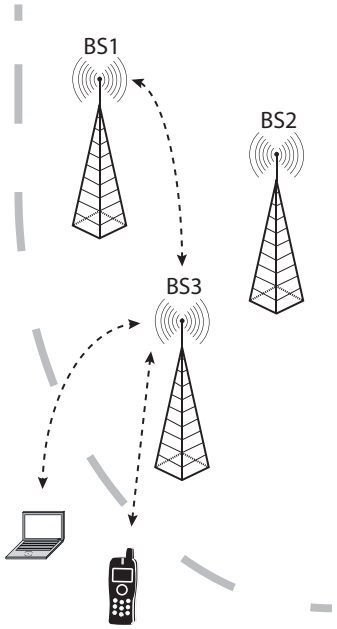

The problem in this scenario is that many of these devices are not designed to operate in conjunction with other smart sensors. Indeed, a central controlling device is needed to regulate the operation of all devices and designate a specific time and frequency for each transmission (RAMAN; YATES; MANDAYAM, 2005). The central cognitive controller tries to detect white spaces and simultaneously communicate with multiple devices.

Figure 1.4: Example of a digital home scenario.

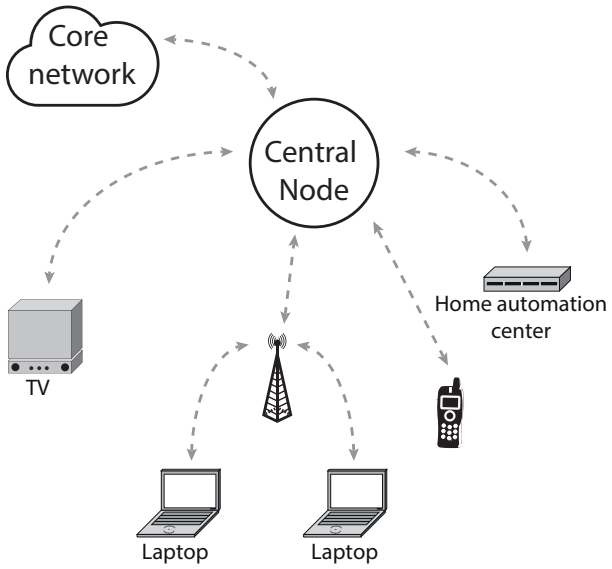

1.3 Motivation

The available transmission frequencies are becoming overcrowded as a consequence of a great necessity of new high speed/capacity wireless technologies; hence, it is extremely necessary to develop efficient methods to transmit/access the spectrum. Once all wireless spectrum is ruled by an specific agency - FCC is case of United States of America or Anatel (Agência Nacional de Telecomunicações - Brazilian National Telecommunications Agency) in case of Brazil - recent studies are aiming to develop efficient technologies to increase number of active users without increasing the necessary bandwidth. Additionally, spectrum has been proved to be underutilized. For example, (MCHENRY; LANE-ROBERTS, 2004) shows that, even during peak time, only 13% of all spectrum opportunities are effectively used. In order to overcome this problem, many researches proposed a powerful alternative, the CRN, which allows the implementation of dynamic spectrum access (BIGLIERI; GOLDSIMITH; GREENSTEIN, 2012).

This work aims to develop and obtain efficient analysis and optimization tools applied to cognitive radio in order to optimize spectrum and power usage. Capacity, performance, computational complexity and power/spectrum usage have to be studied so all proposed methods/technologies are able to actually implement useful changes/improvements to CRN.

1.4 Developed Topics in Cognitive Radio

This Dissertation is intended to study CRN architectures, its characteristics and develop mathematical tool to be applied on future Cognitive Radio systems. The studies with CRN were started during the under graduation period. After commencing this Masters, the following topics have been closer considered:

- Spectrum Sensing in Cognitive Radio Networks;
- Analysis of realistic channels for CRN;
- Non-linear optimization techniques applied to problem solving in CRN;
- Precoding optimization for Cognitive Radio Networks;
- Study of channel estimation techniques for CRN;

This work has firstly analyzed single band Spectrum Sensing (SS) methods for CRN and compared its complexity and performance. The study of SS methods

worked as an introduction to CR technologies and helped to develop the next step of this work, which is the performance analysis of Hadamard Ratio Sensor used as spectrum sensor for cognitive radio networks.

The third study of this Masters project consists of applying non-linear optimization techniques to maximize the sum capacity of a CRN. As an outcome of this study, a methodology of cancelling interference between SUs and PUs and also optimally allocation power between all SUs has been developed. The performance of this technique has been evaluated in terms of performance and capacity figures. In addition, we have used the capacity results to design a tool for choosing the optimum number of secondary users to achieve maximum capacity for a given scenario with n_{BS} transmission antennas and M primary users.

The fourth study consists of analyzing a realistic threat present in CRN: the imperfect channel estimation. Once the precoding design is based on knowledge of channel matrix; if this matrix is poorly estimated, harmful impacts may arise. This study is responsible for identifying techniques to accurately estimate the channel between SUs and PUs and offer the best estimative possible for SUs design an optimal precoder and avoid great capacity/performance losses.

The rest of this text is divided in chapters, where each one presents results and findings obtained in an specific article and also gives all necessary theory for a complete understanding of such results. Chapter 2 introduces some basics about SS techniques, popular performance metrics used to compare different methods and results obtained with this research, which has been presented in both articles: a) *Spectrum Sensing Methods for Cognitive Radio Networks - A Review* and b) *Hadamard Ratio Sensor in Realistic CRN Scenarios* (Appendix A.1 and A.2). Chapter 3 gives a basic understanding regarding precoding techniques and the respective findings have been reported in the paper *Efficient ZF-WF Strategy for Sum-Rate Maximization of MU-MISO Cognitive Radio Networks* (Appendix A.3). Chapter 4 summarizes the two investigated channel estimation techniques, and the effect of imperfect channel state information on design of precoders. Finally, Chapter 5 offers the main conclusions and possible future directions to further develop the research.

2 Spectrum Sensing in Cognitive Radio Networks

This chapter consists of a broad research about SS techniques applied CRN. Four different topologies were chosen to be compared: Energy Sensor (EnS) (BIGLIERI; GOLDSIMITH; GREENSTEIN, 2012), Matched Filter Sensor (MfS) (CARDOSO et al., 2010), Covariance Absolute Value Sensor (CaV) (ZENG; LIANG, 2009) and Hadamard Ratio Sensor (HrS) (TUGNAIT, 2012). These sensors were chosen due its main characteristics and computational complexity: EnS is a very low complex sensor and relies only on the energy of received signals; the MfS is expected to present better performance but needs a strong knowledge about primary signals; the CaV is a medium complex and needs some statistical knowledge about primary signals. Finally, the HrS is a complex but highly efficient and very robust detector.

SS is one of the most important steps in CRN, once it is responsible for checking the scenario and deciding whether a SU should or not transmit. After a sensing phase, the cognitive device is ready to select adequate transmission techniques (power, modulation, coding, precoding) in order not to interfere/harm any current primary communication. Additionally, SS is also extremely important to guarantee correct spectrum alternatives for a CR transceiver perform adequate *spectrum handoff* without dropping connection with any secondary users (HERNANDES; KOBAYASHI; ABRAO, 2016).

SS may also be divided in two categories: Single Band Spectrum Sensing (SB-SS) and Multi Band Spectrum Sensing (MB-SS). In SB-SS there is an entire sensing process for each desired band; consequently, if a device wishes to sense a wide band, multiple spectrum sensors will be necessary. In contrast, MB-SS is able to sense a wide band with a single sensor. MB-SS are mainly focused on estimating the PSD and identifying idle bands. This chapter deals only with SB-SS.

The first part of this chapter is referred to Appendix A.1, which consists of

a tutorial about basic SS SISO (Single Input Single Output) architectures, its characteristics, performance metrics, sample complexity and other parameters. Next, numerical experiments are proceeded aiming to compare performance figure of all analysed architectures. All results obtained in the article are also detailed in section 2.2.

The second part of this chapter consists of a more detailed analysis of HrS applied to realistic MIMO CR scenarios, which included influence of path loss and multipath fading. This part is based on Appendix A.2, where a brief mathematical background is given and simulations are performed to compare performance figures of HrS and a classical EnS in Rayleigh fading channels. This analysis is valid to help a designer to choose which SS technique is more indicated to be implemented under certain constrains (i.e. QoS (Quality of Service), capacity and BER).

In order to develop a method to verify the state of a certain frequency band, lets consider that a signal $y(t)$ is being observed by a secondary user at instant k; indeed, this signal may be classified as (CARDOSO et al., 2010):

$$y(k) = \begin{cases} n(k) & : \ H_0 \\ h \cdot s(k) + n(k) & : \ H_1 \end{cases} \tag{2.1}$$

where h represents the channel multiplicative effect and $n(k) \sim \mathcal{N}(0, \sigma_n^2)$ is AWGN (Additive White Gaussian Noise). As stated in (2.1), there are two hypothesis: absence of PU (H_0) of presence of primary signals (H_1).

Once the signal of interest has been defined, it is possible to calculate the reception SNR γ, in case where the SU needs to identify the transmitted signal $s(k)$:

$$\gamma = \frac{h \cdot s(k)}{\eta(k)} \tag{2.2}$$

Or, in cases where the sensor is not able to distinguish between signal and interference, the above equation is treated as signal to interference plus noise ratio (SINR)

$$\gamma' = \frac{h \cdot s(k)}{h \cdot s'(k) + \eta(k)} \tag{2.3}$$

where the portion $h \cdot s'(k)$ is referent to all undesired signals.

The situation here consists of designing a system able to present high chances of correct detection ($Pr\{H_1|H_1\}$ or $Pr\{H_0|H_0\}$) and low rates of false alarms ($Pr\{H_1|H_0\}$) while receiving only N samples (the fewer samples the better and

more efficient the detector is).

2.1 Contributions

The main contributions of the work in this chapter are:

1. Study of the main SS techniques;
2. Performance analysis of various SS methods;
3. Comparison between various SS architectures;
4. Analysis of realistic CR scenarios;

2.2 Numerical Results: Spectrum Sensing techniques

In order to corroborate the above theory, numerical experiments were proceeded under different constraints and scenarios. All necessary theory, mathematical background, numerical experiments about every studied sensor is detailed in Appendix A.1 and the main results are also analysed in this section. Performance of each sensor is studied in terms of ROC (Receiver Operating Characteristics), 3D surfaces which involves sample complexity, SNR, P_d and SNR Wall. Individual results will be firstly presented and then a comparison with all sensor will be done under different circumstances.

It is important to notice that results of sections 2.2.1, 2.2.2 and 2.2.3 are based on AWGN scenarios, whereas sections 2.2.4 and 2.3 also include two cases of Rayleigh fading scenarios: slow and fast fading. For slow fading cases, the channel state changes at each block of N_c samples and for fast fading cases the channel changes at every sample.

2.2.1 Energy Detector

As stated in Appendix A.1, detection probability for an Energy Sensor in AWGN channel is given by:

$$P_d^{\text{ED}} = Q\left(\frac{\lambda_{\text{ED}} - \mu_1}{\sigma_1^2}\right) \tag{2.4}$$

where λ_{ED} is an energy threshold, $\mu_1 = \sigma_n^2(1+\gamma)$, $\sigma_1^2 = \frac{\sigma_n^2}{\sqrt{N}}\sqrt{2\cdot\gamma+1}$ and σ_n^2 is the noise variance. Consequently, it can be seen that changes in SNR, threshold

and number of samples will somehow affect performance of a EnS.

Figure 2.1 presents ROC results for an EnS in AWGN channels, where SU is acquiring 1000 samples to sense the spectrum. As expected, increase in SNR positively affects the sensor, once a higher P_d^{ED} can be achieved with much lower P_f^{ED}.

Figure 2.1: ROC for an Energy detector with N=1000 samples.

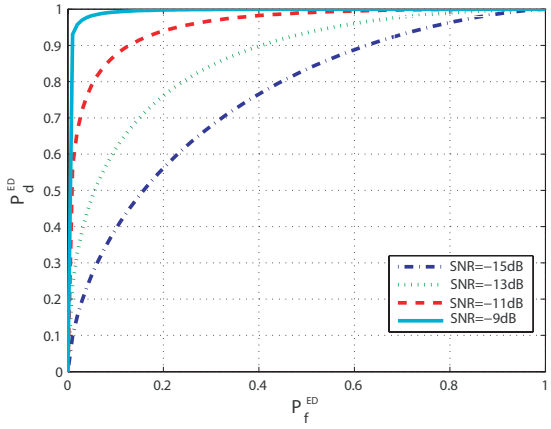

Figure 2.2: P_d^{ED} dependency on N and SNR for $P_f^{\text{ED}} = 0.1$.

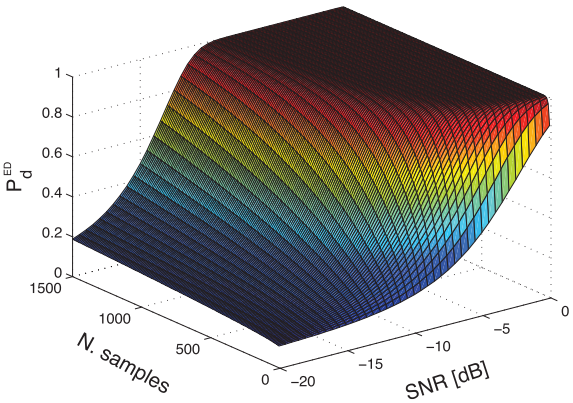

A target detection probability $P_d^{\text{ED}} = 0.8$ is desired for a P_f^{ED} not greater than 0.1. Indeed, from figure 2.2, it is seen that an acceptable performance is obtained with samples ranging from 500 to 1500 for $\gamma > -10$dB.

Once an EnS relies on signal's strength (energy), it is expected that low SNR scenarios are not indicated for this sensor. However, EnS is known to be one of the most simple sensors to be implemented, which is the reason for many works to choose it.

2.2.2 Matched Filter Sensor

Similar simulations were proceeded for a MfS in AWGN channel; results in terms of ROC and 3D surfaces were obtained in order to give an overview about the sensor's performance and influence of the threshold λ_{MF}, number of samples and SNR. Probability of detection in AWGN channels may be written as (MCDONOUGH et al., 1995; BHARGAVI; MURTHY, 2010):

$$P_d^{\text{MF}} = Q\left(\frac{\lambda_{\text{MF}} - \varepsilon}{\sqrt{\varepsilon\sigma_n^2}}\right) \tag{2.5}$$

where $\varepsilon = \sum_{k=1}^{N} x^2[k]$ is the pilot signal's power.

Observation of figure 2.3 shows a much lower range of SNR. This is expected

because, differently from EnS, a MfS does not rely only on energy of a signal. A matched filter detector makes use of a pilot sequence to analyse if there is a real signal or if the measurement consists of noise only. Additionally, the range of number of samples in figure 2.4 is similar to the EnS case, which indicates that both have the same sample complexity; however, MfS is able to work in much lower SNR scenarios.

Figure 2.3: ROC for a MfS detector. **Figure 2.4:** P_d^{MF} dependency on N and SNR for $P_f^{\mathrm{MF}} = 0.1$.

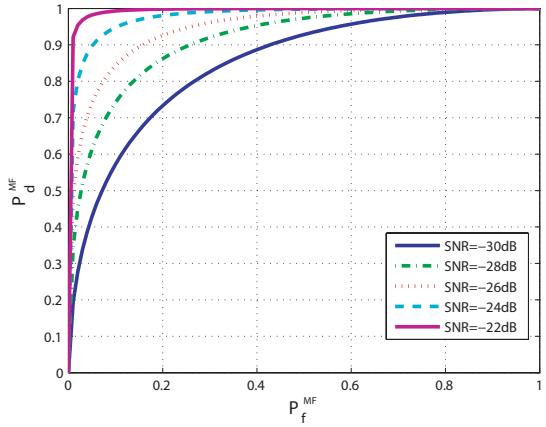

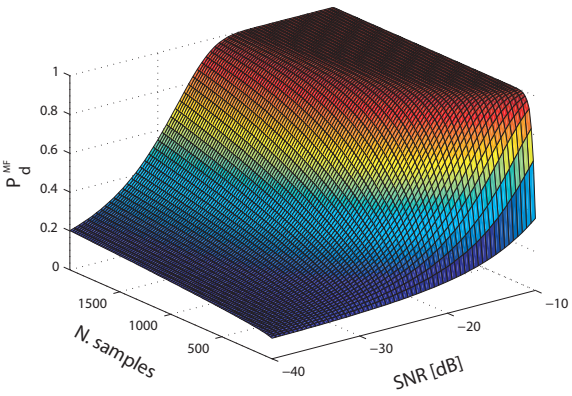

MfS has already showed to present better performance results for low SNR scenarios; however, there is a tradeoff between performance and computational complexity in this case. MfS requires a replica of a pilot sequence at the secondary user so the detector is able to correlate a received signal with the pilot sequence. This fact not only increase computational complexity but also makes necessary the presence of pilot sequence, which is not always available in wireless transmissions.

2.2.3 Covariance Absolute Value Detector

CAV detectors are based on second order statistics of the sensing signal. Out of all N received samples, the sensor analyse the correlation matrix of L consecutive samples, where L is known as smoothing factor. As a consequence, the vector form of signals in (2.1) have to be analyzed here:

$$\mathbf{y}(k) = [y(k) \;\; y(k-1) \;\; \cdots \;\; y(k-L+1)]^T \tag{2.6}$$

$$\mathbf{s}(k) = [s(k) \;\; s(k-1) \;\; \cdots \;\; s(k-L+1)]^T \tag{2.7}$$

$$\mathbf{n}(k) = [n(k) \;\; n(k-1) \;\; \cdots \;\; n(k-L+1)]^T \tag{2.8}$$

The point is, if there actually exists a primary signal on these samples, the

correlation matrix $\mathbf{R}_y = \mathbb{E}\left[\mathbf{y}(k)\mathbf{y}(k)^T\right] = \mathbb{E}\left[\mathbf{s}(k)\mathbf{s}(k)^T\right] + \mathbb{E}\left[\mathbf{n}(k)\mathbf{n}(k)^T\right] = \mathbf{R}_s + \sigma_\eta^2\mathbf{I}_L$ will present its off-diagonal elements correlated. In contrast, if the signal is absent, $\mathbf{R}_s = 0$ and $\mathbf{R}_y$ has all off-diagonal elements equals to zero.

In practice, N samples are received, but the system is usually limited to work with L samples at a time. The covariance matrix $\mathbf{R}_y$ is then estimated via the sample covariance matrix:

$$\widehat{\mathbf{R}}_y = \begin{bmatrix} \beta(0) & \beta(1) & \cdots & \beta(L-1) \\ \beta(1) & \beta(0) & \cdots & \beta(L-2) \\ \vdots & \vdots & \ddots & \vdots \\ \beta(L-1) & \beta(L-2) & \cdots & \beta(0) \end{bmatrix} \tag{2.9}$$

$$\text{where} \qquad \beta(\ell) = \frac{1}{N}\sum_{n=0}^{N-1} y(n)y(n-\ell), \qquad \ell = 0, 1, ..., L-1 \tag{2.10}$$

Two test metrics are consequently deployed:

$$\widehat{T}_1 = \frac{1}{L}\sum_{i=1}^{L}\sum_{j=1}^{L}|\widehat{r}_{ij}| \tag{2.11}$$

$$\widehat{T}_2 = \frac{1}{L}\sum_{i=1}^{L}|\widehat{r}_{ii}| \tag{2.12}$$

where $\widehat{r}_{ij}$ is the ij-th element of the sample covariance matrix, $\widehat{\mathbf{R}}_y$. In fact, $\widehat{T}_1$ has all non-negative elements of $\mathbf{R}_y$ and $\widehat{T}_2$ presents only the diagonal ones.

As a consequence, P_d^{CAV} and P_f^{CAV} will also depend of a correlation strength factor Υ_L, as illustrated in equations (2.13) and (2.14) (ZENG; LIANG, 2009; GEETHU; NARAYANAN, 2012).

$$P_f^{\text{CAV}} = Pr\left\{\frac{\widehat{T}_1}{\widehat{T}_2} > \lambda_{\text{CAV}}\middle| H_0\right\} = 1 - Q\left(\frac{\frac{L-1}{\lambda_{\text{CAV}}}\sqrt{\frac{2}{N\pi}} - 1}{\sqrt{2/N}}\right) \tag{2.13}$$

$$P_d^{\text{CAV}} = Pr\left\{\frac{\widehat{T}_1}{\widehat{T}_2} > \lambda_{\text{CAV}}\middle| H_1\right\} = 1 - Q\left(\frac{\frac{1}{\lambda_{\text{CAV}}} + \frac{\Upsilon_L\gamma}{\lambda_{\text{CAV}}(\gamma+1)} - 1}{\sqrt{2/N}}\right) \tag{2.14}$$

where the correlation strength Υ_L and the correlation coefficient $\widehat{\Upsilon}_L$ are given,

respectively, by (2.15) and (2.16):

$$\Upsilon_L \triangleq \frac{2}{L}\sum_{\ell=1}^{L-1}(L-\ell)|\alpha_\ell| \tag{2.15}$$

$$\widehat{\Upsilon}_L = \frac{\Upsilon_L}{\sigma_s^2\sigma_\eta^2} \tag{2.16}$$

and

$$\alpha_\ell = \frac{\mathbb{E}[\mathbf{s}(n)\mathbf{s}(n-\ell)]}{\sigma_s^2} = \frac{\mathbf{R}_s(\ell)}{\sigma_s^2} \tag{2.17}$$

A primary analysis of figures 2.5 and 2.6 shows that SNR range is between EnS and MfS cases. However, it is worth to emphasize that Υ_L is plays an important role in performance of CAV detectors. Indeed, estimation observation of correlation strength in CRN scenarios is extremely important decide whether a CAV detector is suitable or not.

Figure 2.5: ROC for a CAV detector with $L = 10$, $\Upsilon_L = 2$ and $N = 10000$.

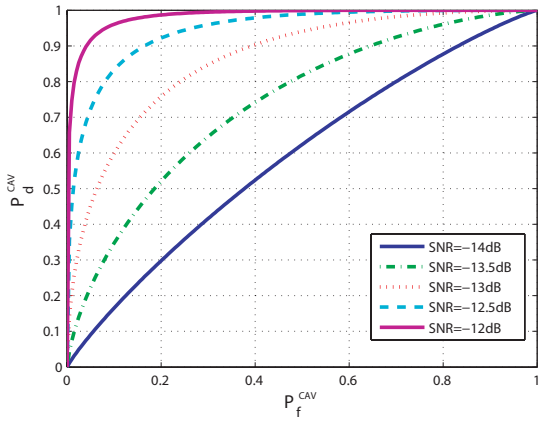

Figure 2.6: ROC for a CAV detector with $L = 10$, $\Upsilon_L = 3$ and $N = 10000$.

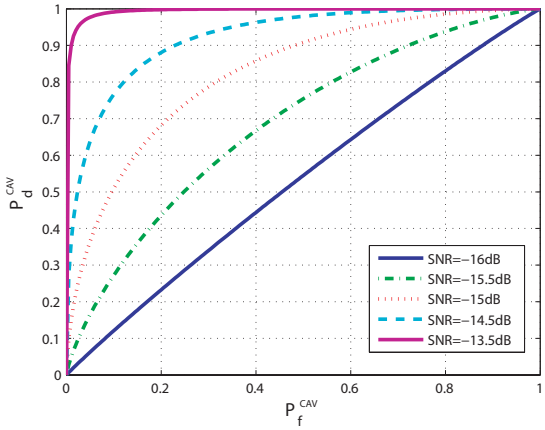

For this sensor, P_d^{CAV} dependency on N and γ has also been analyzed. Figure 2.7 confirms the SNR range described before; additionally, it shows that a much higher number of samples is needed to achieve the same detection probabilities of EnS and MfS. It is expected because second order statistics usually have to be acquired over a long observation of signals. Indeed, even with a higher smoothing factor L, many samples will still be needed.

2.2.4 Hadamard Ratio Based Spectrum Sensor

The HrS is a relatively new spectrum sensing method, even tough it is based on the well known Generalized Likelihood Theory, its literature is a little limited for CR scenarios. The HrS relies on spatial diversity of signals at receiver antennas

Figure 2.7: P_d^{CAV} dependency on N and γ for $P_f^{\text{CAV}} = 0.1$.

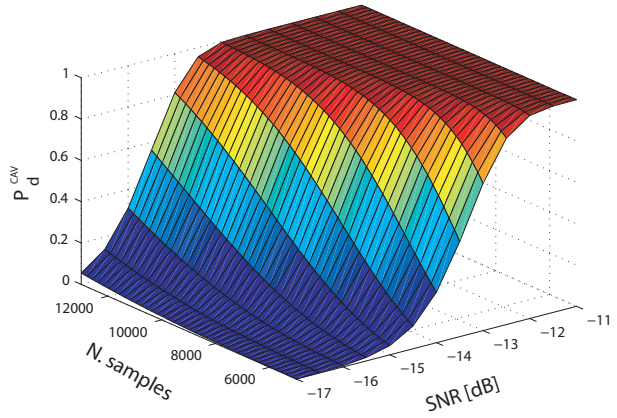

(MARIANI; GIORGETTI; CHIANI, 2012; HUANG et al., 2015). This ends up, as shown in Appendix A.1, offering better results and enhances performance when more users/antennas are sensing the spectrum.

All statistic tests for a HrS are derived based on a MIMO CRN configuration with M and K transmit and receive antennas, respectively. Indeed, all variables in equation (2.1) have to be transformed into its vector form:

$$\mathbf{s}(k) = [s_1(k) \;\; s_2(k) \;\; \cdots \;\; s_M(k)]^T \tag{2.18}$$

$$\mathbf{n}(k) = [n_1(k) \;\; n_2(k) \;\; \cdots \;\; n_K(k)]^T \tag{2.19}$$

$$\mathbf{y}(k) = [y_1(k) \;\; y_2(k) \;\; \cdots \;\; y_K(k)]^T \tag{2.20}$$

And the received signal is written as:

$$\mathbf{y}(k) = \begin{cases} \mathbf{n}(k) & : H_0 \\ \mathbf{Hs}(k) + \mathbf{n}(k) & : H_1 \end{cases} \tag{2.21}$$

The observation vector is assumed to be Gaussian distributed $\mathbf{y}|H_i \sim \mathcal{N}\left(0, \mathbf{\Sigma}^{(i)}\right)$, $i = 0, 1$, where $\mathbf{\Sigma}^{(i)}$ is the received signal covariance matrix. Under H_0 (without primary signals) $\mathbf{\Sigma}^{(0)}$ becomes $\mathbf{\Sigma}^{(0)} = \text{diag}\,(\sigma_1, \ldots, \sigma_K)$, which is a diagonal matrix. However, under H_1, $\mathbf{\Sigma}^{(1)} \triangleq (\sigma_{ij})_{K\times K}$.

Following these assumptions, the likelihood function of all received samples under a general hypothesis H_i is expressed by (HUANG et al., 2015; MARIANI; GIORGETTI; CHIANI, 2012):

$$\mathcal{L}\left(\mathbf{Y}|\widehat{\mathbf{\Sigma}}^{(i)}\right) = \frac{1}{\left|\widehat{\mathbf{\Sigma}}^{(i)}\right|^N} \exp\left(-N \cdot \text{tr}\left(\left[\mathbf{\Sigma}^{(i)}\right]^{-1} \widehat{\mathbf{\Sigma}}\right)\right) \tag{2.22}$$

where $\widehat{\mathbf{\Sigma}} = \frac{1}{N}\mathbf{Y}\mathbf{Y}^H$ is the sample covariance matrix and $\mathbf{Y} = [\mathbf{y}_1, \ldots, \mathbf{y}_N]$. It is

important to notice that $\widehat{\mathbf{\Sigma}}^{(0)} = \text{diag}\left(\widehat{\mathbf{\Sigma}}\right)$ and $\widehat{\mathbf{\Sigma}}^{(1)} = \widehat{\mathbf{\Sigma}}$.

The Generalized Likelihood Ratio Test (GLRT) accounts probabilities of these two hypothesis and compare them with a preset threshold λ_{HR}:

$$\xi_{\text{HR}} = \frac{\mathcal{L}\left(\mathbf{Y}|\widehat{\mathbf{\Sigma}}^{(0)}\right)}{\mathcal{L}\left(\mathbf{Y}|\widehat{\mathbf{\Sigma}}^{(1)}\right)} = \frac{\left|\widehat{\mathbf{\Sigma}}^{(1)}\right|}{\left|\widehat{\mathbf{\Sigma}}^{(0)}\right|} \underset{H_1}{\overset{H_0}{\gtrless}} \lambda_{\text{HR}} \tag{2.23}$$

The exact behavior of ξ_{HR} may assume complex values; however, its moments can be easily expressed and matched with a beta distribution. Indeed, the first and second negative moments of beta distributed random variable Z is defined as (JOHNSON; KOTZ; BALAKRISHNAN, 1995):

$$\mathcal{M}_{-1} = \mathbb{E}\left\{Z^{-1}\right\} = \frac{\alpha+\beta-1}{\alpha-1} \tag{2.24}$$

$$\mathcal{M}_{-2} = \mathbb{E}\left\{Z^{-2}\right\} = \frac{(\alpha+\beta-1)(\alpha+\beta-2)}{(\alpha-1)(\alpha-2)} \tag{2.25}$$

$$\tag{2.26}$$

where α and β are the Beta distribution parameters.

Solving (2.24) and (2.25) for α and β:

$$\alpha = \frac{\mathcal{M}_{-1} - \dfrac{2\mathcal{M}_{-2}}{\mathcal{M}_{-1}} + 1}{\mathcal{M}_{-1} - \dfrac{\mathcal{M}_{-2}}{\mathcal{M}_{-1}}} \tag{2.27}$$

$$\beta = (1-\mathcal{M}_{-1})(1-\alpha) \tag{2.28}$$

Finally, the probability of detection for a HrS is defined as (HUANG et al., 2015):

$$P_d^{\text{HR}} \triangleq Pr\left(\xi_{\text{HR}} < \lambda_{\text{HR}}|\text{H}_1\right) = \frac{B_x(\alpha,\beta)}{B(\alpha,\beta)} \tag{2.29}$$

where $B(\alpha,\beta)$ is the beta function and $B_x(\alpha,\beta)$ is the incomplete beta function.

Figures 2.8 and 2.9 show ROC performance of a HrS under AWGN channels. Comparison of both figures presents an important fact which wasn't mentioned until now is the performance enhancement due to higher spatial diversity. This result allows us to closer study this fact and also analyze HrS under different channels and scenarios.

Figure 2.8: ROC for HrS with $N = 1000$ and $M = 1$.

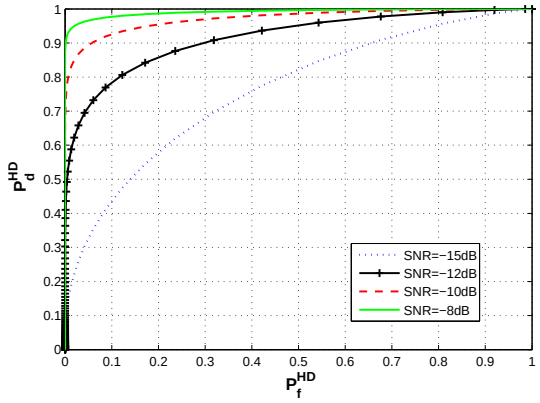

Figure 2.9: ROC for HrS with $N = 1000$ and $M = 3$.

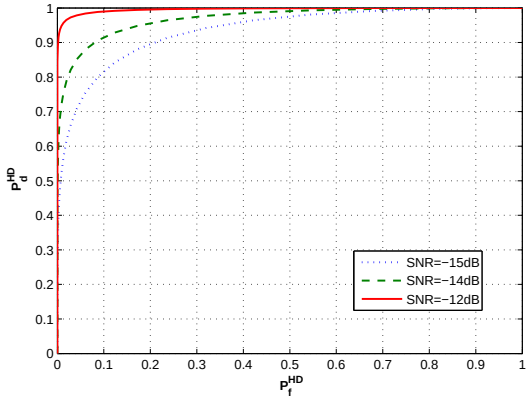

2.2.5 SNR Walls in CR-SS

Another important contribution of this work is the analysis and correct formulation of SNR Walls for spectrum sensors. This asymptotic behavior has already been pointed out for SS devices (TANDRA; SAHAI, 2008; SAHAI; TANDRA, 2009). Theoretically, decrease in SNR could be mitigated by increase in number of samples; however, this it not what actually happens. At some limit point, the "*sample complexity blows up to infinity as the detector sensitivity approaches certain critical values*" (TANDRA; SAHAI, 2008). For example, observing Fig. 2.10, a SNR wall is seen at -46dB and the black dashed line indicates the hypothetical sensor's behavior.

Figure 2.10: SNR Wall characteristics.

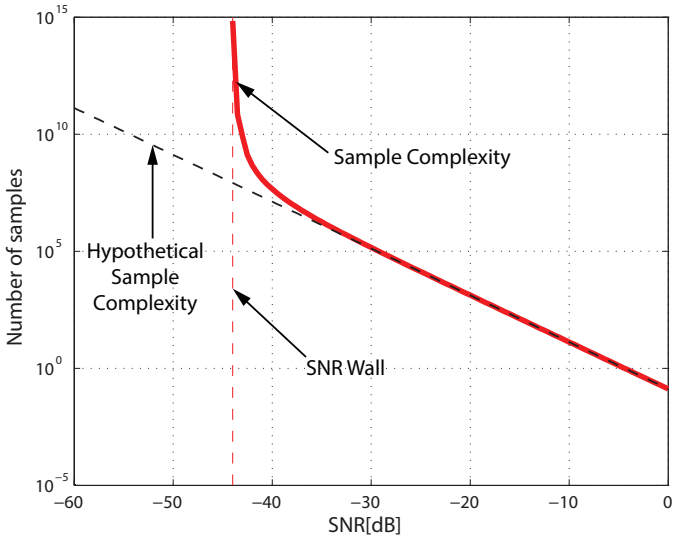

Observing equations of each sensor, it is possible to relate P_d, P_f, and γ to find N.

The sample complexity for an EnS is found with help of a factor $\rho = 10^{x/10}$, which quantifies the level of uncertainty in the noise power, where the noise variance has xdB of uncertainty. As a result, the sample complexity for an EnS is given by (TANDRA; SAHAI, 2008):

$$N^{\text{ED}} = \frac{2\left[Q^{-1}(P_f^{\text{ED}}) - Q^{-1}(P_d^{\text{ED}})\right]^2}{\left[\gamma - \left(\frac{\rho^2 - 1}{\rho^2}\right)\right]^2} \tag{2.30}$$

Consequently, the SNR wall is the point of discontinuity of (2.30):

$$\left[\gamma - \left(\frac{\rho^2 - 1}{\rho^2}\right)\right]^2 = 0 \qquad \Rightarrow \qquad \therefore \quad \text{SNR}_{\text{wall}}^{\text{ED}} = \frac{\rho^2 - 1}{\rho^2} \tag{2.31}$$

Similarly, authors of (TANDRA; SAHAI, 2007) states that MfS is divided such that the signal is coherently sensed within a coherence block with N_c samples and then detected via an energy sensor. Indeed, the sample complexity for a MfS is a modified version of (2.30) with addition of a variable $\theta \in \mathbb{R}|0 \leq \theta \leq 1$ that represents the fraction of a pilot tone power and N_c representing the influence of coherence time:

$$N^{\text{MF}} = \frac{2N_c\left[Q^{-1}(P_f^{\text{ED}}) - Q^{-1}(P_d^{\text{ED}})\right]^2}{\left[\theta N_c\gamma - \left(\frac{\rho^2 - 1}{\rho^2}\right)\right]^2} \tag{2.32}$$

Similarly, the SNR wall for a MfS is found with analysis of the denominator of (2.32):

$$\left[\theta N_c\gamma - \left(\frac{\rho^2 - 1}{\rho^2}\right)\right]^2 = 0 \qquad \therefore \qquad \text{SNR}_{\text{wall}}^{\text{MF}} = \frac{\rho^2 - 1}{\theta N_c \rho^2} \tag{2.33}$$

For the CAV, P_d and P_f are given respectively by (2.14) and (2.13); as a consequence, λ_{CAV} can be isolated from both equations:

$$\lambda_{\text{CAV}} = \frac{1 + (L-1)\sqrt{\frac{2}{N\pi}}}{1 - Q^{-1}(P_f^{\text{CAV}})\sqrt{2/N}} \tag{2.34}$$

$$\lambda_{\text{CAV}} = \frac{1 + \frac{\Upsilon_L\gamma}{1+\gamma}}{1 + \sqrt{2/N}Q^{-1}(P_d^{\text{CAV}})} \tag{2.35}$$

Combining (2.34) and (2.34), the sample complexity for a CAV detector is obtained as:

$$N^{\text{CAV}} = \frac{2\phi^2}{\left(\delta - \sqrt{\delta^2 - 2\Delta\phi}\right)^2} \tag{2.36}$$

where:

$$\delta = Q^{-1}(1 - P_d^{\text{CAV}}) + \frac{(L-1)}{\sqrt{\pi}} + Q^{-1}(P_f)\left[1 + \frac{\Upsilon_L \gamma}{1+\gamma}\right]$$

$$\phi = \frac{2(L-1)}{\sqrt{\pi}} Q^{-1}(1 - P_d^{\text{CAV}})$$

$$\Delta = -\frac{\Upsilon_L \gamma}{1+\gamma}$$

The SNR wall for CAV detectors is also extracted from (2.36):

$$\left(\delta - \sqrt{\delta^2 - 2\Delta\phi}\right)^2 = 0 \qquad \Rightarrow \qquad \therefore \quad 2\Delta\phi = 0$$

$$2\left(\frac{\Upsilon_L \gamma}{1+\gamma}\right) \cdot \left(\frac{1(L-1)}{\sqrt{\pi}} Q^{-1}(1 - P_d)\right) = 0 \tag{2.37}$$

There are two possibilities for the denominator to be set to zero: a) $L = 1$; b) $\Upsilon_L = 0$. This shows that, for fixed and valid values of L and Υ_L, the sample complexity for a CAV detector will not present a discontinuity point in terms of SNR.

Exact calculation of SNR Wall values based on limit analysis of the above equations is more detailed in Appendix A.1. Numerical results are depicted in figure 2.11, where it is possible to observe a wall located at -13.4dB for EnS and -43dB for MfS. However, CAV dos not presents an SNR Wall. This fact had already been pointed ou by Tandra (TANDRA; SAHAI, 2007), which stated that *feature detectors*, like CAV, do not present a wall when working in certain types of channels. This has now been confirmed by analysis of equation (2.36) and observation of figure 2.11.

Figure 2.11: Sample complexity for CRN sensors.

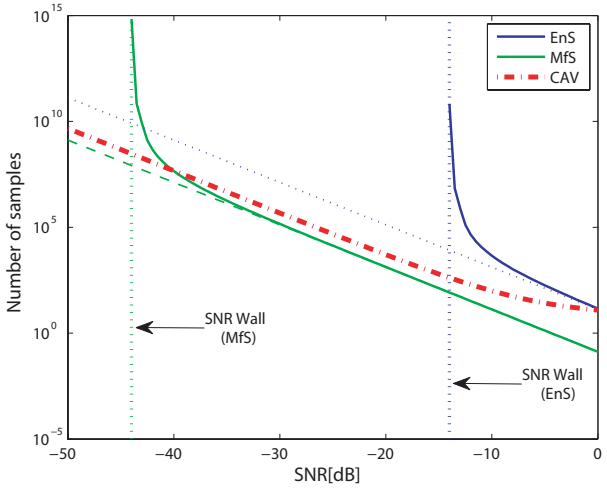

2.3 Numerical Results: Hadamard Ratio Sensor

This study of HrS technologies started at the graduation's final project, where the student performed an extensive research on likelihood theory, which is basic knowledge for a HrS. Additionally, performance metrics and basic results were also developed at that stage. Later, at the Master's step, more realistic scenarios were studied and deeper comparison/analysis of HrS topologies was proceeded. In order to allows a better understanding of HrS' operation, figure 2.12 exemplifies a basic spectrum sensing process of a Hadamard Ratio-based SS. Firstly, M PUs generate and transmit their data over a channel $\mathbf{H}$, which is d meters aways from a SU. The sensing device collects N samples and group them into a matrix $\mathbf{Y}^{K\times N}$, where K is the number of SU's receiver antennas. Then, a sample covariance matrix is calculated and the maximum likelihood of this received signal is estimated. Indeed, the test statistic ξ_{ED} is calculated and the final decision (H_0 or H_1) is taken based on a threshold γ_{ED}.

Figure 2.12: Block diagram for a generic HrS.

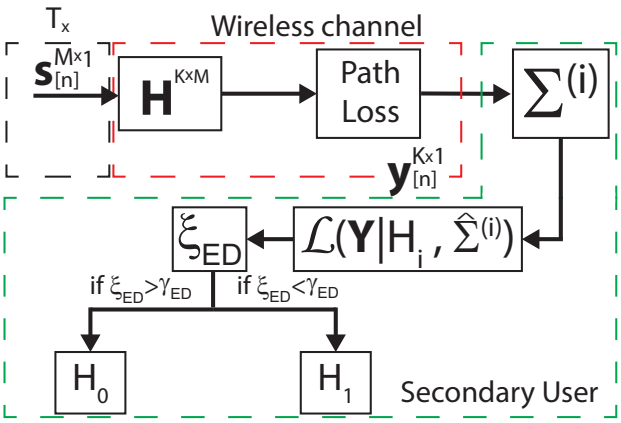

HrS methodology does not provide a closed expression probabilities of detection and false alarm involving all variables, as all previous studied sensors. In contrast, a moment matching strategy is needed. Observing ξ_{ED}, a great similarity to a Beta distributed random variable ($r.v.$) could be detected (HUANG et al., 2015; TUGNAIT, 2012; MARIANI; GIORGETTI; CHIANI, 2012; ABOURIZK; HALPIN; WILSON, 1994). As a consequence, via calculation of first and second positive/negative moments of ξ_{ED} probabilities are calculated via $p.d.f$ (probability density function) integration, which is the C.D.F (Cumulative Density Function) of a Beta $r.v.$

The studied scenario modelling allows insertion of a Doppler spread factor f_d, which represents mobility of secondary users. Indeed, simulations with slow and fast fading could be designed. Additionally, in wireless systems, distance

Table 2.1: Reference values used for simulations

Parameter	Value
Avg. PU power	$P_t \in [-100, -20]$dBm
PU-SU dist.	$d = 1000$m
Noise power	$P_{\text{noise}} = -100$dBm
SNR	$\gamma \in [-3, 7]$dB
# samples	$N \in [32, 1024]$
# SU antennas	$K = 12$
# PU	$M = 5$
Doppler freq.	$f_d \in \{5, 200\}$Hz
Path-loss exponent	$\psi = 4$

between transmitter and receiver does not significantly harm the transmission; however, it demands more transmission power. In order to calculate a path loss effect, the distance d was considered to be the average SU-PU separation. Table 2.1 presents all values and parameters used on simulation runs in this section.

Results are next presented if terms of ROC. Firstly, figure 2.13 compares HrS and EnS for a fast fading environment, where the maximum Doppler shift $f_d = \frac{v}{c} f_c = 200$Hz ($v$ is the user's velocity, f_c is the carrier frequency and c is the light velocity and $d = 1$km. As stated in results of section 2.2.1, an EnS already presents excellent performance at $\gamma = -3$dB in AWGN scenarios; however, figure 2.13 shows that EnS performs poorly in fading channels even at $\gamma = 7$dB. In contrast, HrS presents acceptable performance ($P_d \geq 0.1$ and $P_f \leq 0.2$) at fading scenarios with $\gamma = -3$dB (as shown in the blue dashed curve of figure 2.13).

Figure 2.13: ROC comparison for EnS and HrS.

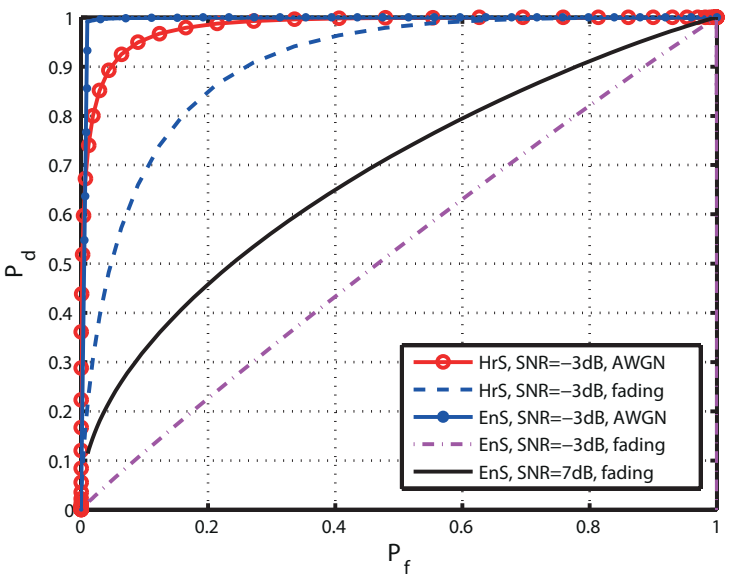

This result justify utilization of HrS as a SS method to be applied in CRN, once the secondary user is usually a portable device, which is in constant move-

ment (fading channel). Next, difference between slow and fast fading and how number of samples affect performance of detection in HrS in described. For the slow fading case, all N samples are subject to the same channel state, while on fast fading there is a change in channel state at each received sample.

The following simulation has been proceeded for a fixed transmitting power equals to -20dBm, $K = 12$ antennas, $M = 5$ users and $d = 1000$m, which results in $\gamma = 0$dB. The scale of x-axis has been changed to logarithmic in order to provide a closer view of the effect of changing the number of samples. Firstly, the slow fading case (2.14 shows that a marginal increase in number of samples effects minimally the performance (change from 128 to 150 samples); however, a great change in N also poses a great increase in P_d). The fast fading case is a little different: it seems to present a limit performance with $N = 128$. This is proved by abruptly increasing samples from 128 to 1024 and, as a consequence, negligible performance improvement is observed. This may indicate the existence of a SNR wall at around 128 samples.

Figure 2.14: Slow fading.

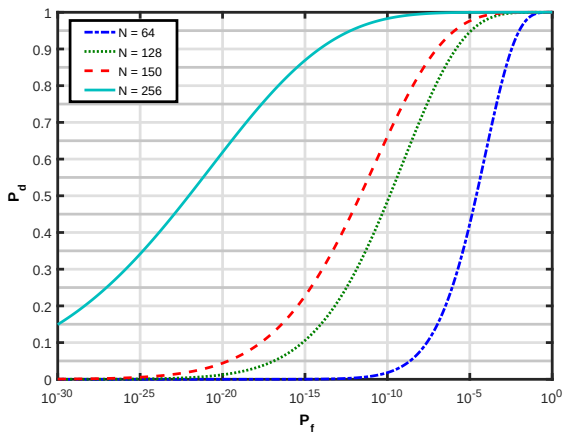

Figure 2.15: Fast fading.

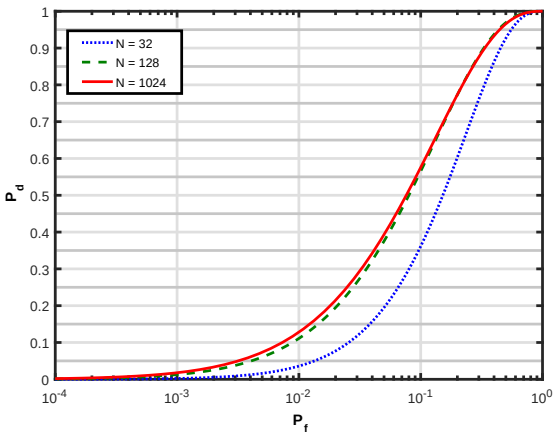

3 Precoding Techniques in Cognitive Radio Networks

Previous chapter has studied efficient spectrum sensing techniques and how it affects a cognitive communication. After the SS stage, a CR has to effectively adapt its transmission strategies (power, code, frequency etc.) to enhance QoS while avoiding interference to PUs. This chapter is devoted to analyze an access strategy based on precoding designing, which is able to reduce/avoid interference between two or more SUs and to PUs.

Precoding is a strategy based on optimization techniques which applies pre-processing on any transmission data aiming to reduce effects of wireless channels. Via exploiting Channel State Information at the Transmitter (CSIT), a precoding matrix $\mathbf{W}$ (or vector $\mathbf{w}$ in MISO scenarios) is designed to encode the information such that overall quality of transmission is enhanced. Precoding is widely used in transceiver design (either at cognitive scenarios or not) to simplify different design criteria and transform the problem into a diagonal/parallel architecture (DANIEL P. PALOMAR, 2007).

The vector $\mathbf{w}$ is usually designed to optimize some transmission characteristics, i.e. capacity, BER, SER, spectrum/power efficiency. The chosen design criteria is the sum rate (SR) optimization for the entire secondary cognitive network, which may have more than one user. A MU-MISO (Multi User MISO) cognitive underlay network was considered. As illustrated in figure 3.1, the network has a central cognitive BS (Base Station) broadcasting information to K SUs while M PUs are also transmitting over the same bandwidth. Each k-th BS-SU link has a channel response modeled by $\mathbf{h}_k \in \mathbb{C}^{n_{\text{BS}} \times 1}$, $k \in \mathcal{K} = \{1, , 2, \ldots, K\}$ and each m-th BS-PU link is represented by $\mathbf{g}_m \in \mathbb{C}^{n_{\text{BS}} \times 1}$, $m \in \mathcal{M} = \{1, , 2, \ldots, M\}$ and is considered a form of interference for any PU. Also, all PUs are constantly transmitting; consequently, their signal is seen as interference at SUs, and the channel vector $\mathbf{q}_{m,k}$ relates each m-th PU and k-th SU.

Given the above scenario, it is possible to assume flat fading channel for all

Figure 3.1: Proposed MISO Cognitive Radio scenario.

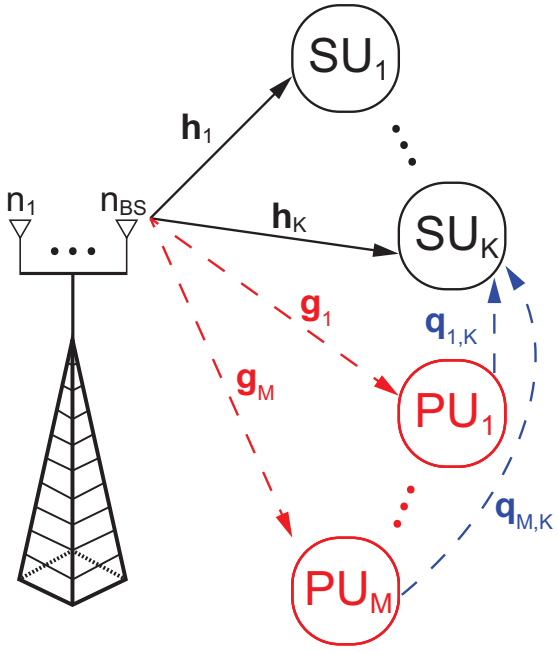

cases. Additionally, as described in (QIU et al., 2012), a CR device usually has a high processing power, which, allied with CSIT, allows and stimulate design of precoding processing techniques to enhance overall quality of communication. Indeed, the work proposed in this chapter is very valid and pertinent to this scenario.

Once the underlay CRN scenarios has been chosen, it is important to adequate every k-th link transmission power in order not to overcome a certain interference limit to any m-th primary user, which is given by I_m. From figure 3.1, the received signal at the k-th SU is written as:

$$\mathrm{y}_k = \mathbf{h}_k^H \mathbf{w}_k \mathrm{x}_k + \sum_{i \in \mathcal{K}, i \neq k} \mathbf{h}_k^H \mathbf{w}_i \mathrm{x}_i + \sum_{j=1}^{M} \mathbf{q}_{j,k}^H \mathbf{z}_j + \eta_k \tag{3.1}$$

where $\eta_k \sim \mathcal{CN}(0, \sigma_k^2)$ is the AWGN (Additive White Gaussian Noise), $\mathrm{x}_k \sim \mathcal{CN}(0, 1)$ is a normalized transmitted symbol and $\mathbf{w}_k$ is the precoding vector. By doing so, $\mathbf{w}_k$ is also responsible for allocating power. Also, there is a transmitted signal $\mathbf{z}_j$ for all M PUs; however, SUs do not have any information about primary users characteristics or its transmitted symbols.

As mentioned before, in an underlay CRN, all PUs are constantly transmitting and SUs do not have any power upon primary transmissions. If all PUs transmit over the entire period of time, for sake of simplicity, an average interference power I_p can substitute calculation of $\mathbb{E}\left[\sum_{j=1}^{M} \left(\mathbf{q}_{j,k}^H \mathbf{z}_j\right)^2\right]$. This constant I_p can be now incorporated into the noise term as $n_k \sim \mathcal{CN}(0, \sigma_k^2 + I_p)$. Consequently, the

received signal at k-th SU is re-written as:

$$\mathrm{y}_k = \mathbf{h}_k^H \mathbf{w}_k \mathrm{x}_k + \sum_{i \in \mathcal{K}, i \neq k} \mathbf{h}_k^H \mathbf{w}_i \mathrm{x}_i + n_k \tag{3.2}$$

Observe that the first term of $\mathbf{y}_k$ in equation (3.2) is relative to the actual information of user k and the second term is referent to interference from other secondary users.

As mentioned before, a transceiver is usually designed to optimize the transmission. This research is focused on optimizing the SR of an entire secondary network constrained by interference and transmission power figures. Indeed, the problem formulation has a general form as follows:

$$\max_{\{\mathbf{w}_1, \ldots, \mathbf{w}_K\}} \quad \sum_{k=1}^{K} C(\mathbf{w}_k) \tag{3.3a}$$

$$\text{s.t}: \quad f_1(\mathbf{w}_k) \, \forall k \in \mathcal{K} \tag{3.3b}$$

$$f_2(\mathbf{w}_k) \, \forall k \in \mathcal{K} \tag{3.3c}$$

Where $f_1(\mathbf{w}_k)$ and $f_2(\mathbf{w}_k)$ represent interference limit and BS transmission power constraints and $C(\mathbf{w}_k)$ is the k-th user channel capacity given by the Shannon's equation (TSE; VISWANATH, 2005):

$$C(\mathbf{w}_k) = \log_2 (1 + \gamma_k) \tag{3.4}$$

where γ_k is the Signal to Interference plus Noise Ratio (SINR), which is formulated as:

$$\gamma_k = \frac{\mathbf{h}_k \mathbf{w}_k \mathbf{w}_k^H \mathbf{h}_k^H}{\sum_{j \neq k}^{K} \mathbf{h}_k \mathbf{w}_j \mathbf{w}_j^H \mathbf{h}_k^H + \sigma_k^2 + I_p} \quad \forall k \in \mathcal{K} \tag{3.5}$$

Differently from other articles that aim to minimize any interference from SUs to PUs as a protection, this work uses interference as a constraint. As stated before, in architecture from figure 3.1, there are basically three types of interference: PUs→SUs, SUs→SUs, SUs→PUs, which will all be considered in the problem formulation. The denominator of (3.5) has already incorporated any interference to secondary users; however, interference to primary users still needed to be considered as a constraint, which is:

$$f_1(\mathbf{w}_k) = \sum_{k \in \mathcal{K}} \mathbf{g}_m \mathbf{w}_k \mathbf{w}_k^H \mathbf{g}_m^H \leq I_m, \quad \forall m \in \mathcal{M} \tag{3.6}$$

In addition, as the great majority of wireless transmission systems, a CRN also has limited transmission power P_{BS}. Indeed, it is possible to write another constraint to our optimization problem:

$$f_2(\mathbf{w}_k) = \mathbf{w}_k^H \mathbf{w}_k \leq P_{\text{BS}} \quad \forall k \in \mathcal{K} \tag{3.7}$$

which states that all allocated power resultant from precoding design must stay below the available power resources.

Grouping all the above equations together, the initial resource allocation optimization problem is finally written as:

$$\max_{\{\mathbf{w}_1,\ldots,\mathbf{w}_K\}} \quad \sum_{k=1}^{K} \log_2(1+\gamma_k) \tag{3.8a}$$

$$\text{s.t}: \quad \mathbf{w}_k^H \mathbf{w}_k \leq P_{\text{BS}}, \ \forall k \in \mathcal{K} \tag{3.8b}$$

$$\sum_{k\in\mathcal{K}} \mathbf{g}_m \mathbf{w}_k \mathbf{w}_k^H \mathbf{g}_m^H \leq I_m, \ \forall m \in \mathcal{M} \tag{3.8c}$$

As every optimization problem, the first step to solve it is the proof of convexity. Appendix A.3 brigs an extensive discussion about it, and shows the non-convexity of the cost function (3.8a), which motivate us to transform the problem and identify, at least, a suboptimal solution.

3.1 Zero Forcing-Water Filling Technique

Zero Forcing (ZF) technique is largely applied as precoding/decoding strategy to minimize channel effects in wireless transmission systems. In order to divide channel effect cancellation and power allocation, the precoding vector was rewritten as $\mathbf{w}_k = \sqrt{p_k}\mathbf{t}_k$ such as $\mathbf{h}_i^H \mathbf{t}_k = 0$, $\forall i \in \mathcal{K}$, $i \neq k$ and $\mathbf{g}_m^H \mathbf{t}_k = 0$, $\forall m \in \mathcal{M}$. The ZF criterion implies in an interference free system only if the following equation is held:

$$\mathbf{F}_{-k}^H \mathbf{t}_k = \mathbf{0} \tag{3.9}$$

where $\mathbf{F}_{-k} \triangleq \{\mathbf{g}_1, \ldots, \mathbf{g}_M, \mathbf{h}_1, \ldots, \mathbf{h}_{k-1}, \mathbf{h}_{k+1}, \ldots, \mathbf{h}_K\} \in \mathbb{C}^{n_{\text{BS}} \times (M+K-1)}$. If the above criterion is respected, the original problem is simplified and the cost function becomes convex (for more details, the reader should refer to Appendix A.3).

Indeed, the optimization problem is simplified to:

$$\max_{\{\mathbf{t}_k\},\mathbf{p}} \quad \sum_{k=1}^{K} \log_2\left(1+\gamma_k\right) \tag{3.10a}$$

$$\text{s.t}: \quad \sum_{k=1}^{K} p_k \mathbf{t_k}^H \mathbf{t}_k \leq P_{\text{BS}},\ \forall k \in \mathcal{K} \tag{3.10b}$$

$$\mathbf{F}_{-k}^H \mathbf{t}_k = \mathbf{0} \tag{3.10c}$$

1. When $(M+K-1) < n_{\text{BS}}$, $\text{rank}\left(\mathbf{F}_{-k}\right) < n_{\text{BS}}$; consequently, $\mathbf{F}_{-k}^H \mathbf{t}_k = \mathbf{0}, \forall k$ presents an infinite number of solutions, including the optimal $\mathbf{W}^* = \mathbf{T} \cdot \text{diag}\left(\sqrt{\mathbf{p}^*}\right)$, where $\mathbf{T}$ is the classical ZF solution: $\mathbf{T}^* = \mathbf{T}'\left(\mathbf{T}'\mathbf{T}'^H\right)^{-1}$, where $\mathbf{T}' = \left(\mathbf{I} - \mathbf{G}^H\mathbf{G}\right)\mathbf{H}^H$ and $\mathbf{p}^*$ is an optimal power allocation. Note that $\mathbf{H} = [\mathbf{h}_1, \ldots, \mathbf{h}_k]$ is the collection of all BS-SU channel vectors and $\mathbf{G} = [\mathbf{g}_1, \ldots, \mathbf{g}_M]$ refers to BS-PU power linkage link.

2. When $(M+K-1) > n_{\text{BS}}$, $\text{rank}\left(\mathbf{F}_{-k}\right) = n_{\text{BS}}$ and $\mathbf{F}_{-k}\mathbf{t}_k = \mathbf{0}$ only has the trivial solution $\mathbf{t}_k^* = \mathbf{0}$, which implies that all SUs are deactivated. In order to avoid this effect, we will ensure that a set $\mathcal{S} \subset \mathcal{K}$ of active SUs is used to keep $(M+K-1) < n_{\text{BS}}$.

After finding $\mathbf{t}_k$, the problem is narrowed down to optimally allocating power, which has a well known solution given by the Water Filling (WF) algorithm:

$$\max_{\mathbf{p}\geq 0} \quad \sum_{k\in\mathcal{S}} \log_2(1+\gamma_k) \tag{3.11a}$$

$$\text{s.t}: \sum_{k\in\mathcal{S}} p_k \left|\mathbf{t}_k^*\right|^2 \leq P_{\text{BS}} \tag{3.11b}$$

where:

$$p_k = \frac{1}{b_k}\left[\mu - b_k\right]^+, \text{ for } \sum_{k\in\mathcal{S}} \left[\mu - b_k\right]^+ = P_{\text{BS}} \tag{3.12}$$

b_k denotes the k-th diagonal element of $\left(\mathbf{H}\mathbf{H}^H\right)^{-1}$, μ is the water level and $[\cdot]^+ = \max\{0, \cdot\}$

This two step optimization problem is the proposed Zero Forcing-Water Filling (ZFWF) technique to sub-optimally maximize the SR of a CRN under certain physical constraints. The sub-optimality comes from the fact that, given the set of all possible solutions to the original problem (3.8a), we have selected a special case of $\mathbf{w}_k$ that guarantees an interference-free transmission, has a closed form solution and narrows down the problem to a simple power allocation strategy.

This proposed solution turns out to be more complicated with increasing number of primary or secondary users. Considering the zero-forcing constraint

(3.9), it is possible to observe that, if K or M become very large, it will be very difficult to find a precoding vector lying in the null-space of $\mathbf{F}_{-k}$, which turns out not to completely force interferences to zero. This fact may harm the transmission in a way that, if more users are present in the network, capacity will actually decrease, which is the opposite from what we are designing the precoding for.

3.2 Contributions

The main contributions of the work in this chapter are:

1. Characterization of a MISO-CR scenario;
2. Complete convexity analysis of a SR problem in MISO-CR;
3. Design of SR maximization techniques for CRN;
4. Comparison of different precoding techniques and power allocation strategies.
5. Proposition of linear/exponential approximations of the optimal number of SUs for a given CRN configuration, where only information about n_{BS} and SINR is available.

3.3 Numerical Results

Basically, an optimization problem can be modeled/solved in two ways: robust optimization and stochastic optimization. Wireless systems are usually very sensitive to small interferences and changes (BEYER; SENDHOFF, 2007). Robust optimization techniques seek a complete description/modeling (either additive and multiplicative) (BEN-TAL; GHAOUI; NEMIROVSKI, 2009), while stochastic optimization leads with estimation errors according to some statistical distributions (KALL; WALLACE, 1994).

The theory developed in previous section is based on stochastic optimization, once noise uncertainty was modeled as AWGN and primary interference to SUs was considered a constant. Other works aim to more precisely model these parameters and also other uncertainties in CRN (XU; ZHAO; LIANG, 2015); however, this is not the focus of the proposed study/methodology.

3.3.1 Capacity comparison

The instantaneous capacity for any simulation trial is given by equation (3.4), which assumes perfect channel state information at receiver and transmitter. Assuming a WSS channel (Wide-Sense Stationary), the ergodic capacity $\overline{C}(\cdot)$ is computed via taking the expected value over all calculated instantaneous capacity (equation (3.13)) (COSTA; HAYKIN, 2010). Indeed, taking the expectancy from a sufficient number of trials, we approach the ergodic capacity of the channel.

$$\overline{C}(\mathbf{w}_k) = \mathbb{E}\left[C(\mathbf{w}_k)\right] \tag{3.13}$$

This section will now present all relevant obtained results. As the initial proposition is to maximize the SR of an CRN, an important performance figure is the actual SR, which is calculated after designing a precoding vector and properly allocating power. Later, another figure used to evaluate performance of a transmission system is the Bit Error Rate (BER), which is the number of error bits divided by the total number of transmitted bits. As seen in equation (3.13), our results become valid if a minimum number of trials is used to simulate the transmission. All following results were obtained via Monte Carlo simulations with 10^6 trials.

Capacity of MIMO channels is directly related to number of antennas (TSE; VISWANATH, 2005). Specifically in this work, capacity is dependent on number of secondary users (K) and BS antennas (n_{BS}). Therefore, it is essential to demonstrate all optimization results for various scenario configurations. The following result plotted on figure 3.2 are based on setups of Table 3.1, where we are aiming to vary n_{BS} and K to analyze how the SR of a CRN is affected.

Table 3.1: Reference values used for simulation 1

Parameter	**Value**
SINR	$\gamma \in [-15, 35]$dB
Secondary users	$K \in \{3, 5, 10, 15\}$
Primary users	$M \in \{1, 2\}$
CR-BS antennas	$n_{\text{BS}} \in \{8, 16\}$
PU interference	$I_p = 0$dB
Modulation	4-QAM

The value of I_p appear in decibel scale, which represents 1 watt of interference at any secondary user. Considering that in such CR scenario there is n more than two primary users and secondary users are spread over a certain coverage region, this reference value used for simulation represents a consistent interference power that does not significantly impacts SUs' transmission but limits the sum capacity.

All result following presented will compare performance figures between the proposed ZFWF scheme and the ZFEP (Zero Forcing Equal Power), which is a method that does not make use of optimal power allocation.

Figure 3.2: Sum capacity for ZFWF and ZFEP power allocation schemes.

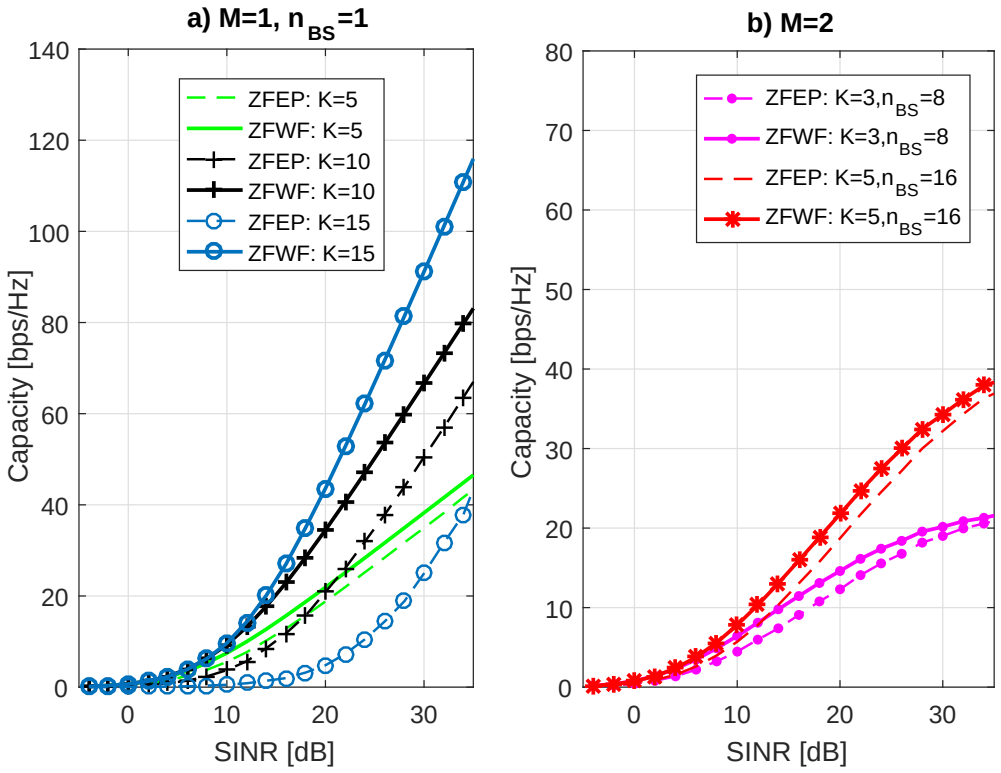

The first important analysis of figure 3.2.a) consists of observing that the proposed algorithm outperforms the case of a transmission that only cares about avoiding interferences on the network. The main idea behind ZFWF is to create a way of doing two important jobs in a CR transmission: interference zeroing and optimal power allocating. Indeed, we are able to see that zero forcing by itself does not offer great advantages for capacity enhancement; however,after applying zero forcing, we are able to deal with parallel channels and apply water filing power allocation, which significantly increases the SR of a secondary network.

The second important analysis of figure 3.2.b) comes from the red and magenta curves, that have two primary users. In both cases, either ZFWF and ZFEP, there is a possible capacity limit. This is probably due to interference constraint imposed by each PU. Even though the SUs have available power, they are limited by an interference threshold, which ends up limiting their capacity. Also, the constant interference I_p increases when $M > 1$ and SUs do not have how to avoid it. This phenomenon is actually prone to happen in cases with $M = 1$; however, for much higher SINR values.

Lastly, it is possible to observe the effect of increasing the spatial diversity.

If n_{BS} or K increases, the water filing algorithm is able to use only the non-faded channels. This is observed by the fact that, as K increases, the ZFWF curve detaches even more from the ZFEP ones (green, black and blue curves).

3.3.2 Optimum number of secondary users

In every wireless transmission network, there are some limiting parameters *i.e.* transmitting power, number of antennas or even distance from BS. In the specific case of an underlay CR MISO broadcasting network, the aim is to attend as much secondary users as we can without interfering primary transmissions. However, there exists a certain number of secondary users that maximizes the SR of the network. A basic explanation is that, the more users are transmitting, the more interference inter SUs will happen, and instead of increasing, the sum capacity will actually decrease. This is seen in figure 3.3, which plots $\mathcal{C}$ as a function of n_{BS} and K for different values of SINR.

Figure 3.3: Ergodic capacity for a ZFWF transmission with varying K, n_{BS} and SINR.

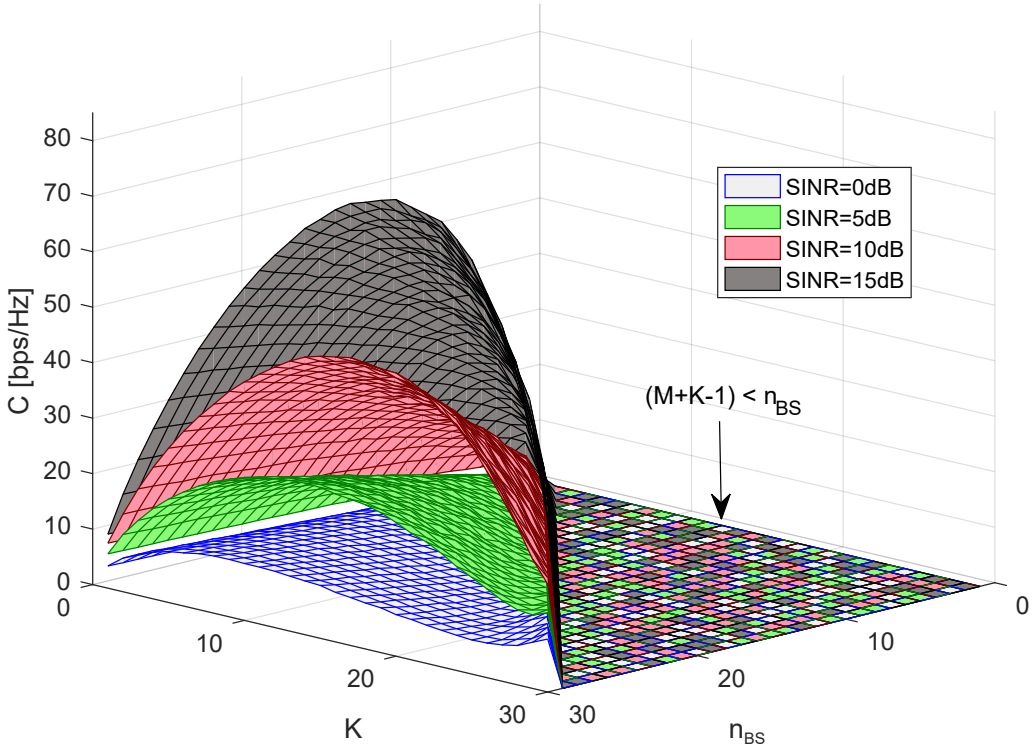

This existence of a optimum K^* is explained by two major facts. Firstly, as SUs are generally low-cost, low-power radios, when K increases, an unavailable amount of transmission power is required to guarantee quality communication for all users, which ends up reducing the secondary sum capacity. Secondly, as the precoding matrix has been designed based on $\mathbf{F}_{-k}$ and its dimension, if K and

n_{BS} increase, the dimension of $\mathbf{F}_{-k}$ also increases; as a consequence, there exists fewer solutions that guarantee a precoding matrix lying in the null space of $\mathbf{F}_{-k}$ and the ZF algorithm is not able to completely null the interference.

As observed in Figure 3.3, for every value of SINR and n_{BS} there is an optimal K^* that maximizes the sum capacity of the entire cognitive network. For massive MIMO architectures it is common to analyze the asymptotic capacity behavior as both n_{BS} and K are usually very large, which simplifies the process of finding a closed expression of K^* (BAI; HEATH, 2014). However, as in CR technologies K is not greater than 20, this asymptotic analysis is invalid. Consequently, it is unfeasible to derivate the sum capacity expression and identify an exact formula for K^*. Differently, we have approximated this value via linear interpolation. Figure 3.4 presents the same ergodic capacity plotted above for the case with $\gamma_k = 15\text{dB}$ and also the points of maximum capacity, which corresponds to a specific value of n_{BS} and K.

Figure 3.4: Ergodic capacity for a ZFWF transmission with varying K, n_{BS} and $\gamma_k = 15\text{dB}$.

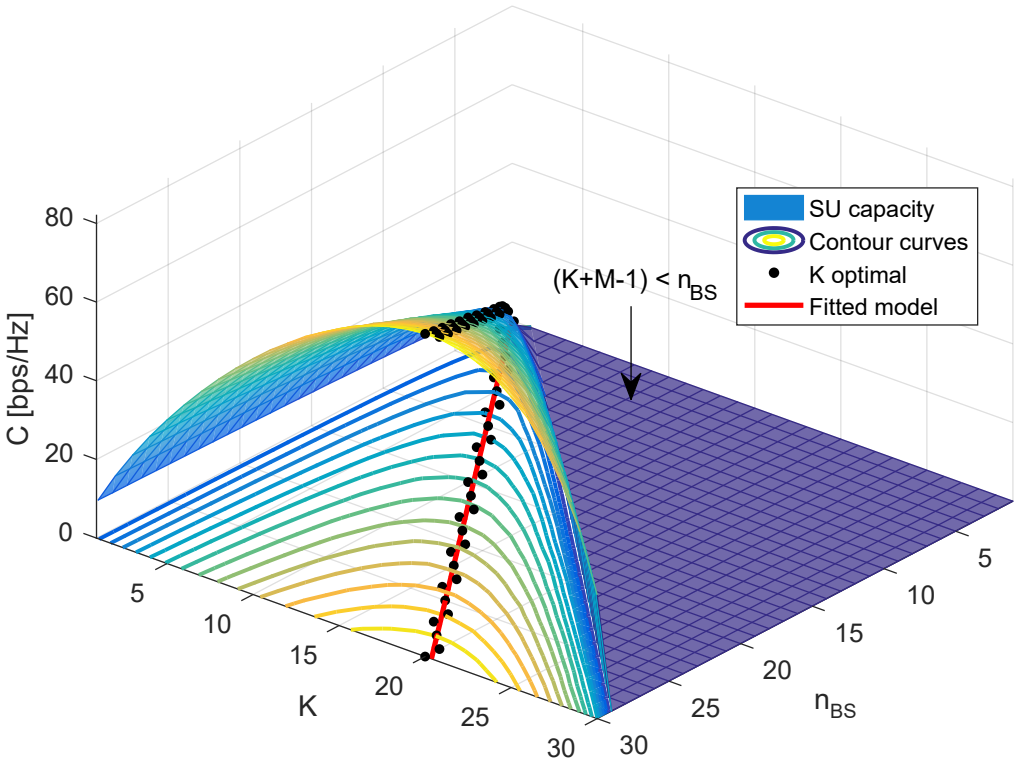

Previous simulation was done for $\gamma_k = 15\text{dB}$, whose linear approximation (red line in Figure 3.4) resulted in the following equation:

$$K^* = 0.6712 \cdot n_{\text{BS}} + 0.2299, \qquad @\gamma_k = 15[dB] \tag{3.14}$$

which gives a solution with mean squared error (MSE) equal to 0.0825. Note

that, in real architectures, K^* can only be an integer number. Indeed, using the function round, a more accurate and realistic result is obtained, with mean squared error equals to 0.0333. Both obtained models and its respective MSE are enumerated in table 3.2.

Table 3.2: Obtained fitting and respective mean squared errors.

Model	MSE
$K^* = 0.6712 \cdot n_{\text{BS}} + 0.2299$	0.0825
$K^* = \text{round}\,(0.6712 \cdot n_{\text{BS}} + 0.2299)$	0.0333

Every linear approximation of K^* is somehow dependent on SINR; consequently, there is a different equation for every value of SINR:

$$\begin{aligned} K^* &= 0.3071 \cdot n_{\text{BS}} + 0.5429, \qquad @\gamma_k = 0[dB] \\ K^* &= 0.5357 \cdot n_{\text{BS}} + 0.3143, \qquad @\gamma_k = 8[dB] \\ K^* &= 0.6893 \cdot n_{\text{BS}} + 0.2190, \qquad @\gamma_k = 16[dB] \\ K^* &= 0.8143 \cdot n_{\text{BS}} - 0.0476, \qquad @\gamma_k = 24[dB] \end{aligned}$$

The next step is to observe how the angular coefficient and the constant term of K^* behave according to SINR and finally get to a general equation as follows:

$$K^* = \tan\left(\varphi(\gamma_k)\right) \cdot n_{\text{BS}} + \beta(\gamma_k) \tag{3.15}$$

which narrows down the job to analysing the slope (related do the angle ϕ of the line) and the constant β (FARIN; HANSFORD, 2004).

Via plotting various lines of K^* and separately all φ and β, it is possible to visually identify their behaviour and then interpolate them to get an equation for $\varphi\left(\gamma_k\right)$ and $\beta\left(\gamma_k\right)$.

Figure 3.5.a) presents four obtained linear approximations of K^* and their respective angle. Subsequently, all obtained angles and constant terms are plotted respectively in figure 3.5.b) and 3.5.c) in order to illustrate their behaviour according to SINR. The red curves of figures 3.5.b) and 3.5.c) were obtained with an exponential fitting where the SINR is the independent variable:

$$\varphi(\gamma_k) = a_1 \cdot \text{SINR}^{b_1} + c_1 \tag{3.16}$$

$$\beta(\gamma_k) = a_2 \cdot \text{SINR}^{b_2} + c_2 \tag{3.17}$$

With help of the Matlab Curve Fitting Tool, all necessary parameters to

Figure 3.5: Fitting of K^*.

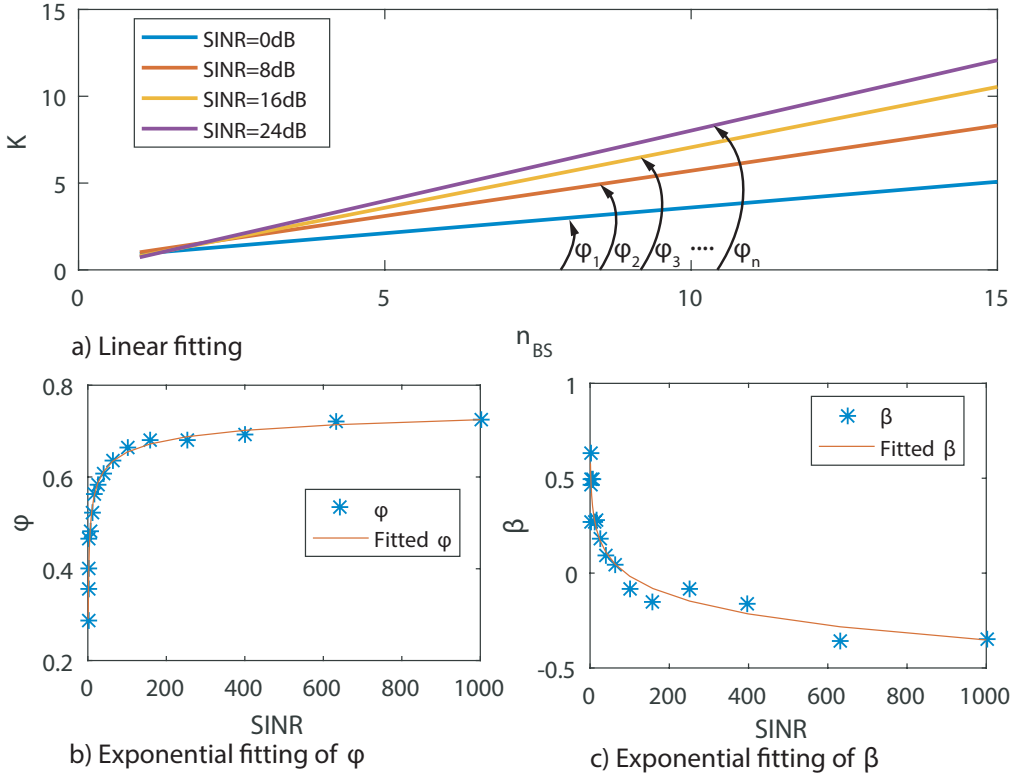

approximate φ and β were accurately obtained as follows:

$$\begin{aligned} a_1 &= -0.5189 \\ b_1 &= -0.2608 \\ c_1 &= 0.8107 \\ a_2 &= -3.2938 \\ b_2 &= 0.0360 \\ c_2 &= 3.8715 \end{aligned}$$

which are now substituted in (3.15):

$$\begin{aligned} K^* &= \tan\left(\varphi(\gamma_k)\right) \cdot n_{\text{BS}} + \beta(\gamma_k) \\ &= \tan\left(-0.5189 \cdot \gamma_k^{-0.2608} + 0.8107\right) n_{\text{BS}} \\ &\quad - 3.2938 \cdot \gamma_k^{0.0360} + 3.8715 \end{aligned} \tag{3.18}$$

Equation (3.18) offers a simple alternative for near-optimally choosing the adequate number of secondary users in a cognitive radio scenario and presents a mean squared error equals to 0.0958.

All results presented until now helped us to find out an alternative way to make use of basic characteristics (number of BS antennas and SINR) to calculate K^*. As observed in (3.14) and (3.18), K^* is linearly dependent of n_{BS} and

exponentially dependent of SINR. This behavior is plotted in surface of Fig. 3.6 All results presented above presented that the proposed maximization scheme

Figure 3.6: Sum capacity of a CRN with optimum number of SUs.

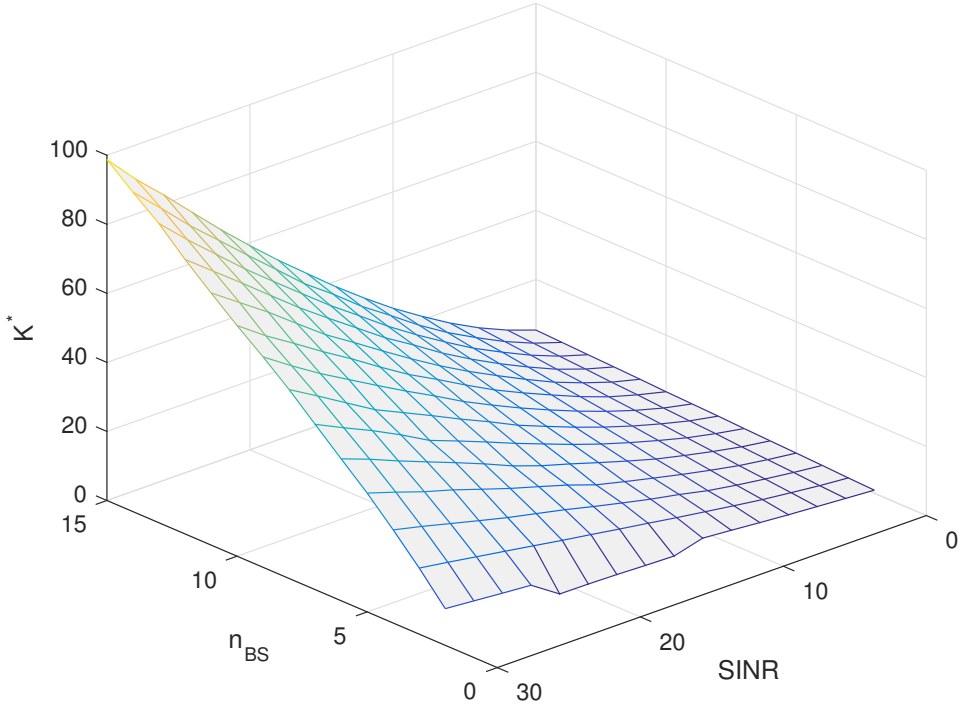

achieves a maximum SR of a given CRN. This maximization is valid only if both techniques (Zero Forcing and Water Filing) are combined, in order to null interference between users, transform the system into parallel channels and finally optimally allocate power for a certain number of secondary users.

3.3.3 Bit Error Rate Comparison

Wireless transmission networks have various parameters that need to be carefully addressed, *i.e.* transmission power, bit error rate, frame error rate, bandwidth, transmission time and capacity. This work has proposed a method to enhance capacity of an entire CRN, which resulted in a combined optimization strategy, where a zero forcing stage is deployed to properly null inter-users interference and a water filing power allocation is used to optimally allocate the available power in order to achieve maximum capacity. This technique has been proved above to correctly solve the initial problem (3.8). However, another important performance metric has to be analyzed in this case: the Bit Error Rate, which indicates how many bits are lost in a certain period of time for a give value of SINR.

It is practically impossible to optimize all parameters of a wireless transmis-

sion. If greater capacity is used, it might result in more package loss; if less power is employed, capacity and BER may be degraded. As previous subsections focused on maximizing SR, it is important to analyze the impact of this precoding technique in BER figures.

In order to make such comparison, at the same time that an algorithm to maximize SR is run, we transmit a data vector under both pre-processing strategies (MMSE and ZFWF) in order to calculate the BER along 10^6 Rayleigh channel realizations. The result is plotted in figure 3.7, where various scenario configurations are tested in the same transmission scheme. Firstly, it is important to

Figure 3.7: BER for ZFWF and ZFEP power allocation schemes.

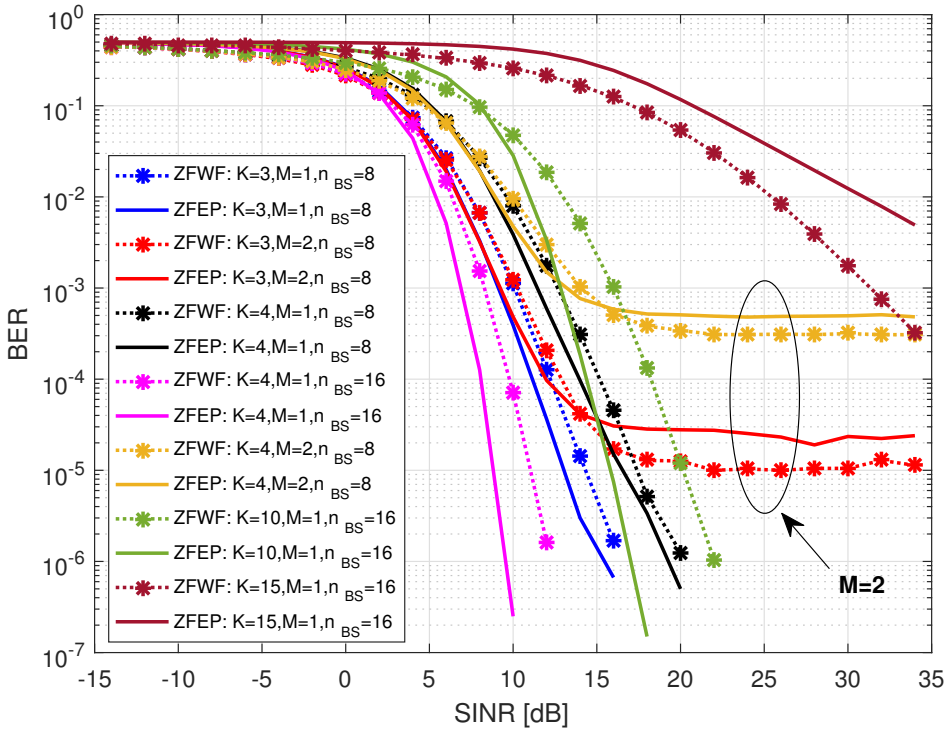

notice that, even though ZFWF was designed to maximize sum capacity, it minimally affects BER values. Also, as expected, BER is dependent on number of users/antennas (spatial diversity order), which is seen from the great separation between the case where n_{BS} and $K = 15$ and all other curves. Also, for all cases with one primary user, the ZFWF presents higher BER than ZFEP for high SINR.

The most interesting result extracted from this simulation is related to curves where there is more than one primary user. Curves red and orange present a BER floor from $\gamma_k \approx 15$dB. There are a few reasons for this phenomenon: firstly, PUs represent a very strong and unavoidable interference to secondary transmission, which confuses SUs channel estimation, decreases SINR and degrades signal detection. Also, once PUs hold transmission license, they have preference over

the bandwidth and, as soon as any PU wish to transmit, SUs must give space or reduce transmission power to avoid overcoming the interference temperature threshold. Both situations, as a consequence of a great need for more transmit power, end up causing an unavoidable BER floor. In order to eliminate, mitigate it or achieve lower BER in scenarios where $M \geq 2$, active interference cancellation is usually required.

3.3.4 MMSE Precoder Comparison

A few precoding techniques have been applied to CRN in order to enhance performance, like *Bivariate Probabilistic Constrained Programming* (BPCP) (LAW; MASOUROS; PESAVENTO, 2017), where the pre-processing matrix is designed to improve Quality of Service (QoS) by considering presence of constructive interference at secondary transmissions and taking advantage of it. Also, *Leakage Rate Limiting* (LRL), which, instead of using an interference temperature constraint, deals with interference leakage rate limiting to sustain a certain QoS (AL-ALI; HO, 2016). However, the classic *Minimum Mean Squared Error* (MMSE) approach to BER minimization can also be applied to CRN, under certain considerations, and offers a simple option to be compared to our proposed ZFWF scheme (ZHOU; THOMPSON, 2008; LEE; LEE, 2011).

ZFWF and MMSE are two distinct precoding approaches: one tries to null interference and achieve maximum capacity without care of correct bit detection, and other looks for the minimum error possible at receiver without taking care of inter user interference or capacity figures. As the main purpose of this work is to maximize the sum capacity of a secondary network, ZFWF's BER figures will not be compared to the MMSE results, once the second is known to present much lower BER and consequently, better performance.

In contrast, the next simulation compares capacity of ZFEP (no optimal power allocation), ZFWF and MMSE precoding techniques, with the MMSE precoding matrix being calculated only with the SU's channel matrix $\mathbf{W}_{MMSE} = \mathbf{H} \cdot \left(\mathbf{H}^H\mathbf{H} + \mathbf{I}_K \cdot \eta_0\right)$ does not present a power allocation strategy. Once seen in previous subsections, presence of more than one PU causes significant BER floors and capacity debasement; as a consequence this simulation does not consider cases where $M \geq 2$ and all other reference values used for generation of figure 3.8 are presented in Table 3.3.

As expected, combination of zero forcing interference nulling and water filing power allocation brings significant capacity improvement, as seen from the dis-

Table 3.3: Reference values used for simulation 2

Parameter	Value
SINR	$\gamma \in [-5, 35]$dB
Secondary users	$K \in \{10, 15\}$
Primary users	$M = 1$
CR-BS antennas	$n_{\mathrm{BS}} = 16$
PU interference	$I_p = 0$dB
Modulation	4-QAM

Figure 3.8: Sum capacity for Zero Forcing and MMSE beamforming techniques. $K = 10$ and $K = 15$ SUs.

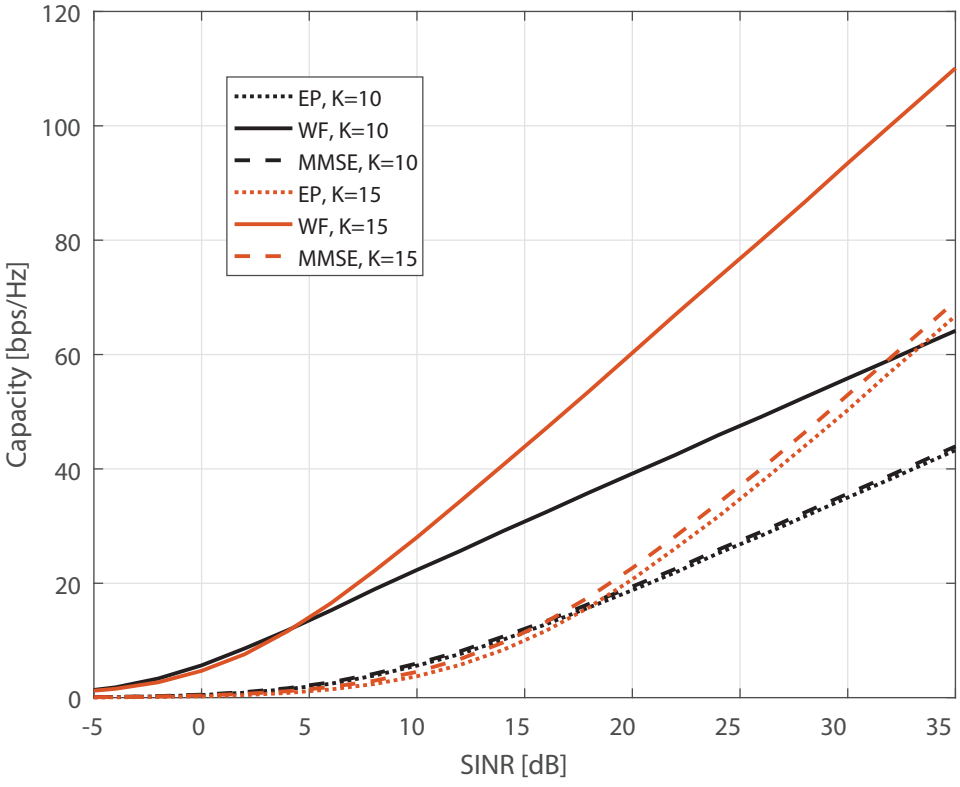

tance between ZFWF and ZFEP/MMSE curves for both scenario configurations. Also, if greater spatial diversity is deployed (red curves), this improvement becomes even more significant. However, as seen in subsection 3.3.2, the optimum K^* must be respected, otherwise the sum capacity will actually decrease, once the null space in which $\mathbf{W}_{ZF}$ must lie on is drastically reduced. Also, as observed in Fig. 3.8, does not present much improvement from simple ZFEP, once none sort of power allocation is employed. Hence, as previous analysed, the combined strategy ZF and WF has proved again to be the optimal choice when aiming to maximize sum capacity of cognitive radio networks.

4 Channel Estimation Error Effect in Cognitive Radio Networks

4.1 Introduction

The wireless network has taken a great turn over when MIMO architectures were introduced, which brought a whole new scenario for development of transmissions strategies able to make efficient use of spatial diversity and/or multiplexing. The emerging cognitive radio technologies also aim to develop transmission methods able to adapt each link of a MIMO channel in order to achieve better overall performance. This efficient use is usually employed if accurate *channel state information* (CSI) is available at the transmitter, which is obtained via channel estimation procedures.

A popular and recent example of application of channel estimation is the introduction of IEEE 802.11n network standard (BING, 2008), which is known to achieve much greater transmission rate and make efficient use of unlicensed spectrum bands. Even though this protocol destined for indoor scenarios, it is a very popular and simple example for explaining the main functionality of training and channel estimation timings. This high throughput standard offers several enhancements to medium access control (MAC) layer and plays an important role in popularization of MIMO technologies. The 802.11n employs high throughput orthogonal frequency division multiplexing (HT-OFDM) by using technologies such as MIMO, channel biding, beamforming and space-time block coding (STBC).

In order to provide means for an accurate channel estimation, the IEEE 802.11n has two operation modes: *mixed* and *green field* modes. As illustrated in Fig. 4.1, there are basically one structural difference between these modes: the time period destined to training and channel estimation, and the data transmission event.

Even though training periods bring possibility of performance enhancement,

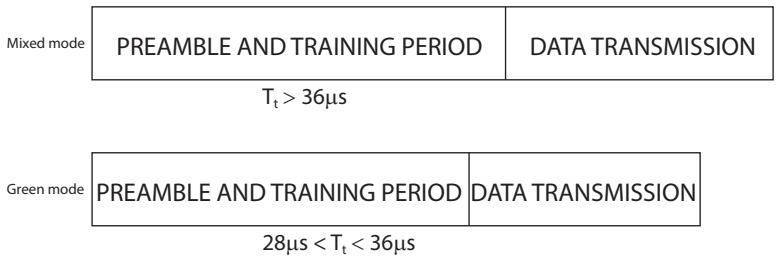

Figure 4.1: IEEE 802.11n HT-PLCP (Physical Layer Convergence Protocol) frame formats.

it also causes spectral/power efficiency loss. Spectral efficiency is defined as the net bit rate over the channel bandwidth. The longer preamble is used, the lower net bit rate is achieved. Consequently, it is desired to keep the training period as low as possible.

The high throughput mesh networks is a promising scenario for cognitive radios (BIGLIERI; GOLDSIMITH; GREENSTEIN, 2012). Also, our previous analysis (CLAUDINO; ABRAO, 2017) have demonstrated that accurate (virtually perfect) CSI estimations bring significant improvements in capacity, once correct interference cancellation and power allocation can be applied together. Indeed, the optimization techniques are deployed in (CLAUDINO; ABRAO, 2017) to design CR precoding strategies aiming at maximizing the sum capacity of a multiple input-single-output cognitve radio networks (MISO-CRNs). The chosen technique is zero-forcing waterfilling (ZFWF). To maximize the sum capacity, the number of secondary users to be supported in a certain CRN is optimally determined. The choice of K^* is based only on the number of basestation (BS) antennas and SINR. This might be very useful when designing and controlling the network, once the BS can select the best quality links and discard the poor ones.

Other studies have proved that different beamforming techniques may cause improvements on the spectral efficiency (KHATAMI; MOHAMEDPOUR; ANDARGOLI, 2017) and also SINR maximization (TOUTOUNCHIAN; VAUGHAN, 2016). Therefore, the following facts are enough reasons to motivate the study of channel estimation techniques and its impact on the performance of CR networks:

- Accuracy in the CSI estimations brings huge improvements to wireless transmissions;
- Accurate CSI estimations allow CR devices to successfully explore powerful interference cancellation techniques;
- The imperfections of the CSI estimations is due to the miss-detection of signals;

- Study of imperfect CSI effects brings means of analyzing possible errors and extrapolation of interference thresholds;
- Current communication protocols allow transmission periods dedicated to training and channel estimation;
- Use of known pilot sequences allows SUs to estimate both SU's and PU's channel matrix.

4.1.1 Contributions

CRN is a recent and promising field of study that needs a closer look and some special analysis. As a consequence of its topology, cognitive transceivers must always be working under high interference. The knowledge of channel characteristics or statistics is essential for precoding design and performance optimization. Hence, this work comes to contribute with the literature on the following CRN aspects:

- Mathematical determination of Linear MMSE (LMMSE) channel estimation for underlay CRN mode with simultaneous transmission of PUs and SUs;
- Proof that knowledge of both primary and secondary pilot sequences are necessary to apply LMMSE channel estimation;
- Simultaneous estimation of both PU and SU channels for underlay CRN, where all users are transmitting over the entire period of time;
- Analysis of impact of imperfect channel estimation on capacity of secondary users;
- Quantification of capacity loss of the underlay CRNs due to imperfect channel estimations.

The reminder of this Chapter is divided as follows: Section 4.2 presents the adopted underlay MU-MISO-CRN system model, evidencing the channel estimation problem in underlay CRNs. In Section 4.2.4 the linear MMSE MU-MISO CRN channel estimator is derived for synchronous scenarios. Numerical results in in Section 4.3 demonstrate the effectiveness of the proposed LMMSE channel estimation method for underlay MU-MISO-CRNs in both asynchronous and synchronous scenarios.

4.2 System model

A single-cell underlay multiuser (MU) MISO-CRN will be considered, where a CR-BS with n_{BS} antennas is communicating with K SUs and M PUs. The secondary transmission is established via a half-duplex link where the CR-BS has means of properly estimating all necessary channel characteristics and make the best use of it to enhance its transmission.

This work consists of separately analyzing uplink (UL) and downlink (DL) of a single cell underlay MU-MISO-CRN. The channel training occurs at uplink, while the data transmission is at the downlink. During uplink, the CR-BS is simultaneously receiving PUs and SUs pilot sequences and estimating both channel matrix. After receiving and processing the data, the CR-BS makes the best use of it to design efficient precoders according to the strategy developed in (CLAUDINO; ABRAO, 2017).

A possible time-slot structure is depicted in Fig. 4.2, where the channel estimation is composed of two stages that must be no longer than N symbols. Firstly, the CR-BS receives all transmitted pilot sequences and then process it to estimate the channel matrix and design efficient transmission precoders according to theory of (CLAUDINO; ABRAO, 2017). Subsequently, the CR-BS transmits the estimated channel to allow the CR node to properly decode the following message; finally, the CR-BS transmits all desired data. An essential condition is that the period T must be smaller than the channel's coherence time $(\Delta t)_c$. This constraint guarantees that all estimated channel parameters at the uplink can be reasonably used on the following downlink data transmission.

Figure 4.2: Frame structure.

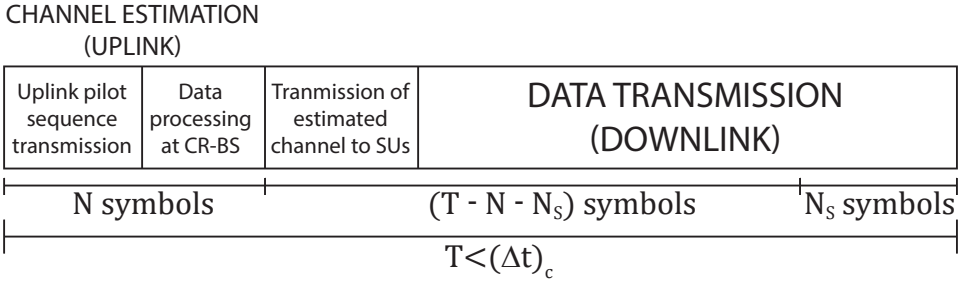

For sake of simplicity and compactness, the system model presented in this work relies on synchronous transmission and assumes orthogonal training sequences, which is not the most realistic case in the uplink direction, once it is impractical to synchronize all PUs and SUs such that its transmitted pilot sequences will be simultaneously received at CR-BS and without overlapping of two

or more consecutive symbols. However, some asynchronous practical cases will be analyzed numerically in Section 4.3, where the pilot sequence is quasi-orthogonal and some overlapping is accepted at the CR-BS.

Next, uplink channel estimation and downlink data transmission will be described. The uplink underlay CRN is used for training and channel estimation, and a few estimation techniques will be studied and hereafter compared. In this case, research of LMMSE technique adapted to MISO-CRN came up with a novelty to prove that knowledge of primary and secondary pilot sequence and noise variances are strictly necessary. Moreover, the downlink data transmission subsection explains how the channel estimative will be used to efficiently design optimal precoders according to the analytical findings in (CLAUDINO; ABRAO, 2017).

4.2.1 Uplink - training and channel estimation

The considered uplink configuration is depicted in Fig. 4.3.a), where vectors $\mathbf{h}_i$, $\mathbf{g}_j \in \mathbb{C}^{n_{BS}\times 1}$, with $i \in \mathcal{K} = \{1, \ldots, K\}$ and $j \in \mathcal{M} = \{1, \ldots, M\}$ are, respectively, secondary and primary channel vectors.

Figure 4.3: Uplink and Downlink underlay MU-MISO-CRN scenarios.

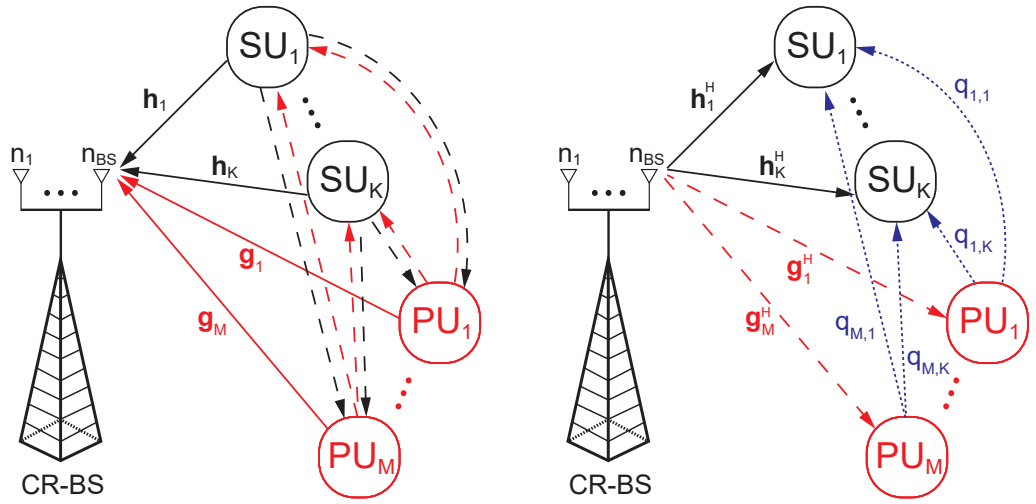

a) UL **b)** DL

Observe that, even though both primary and secondary signals may be interfering on other users signals, our interest herein is to collect the received signal at CR-BS, which is composed by PUs' and SU's pilot sequences. Once an underlay CR transmission is considered, both PUs and SUs are simultaneously transmitting

their training sequence and the CR-BS receives a signal $\mathbf{y} \in \mathbb{C}^{n_{\text{BS}} \times 1}$ as follows:

$$\mathbf{y} = \sum_{i=1}^{K} \mathbf{h}_i p_i + \sum_{j=1}^{M} \mathbf{g}_j p_j + \mathbf{n} \tag{4.1}$$

where p_i is an arbitrary pilot symbol and $\mathbf{n} \sim \mathbb{C}\mathcal{N}(0, \sigma_n^2)$ is the complex Additive White Gaussian Noise (AWGN).

Alternatively, eq. (4.1) can be re-written with the channel matrix $\mathbf{H} \in \mathbb{C}^{n_{\text{BS}} \times K}$, $\mathbf{G} \in \mathbb{C}^{n_{\text{BS}} \times M}$ and the pilot sequences $\mathbf{p}_s \in \mathbb{C}^{K \times 1}$ and $\mathbf{p}_p \in \mathbb{C}^{M \times 1}$:

$$\mathbf{y} = \mathbf{H}\mathbf{p}_s + \mathbf{G}\mathbf{p}_p + \mathbf{n} \tag{4.2}$$

A certain number of training realizations is usually required to properly estimate the channel in MIMO systems (HASSIBI; HOCHWALD, 2003). The lower bound of training symbols is known to be the number of receiving antennas. In this work, the training length N will be larger than n_{BS}, such as $N \gg n_{\text{BS}}$, in order to avoid possible channel estimation uncertainties. However, as explained before, training sequence length directly affect energy/spectral efficiency. Also, as mentioned before, the total frame length must be smaller than the coherence time of the channel.

As a consequence, the pilot symbol vectors $\mathbf{p}_s$ and $\mathbf{p}_p$ can be substituted by its respective matrix form $\mathbf{P}_s \in \mathbb{C}^{K \times N}$ and $\mathbf{P}_p \in \mathbb{C}^{M \times N}$, which results in the following received signal:

$$\mathbf{Y} = \mathbf{H}\mathbf{P}_s + \mathbf{G}\mathbf{P}_p + \mathbf{N} \tag{4.3}$$

Where $\mathbf{Y} \in \mathbb{C}^{n_{\text{BS}} \times N}$ is the received signal, the wireless channels $\mathbf{H}$ and $\mathbf{G}$ are complex Gaussian variables and Rayleigh flat fading assumed to be constant for $(\Delta t)_c > T$ symbols.

4.2.2 Estimating PU's and SU's channel matrices in underlay CRNs

The main idea is to make use of one training period to simultaneously estimate both primary and secondary channel matrix. However, the problem herein is that, for underlay CRN scenarios, PUs are constantly transmitting (and usually SUs are also aiming to do so). As a consequence, the estimators $\widehat{\mathbf{H}}$ and $\widehat{\mathbf{G}}$ have to deal with a constant interference: when estimating $\mathbf{H}$, there is the primary term $\mathbf{G}\mathbf{P}_p$ and, when estimating $\mathbf{G}$, there is an interference referent to $\mathbf{H}\mathbf{P}_s$.

All researches until now focus on estimating $\mathbf{H}$ and $\mathbf{G}$ separately or only one of them. However, the precoder studied in (CLAUDINO; ABRAO, 2017) relies on knowledge of both $\widehat{\mathbf{H}}$ and $\widehat{\mathbf{G}}$, and the fastest way of doing such estimation is to only one received signal of length N to estimate both channel matrix.

Underlay CRNs do not need a spectrum sensing stage, which allows all SUs to make use of the training period only to estimate the channel; consequently, the proposed frame structure of Fig. 4.2 still valid for the underlay MU-MISO CRN scenario.

It is known that some estimation techniques present better results for certain network configuration or are less computationally complex. Indeed, in the following, the *least squares* (LS) and the *linear minimum mean squares error* (LMMSE) estimation techniques will be briefly presented, in order to allow a future analysis of the impact of the use of such estimators on sum capacity and error performance. The classical LS estimator will be firstly introduced and can be straightforwardly adapted to MU-MISO CRN channel estimation application scenarios. However, the LMMSE case can not be easily adapted and some new inferences are presented.

4.2.3 Least Squares MU-MISO CRN Channel Estimator

The LS channel estimator is intended to find a parameter $\boldsymbol{\theta}$ to minimize the function $J_{\text{LS}}(\boldsymbol{\theta})$:

$$\begin{aligned} J_{\text{LS}}(\boldsymbol{\theta}) &= (\mathbf{Y} - \boldsymbol{\theta}\mathbf{P}_i)^2 \\ &= (\mathbf{Y} - \boldsymbol{\theta}\mathbf{P}_i)^H(\mathbf{Y} - \boldsymbol{\theta}\mathbf{P}_i) \\ &= \mathbf{Y}^H\mathbf{Y} - \mathbf{Y}^H\boldsymbol{\theta}\mathbf{P}_i - \boldsymbol{\theta}^H\mathbf{P}_i^H\mathbf{Y} + \boldsymbol{\theta}^H\mathbf{P}_i^H\mathbf{P}_i\boldsymbol{\theta} \end{aligned} \tag{4.4}$$

The gradient of $J_{\text{LS}}(\boldsymbol{\theta})$ is then calculated and set to zero as:

$$\begin{aligned} \frac{\partial J_{\text{LS}}(\boldsymbol{\theta})}{\partial \boldsymbol{\theta}} &= -\mathbf{P}_i^H\mathbf{Y} + \mathbf{P}_i^H\mathbf{P}_i\boldsymbol{\theta} = \mathbf{0} \\ \mathbf{P}_i^H\mathbf{P}_i\boldsymbol{\theta} &= \mathbf{P}_i^H\mathbf{Y} \\ \boldsymbol{\theta} &= \left(\mathbf{P}_i^H\mathbf{P}_i\right)^{-1}\mathbf{P}_i^H\mathbf{Y} \end{aligned} \tag{4.5}$$

where the training matrix $\mathbf{P}_i$ can be referent to SUs ($\mathbf{P}_s$) or PUs ($\mathbf{P}_p$); the pseudo-inverse matrix of $\mathbf{P}_i$ is given by $\mathbf{P}_i^{\dagger} = \left(\mathbf{P}_i^H\mathbf{P}_i\right)^{-1}\mathbf{P}_i^H$.

It is important to remember that, differently from other traditional MIMO architectures, an underlay CR has to use the same received signal $\mathbf{Y}$ to estimate

two distinct channel matrices, which may result in poor performance. Consequently, estimative of $\mathbf{H}$ has to lead with interference from PUs and vice-versa. From (4.5), each LS estimator (secondary and primary) can be written as (KAY, 1993):

$$\widehat{\mathbf{H}}_{\text{LS}} = \mathbf{Y}\mathbf{P}_s^{\dagger} \tag{4.6}$$

$$\widehat{\mathbf{G}}_{\text{LS}} = \mathbf{Y}\mathbf{P}_p^{\dagger} \tag{4.7}$$

4.2.4 Linear MMSE MU-MISO CRN Channel Estimator

The LMMSE estimator has a general form $\widehat{\mathbf{H}}_{\text{LMMSE}} = \mathbf{Y}\mathbf{A}^*$, where the matrix $\mathbf{A}^*$ is responsible for minimizing the difference between $\mathbf{H}$ and $\widehat{\mathbf{H}}_{\text{LMMSE}}$ as follows:

$$\begin{aligned}\mathbf{A}^* &= \arg\min_{\mathbf{A}} \mathbb{E}\left\{||\mathbf{H} - \widehat{\mathbf{H}}_{\text{LMMSE}}||_F^2\right\} \\ &= \arg\min_{\mathbf{A}} \mathbb{E}\left\{||\mathbf{H} - \mathbf{Y}\mathbf{A}||_F^2\right\}\end{aligned} \tag{4.8}$$

This approach is named *Linear* MMSE because the estimated channel matrix is a linear weighted combination of received signals.

The classical solution for problem (4.8) is applicable for SISO, SIMO and MIMO scenarios. In these cases, an arbitrary estimated channel matrix $\widehat{\mathbf{H}}_a$ is calculated based on the cross-correlation between $\mathbf{H}_a$ and the received signal $\mathbf{Y}$, namely matrix $\mathbf{R}_{H_aY}$, the inverse of the autocorrelation of $\mathbf{Y}$, *i.e.,* $\mathbf{R}_{YY}^{-1}$, and the proper received signal $\mathbf{Y}$ (BIGUESH; GERSHMAN, 2004):

$$\widehat{\mathbf{H}}_a = \mathbf{R}_{H_aY}\mathbf{R}_{YY}^{-1}\mathbf{Y} \tag{4.9}$$

A more detailed description of the classic LMMSE definition is written on Appendix A.4.

The novelty regarding the CRN channel estimation is the adaptation of eq. (4.9) to MU-MISO-CRN scenarios. Such analysis presents some peculiarities that must be properly unveiled. Considering the ideal synchronized received signal with orthogonal training sequences[1], eq. (4.3). It is necessary to adapt the

[1]Note that this case is specific for synchronized SU's and/or PU's transmitters, once no overlapping between consecutive samples is considered in such received signal expression. Even though this characterizes a not completely realistic configuration, it makes simpler the process of developing mathematical expressions for both estimated channels. The numerical results in Section 4.3 will present some analysis regarding non-synchronized transmitters and also non-orthogonal training sequences.

classic cross-correlation[2] and autocorrelation matrix from (4.9) for the MISO-CRN, where there exists two major series of pilot sequences and channel matrix. Indeed, the following has to be calculated:

$$\widehat{\mathbf{H}}_{\text{LMMSE}} = \mathbf{R}_{HY}\mathbf{R}_{YY}^{-1}\mathbf{Y} \tag{4.10}$$

$$\widehat{\mathbf{G}}_{\text{LMMSE}} = \mathbf{R}_{GY}\mathbf{R}_{YY}^{-1}\mathbf{Y} \tag{4.11}$$

where the correlation matrix $\mathbf{R}_{HH}$, $\mathbf{R}_{YY}$, $\mathbf{R}_{HY}$ and $\mathbf{R}_{GY}$ have the following specific forms:

$$\mathbf{R}_{HH} = \mathbb{E}\left\{\mathbf{H}\mathbf{H}^H\right\} = \sigma_h^2\mathbf{I}_K \tag{4.12}$$

$$\mathbf{R}_{YY} = \mathbb{E}\left\{\mathbf{Y}\mathbf{Y}^H\right\} = \sigma_h^2\mathbf{P}_s\mathbf{P}_s^H + \sigma_g^2\mathbf{P}_p\mathbf{P}_p + \sigma_n^2\mathbf{I}_N \tag{4.13}$$

$$\mathbf{R}_{HY} = \mathbb{E}\left\{\mathbf{H}\mathbf{Y}^H\right\} = \sigma_h^2\mathbf{P}_s^H \tag{4.14}$$

$$\mathbf{R}_{GY} = \mathbb{E}\left\{\mathbf{G}\mathbf{Y}^H\right\} = \sigma_g^2\mathbf{P}_p^H \tag{4.15}$$

The above result, even though obtained for a synchronous case, describes that for underlay CRN it is strictly necessary knowledge of both primary and secondary pilot sequences and channel variances. This interesting result puts some serious constraints regarding possible standards to regulate the CR transmission scheme: primary users, apart from allowing secondary users to transmit over a specific bandwidth, must at least share its pilot sequence indexes in order to allow SUs to efficiently design precoders/decoders while avoiding (or smartly reducing) possible interferences.

Until now, two estimation methods have been studied: the classic LS and LMMSE. The LS can be straight forwardly applied to MISO-CRN; however, the above research unveiled that LMMSE needs some special care regarding knowledge of pilot sequences and signals statistics. The next step is to apply these results to precoder ZFWF studied in (CLAUDINO; ABRAO, 2017), which requires knowledge of $\mathbf{H}$ and $\mathbf{G}$ to optimally design a precoder to maximize the sum capacity of a CRNs.

[2]The analysis of effect of non-orthogonal training sequences will be done with help of Gold sequences, which has already been proved to offer better performance results in realistic asynchronous scenarios if compared to other non-orthogonal sequences (KOBAYASHI; ABRAO, 2017).

4.2.5 Downlink: Data Transmission

This work has already revealed that SUs must know the primary pilot sequence and channel variance, apart from its pilot sequence, to accurately estimate the channel matrix via LMMSE estimation. Additionally, this Section intended to study the effect of channel estimation error on the CR transmissions. Notice that two estimation algorithms can be derived for UL channel estimation from the previous section 4.2.1, which results in four CR channel estimation matrices, $\widehat{\mathbf{H}}_{\text{LS}}$, $\widehat{\mathbf{G}}_{\text{LS}}$, $\widehat{\mathbf{H}}_{\text{LMMSE}}$ and $\widehat{\mathbf{G}}_{\text{LMMSE}}$. These results will now be used to design efficient precoders according to (CLAUDINO; ABRAO, 2017), which is summarized by the optimization problems in eqs. (15)–(17) of such reference.

Even though the channel estimation is proceeded during the uplink transmission, all collected data and estimated channel matrix can be used for a downlink transmission, once the coherence time has been considered greater than a frame transmission period. This is known as the *uplink-downlink duality*, which says the channel matrix estimations obtained during uplink can be transposed and deployed for a downlink transmission purpose, with sum power constraint modification (SCHUBERT; BOCHE, 2004; WIESEL; ELDAR; SHAMAI, 2006).

In the DL transmission, for the purpose of data transmission, the n_{BS} antennas CR-BS broadcasts the signal to K SUs, while M PUs are constantly transmitting, as described in Fig. 4.3.b). With the purpose of maximizing the sum capacity, the CR-BS employs a ZFWF precoder $\widehat{\mathbf{W}}$ based on the previous obtained channel matrix estimations $\widehat{\mathbf{H}}$ and $\widehat{\mathbf{G}}$ in a same way of (CLAUDINO; ABRAO, 2017, eq. (13)), having the following form:

$$\widehat{\mathbf{W}} = \text{diag}\left(\sqrt{\widehat{\mathbf{p}}}\right)\widehat{\mathbf{T}}^{\dagger} \tag{4.16}$$

where the pseudo-inverse matrix $\widehat{\mathbf{T}}^{\dagger}$ is the ZF solution given as:

$$\widehat{\mathbf{T}}^{\dagger} = \widehat{\mathbf{T}}\left(\widehat{\mathbf{T}}\widehat{\mathbf{T}}^{H}\right)^{-1} \tag{4.17}$$

and $\widehat{\mathbf{T}} = \left(\mathbf{I} - \widehat{\mathbf{G}}\widehat{\mathbf{G}}\right)\widehat{\mathbf{H}}$ is based on the estimated PU's and SU's channel matrices. Besides, the vector $\widehat{\mathbf{p}}$ is an optimal power allocation resultant from the WF algorithm, which has been described by (CLAUDINO; ABRAO, 2017, eq. (17)).

The above precoder is a sub-optimal solution for the sum capacity problem. Once the optimal one is based on perfect channel state information at the transmitter, if an estimated version of $\mathbf{H}$ or $\mathbf{G}$ is used, the ZF does not completely forces inter users interferences and, consequently, the WF algorithm is erroneously

applied to non-parallel channels. Hence, the received signal at k-th SU when the ZFWF precoder is not perfectly designed presents interference from others SUs and PUs and is given by:

$$\tilde{y}_k = \mathbf{h}_k^H \widehat{\mathbf{w}}_k x_k + \sum_{i \in \mathcal{K}, i \neq k} \mathbf{h}_k^H \widehat{\mathbf{w}}_i x_i + \sum_{j=1}^{M} q_{j,k} z_j + \eta_k \tag{4.18}$$

where x_k a transmitted symbol destined to SU k, $\widehat{\mathbf{w}}_k$ is the associated sub-optimal precoder, z_j is the j-th PU transmitted symbol, $q_{j,k}$ is the complex channel gain relating PU j and SU k and $\eta_k \sim \mathcal{CN}(0, \sigma_k^2)$ is the AWGN. All information symbols are normalized, *i.e.,* $x_i \sim \mathcal{CN}(0,1)$; hence, the kth transmitted power is determined only by the precoder $\widehat{\mathbf{w}}_k$.

An important point to be considered in CRN is the absence of knowledge about primary transmission information. Indeed, SUs have to lead with a constant interference coming from PUs. For sake of simplicity, once PUs are considered to be always transmitting, an average constant interference power I_p can be used instead of determining $\mathbb{E}\left[\sum_{j \in \mathcal{M}} q_{j,k} z_j\right]$. For a large number of PU's or antennas, the interference can be considered Gaussian distributed. Even though this assumption is not so accurate for fewer antennas/users, it will be used to model the interference power, which will be incorporated into the noise term in (4.18), such that the noise variance is increased, $n_k \sim \mathcal{CN}(0, \sigma_k^2 + I_p)$. Consequently, the received signal at k-th SU can be simplified as:

$$\tilde{y}_k = \mathbf{h}_k^H \widehat{\mathbf{w}}_k x_k + \sum_{i \in \mathcal{K}, i \neq k} \mathbf{h}_k^H \widehat{\mathbf{w}}_i x_i + n_k \tag{4.19}$$

As seen in (4.19), every k-th SU link is subject to interference from SU's and additive noise. Hence, the signal to interference plus noise ratio (SINR) of SU k is ready defined as:

$$\widehat{\gamma}_k = \frac{\mathbf{h}_k^H \widehat{\mathbf{w}}_k \widehat{\mathbf{w}}_k^H \mathbf{h}_k}{\sum_{j \neq k} \mathbf{h}_k^H \widehat{\mathbf{w}}_j \widehat{\mathbf{w}}_j^H \mathbf{h}_k + \sigma_k^2 + I_p} \tag{4.20}$$

where the notation $\widehat{\cdot}$ comes from the channel error estimation impact on the precoder vector calculation. Consequently, the sum capacity of the K active SUs is written as:

$$\widehat{\mathcal{C}} = \sum_{k=1}^{K} \widehat{\mathcal{C}}_k = \sum_{k=1}^{K} \left[\log_2\left(1 + \widehat{\gamma}_k\right)\right] \tag{4.21}$$

Notice that, when perfect channel state information is attained at the transmitter side, $\widehat{\mathbf{H}} = \mathbf{H}$, $\widehat{\mathbf{G}} = \mathbf{G}$ and the precoder is optimally designed ($\widehat{\mathbf{W}} = \mathbf{W}$). As a consequence, the ZF stage will perfectly force interferences to zero and (4.20) will

be reduced to:

$$\gamma_k = \frac{\mathbf{h}_k^H \mathbf{w}_k \mathbf{w}_k^H \mathbf{h}_k}{\sigma_k^2 + I_p} \tag{4.22}$$

The impact of imperfect channel estimation will be quantized and compared to the ideal case in the next section. As mentioned before, all mathematical discussion was based on synchronous transmission at the uplink and use of orthogonal pilot sequences, which eases the process of finding a closed solution for all channel estimators. However, this is not a realistic scenario. In order to corroborate our theoretical findings and verify how harmful the imperfect channel estimation actually is, the presented numerical results considering asynchronous reception and non-orthogonal pilot sequences are analyzed in the sequel and compared to the ideal case.

4.3 Numerical results

All numerical results presented in this section aim to analyze and quantify the effect of imperfect channel estimation on the sum capacity optimization problem. In order to do so, a block fading channel model will be considered, where the channel coefficients remain static for a period of at least $T + 1$ symbols (MARZETTA; HOCHWALD, 1999). Indeed, results from channel estimation during N symbols can be fairly used on downlink transmission.

Basically two scenarios will be analyzed in this Section. Firstly, a potential market for CR technologies, which is the use of white spaces to offer reliable bandwidth to emergency and public safety communications (VILLARDI; ABREU; HARADA, 2012). In such scenario, there exists few users allocated around the city, but they need a reliable and constant link to communicate in case of an emergency. Secondly, a network with greater spatial diversity will be considered, which illustrates, for example, a sensor network with many sensors and one central multi antenna CR-BS.

Apart from considering two potential markets for CRN, this section will also analyze the effect of asynchronous transmitter, where the received pilot sequences at CR-BS arrive delayed and overlapped. A comparison between the classical LS and the adapted LMMSE for synchronous and asynchronous transmitter with two different pilot sequences sets, Walsh-Hadamard (W-H) and Gold codes will be employed to simulate the results in terms of sum capacity and capacity loss. For all synchronous cases, the Walsh-Hadamard code sequences have been used, once it was proved in (KOBAYASHI; ABRAO, 2017) to present the better perfor-

mance. However, for the asynchronous situation, W-H codes actually degrades the transmission. As a consequence, for all asynchronous CRNs scenarios simulations the Gold sequences were deployed.

Table 4.1 presents the main parameters and its reference values used to simulate both scenarios, here named *not crowded* and *sensor network*:

Table 4.1: Reference values for simulations

Parameters	**Not Crowded**	**Sensor Network**
SINR	$\gamma \in [-10, 20]$dB	$\gamma \in [-10, 20]$dB
SUs	$K = 4$	$K = 30$
PUs	$M = 1$	$M = 1$
CR-BS antennas	$n_{\text{BS}}6$	$n_{\text{BS}}40$
PU interference	$I_p = 0$dB	$I_p = 0$dB
Pilot sequence	$N = 64$	$N = 64$

4.3.1 White Spaces – Not Crowded Scenarios

The first simulation makes use of the ideal case with synchronous transmission and orthogonal pilot sequence. The chosen pilot sequence set is the W-H with $N = 64$ symbols for a configuration with $K = 4$, $M = 1$ and $n_{\text{BS}} = 6$ with varying uplink SINR (estimation). It is expected that higher uplink SINR scenarios lead to more accurate channel estimative; consequently, the precoder matrix is more efficiently designed and higher capacity is achieved. In order to analyze this effect, Fig. 4.4.a) presents the sum capacity for a MU-MISO CRN, where the channel estimation has been proceeded with LS or LMMSE methods. For this simulation, the capacity curves were averaged over 1000 Monte Carlo trials.

The perfect CSI case in Fig. 4.4 (blue solid line) consists of designing the precoder matrix $\mathbf{T}^*$ assuming $\widehat{\mathbf{H}} = \mathbf{H}$. As expected, a channel estimation in lower uplink SINR scenarios leads to poorer capacity for the downlink transmission. It is firstly observed that channel estimation causes a great decrease in the sum capacity. As expected, the lower uplink SINR is used, the poorer capacity. Usually, transmission systems seek to operate at high SINRs to estimate the channel, which imposes less interference and, consequently, a more accurate estimative.

The asynchronous case presented in Fig. 4.4.b) considers 10% delayed received signals and non-orthogonal pilot sequences. Comparison of both solid and dotted lines of Fig. 4.4.b) corroborates, as expected, de-synchronization and correlated sequences significantly negatively impact the sum capacity.

Figure 4.4: Sum capacity for different values of γ at the uplink channel estimation process for a MU-MISO CRN with $n_{\text{BS}} = 6, K = 4, M = 1$.

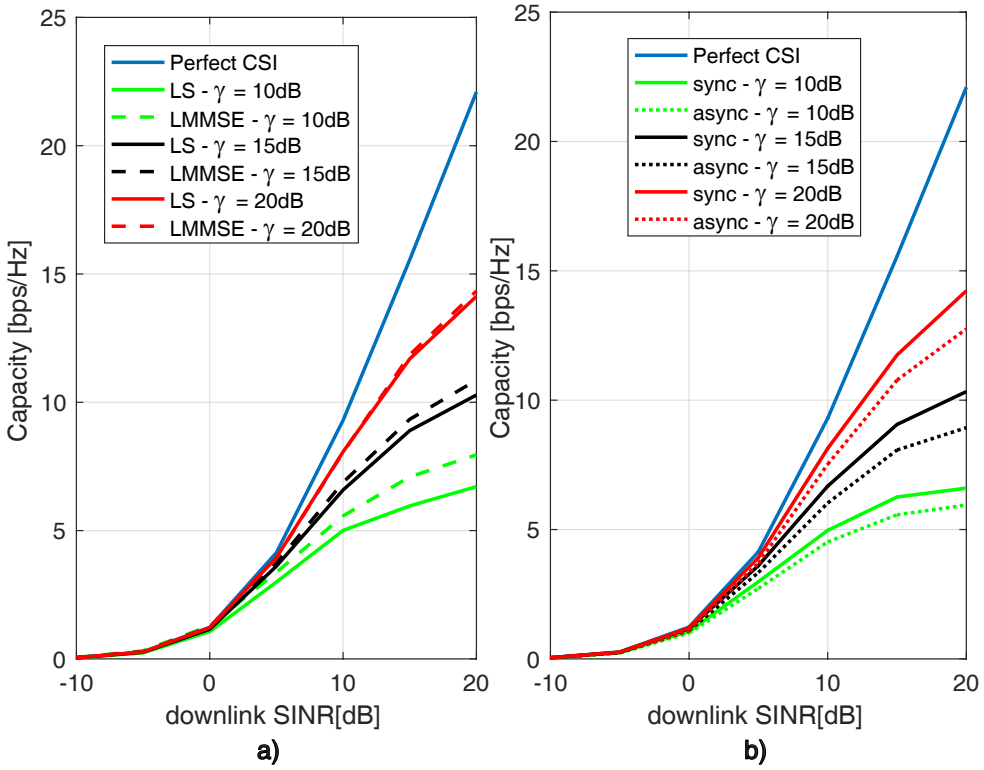

Figure 4.5: Capacity loss for different values of γ at the uplink channel estimation process for a MU-MISO CRN with $n_{\text{BS}} = 6, K = 4, M = 1$.

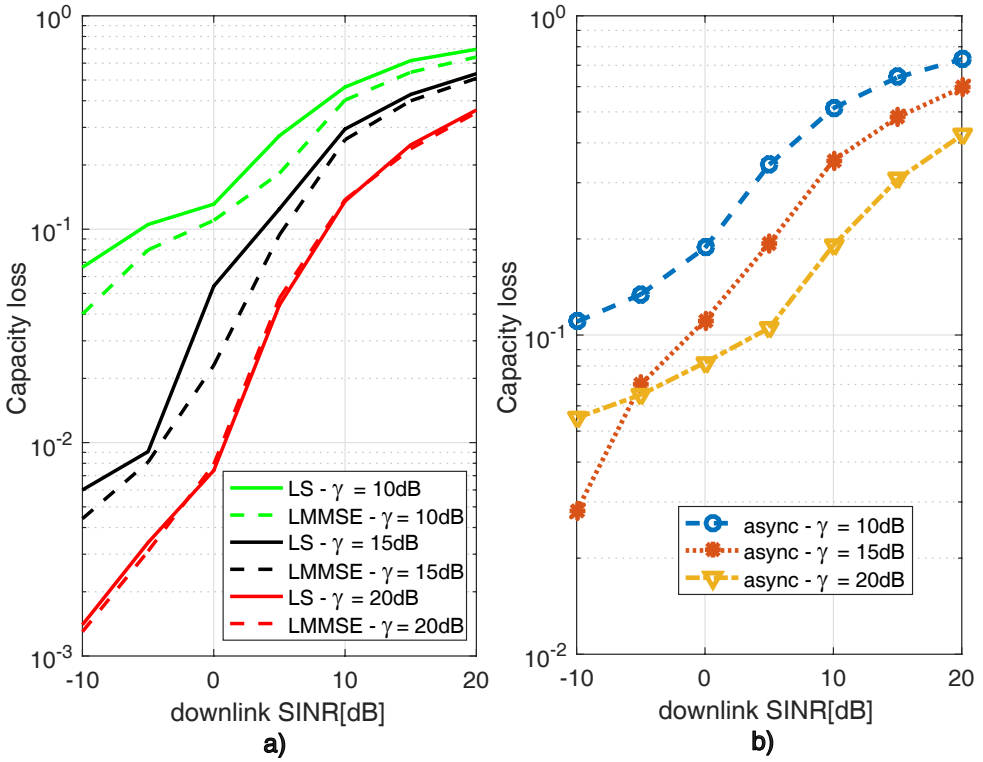

Considering the perfect CSI capacity as $\mathcal{C}$ and that capacity $\widehat{\mathcal{C}}$ achieved using precorders with imperfect channel estimations $\widehat{\mathbf{w}}$; hence, the *capacity loss* is expressed simply by:

$$\mathcal{L} = 1 - \frac{\widehat{\mathcal{C}}(\widehat{\gamma}, \widehat{\mathbf{G}}, \widehat{\mathbf{H}})}{\mathcal{C}(\gamma, \mathbf{G}, \mathbf{H})} \tag{4.23}$$

Fig. 4.5 expresses the capacity loss for every CRN system configuration previously analyzed. It is observed that, the more accurate channel estimator is used, the higher capacity is achieved (Fig. 4.4), and the lower capacity loss is resultant. However, once all cases with use of estimated channels limit the maximum system capacity, for high downlink SINR values the capacity loss increases significantly. Fig. 4.5.a) shoes that there is not a significant improvement from LS to LMMSE in therms of capacity loss. In addition, comparing the capacity losses in Figs. 4.5.a) and 4.5.b), one can conclude that for high quality SINR scenarios the de-synchronization does not poses great harm; however, it significantly impacts on the capacity loss when the CRN system operates under low SINR scenarios. Indeed, under low γ's the capacity losses in Fig. 4.5.b) are significant when compared with the synchronous case of Fig. 4.5.a).

Analysis of both figures shows that the uplink SINR imposes a capacity limit on downlink transmissions. In all cases, for higher downlink SINR values, the capacity loss increases significantly. Even though the estimation is done with $\gamma = 20$dB, the capacity loss overcomes 10%. This comes from the fact that, with perfect channel estimation, the precoder optimally allocates power for all users; however, LS and LMMSE estimators necessary imply in imperfect PU's and SU's channel matrix estimations, and consequently, they are not optimal.

Previous analyses of Figs. 4.4 and 4.5 prove that channel estimation poses a very important point on CRN, once it significantly impacts the results of precoder design; consequently, performance and capacity will also be affected. Once, in real scenarios, the synchronization is impossible to be achieved, transceivers and CR-BS must design robust precoders and decoders able to tackle with such unavoidable interference.

4.3.2 Sensor Network – Great Spatial Diversity

Similarly to previous results, in this subsection the effect of channel estimation under a few different circumstances will be analyzed, *i.e.,* under massive number of CR-BS antennas and a high number of SU's nodes. However, we will explore a greater diversity scenario, where the asynchronous transmission condition has

chances of lowering even more the sum capacity.

Firstly, from Fig. 4.6, it is observed that not only the overall DL capacity increases remarkably, but also the difference between the curves resultant from LS and LMMSE. Previously, both techniques had similar impact on sum capacity $\mathcal{C}$. However, in this scenario the LMMSE algorithm shows a significant decrease in capacity performance compared to LS estimator. Such LMSE difference in performance is even more pronounced for low SINR's.

Figure 4.6: Sum capacity for different values of γ at the uplink channel estimation process for a MU-MISO CRN with $n_{\text{BS}} = 40, K = 30, M = 1$.

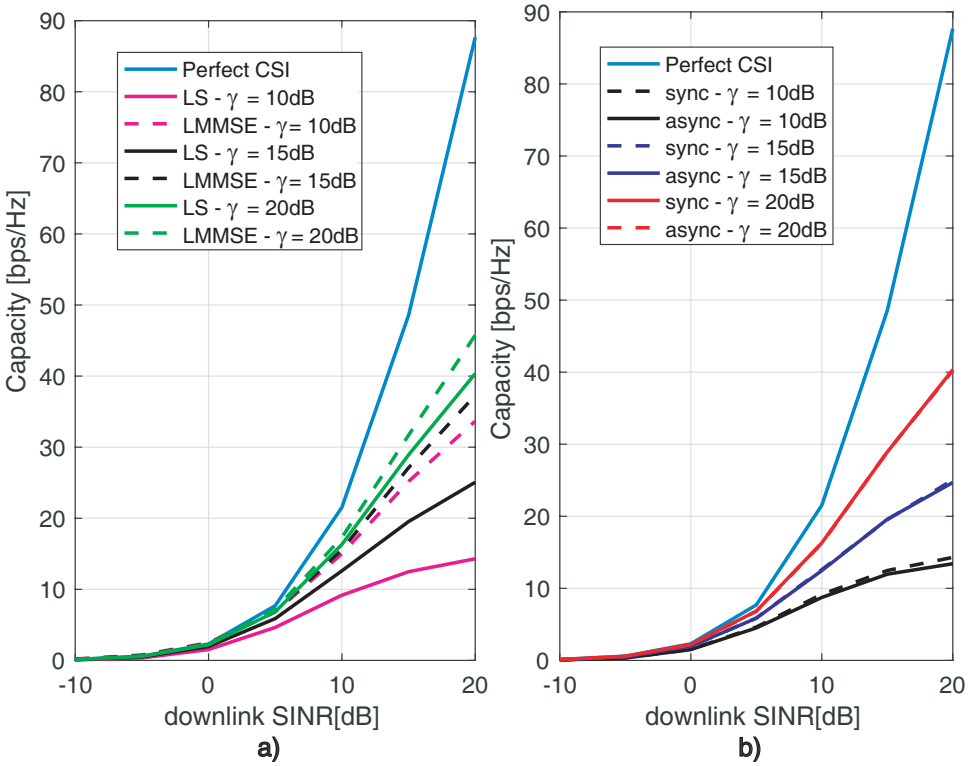

Also, observation of Fig. 4.7 reinforces that, for CRN systems with greater spatial diversity the use of Gold sequence sets, which has been proven to be better than W-H sets for asynchronous transmission system (KOBAYASHI; ABRAO, 2017), result in similar sum capacity for MU-MISO CRN. Simulations proved that, for this scenario configuration, the LMMSE has been presented better results in terms of sum capacity. As consequence, if only sum capacity is desired to be maximized, LMMSE showed to be the best option due its greater resultant sum capacity. Its However, the tradeoff capacity and complexity has to be analyzed, once the LMMSE algorithm needs some extra knowledge about pilot sequence and channel statistics if compared to LS technique.

Figure 4.7: Capacity loss for different values of γ at the uplink channel estimation process for a MU-MISO CRN with $n_{\text{BS}} = 40, K = 30, M = 1$.

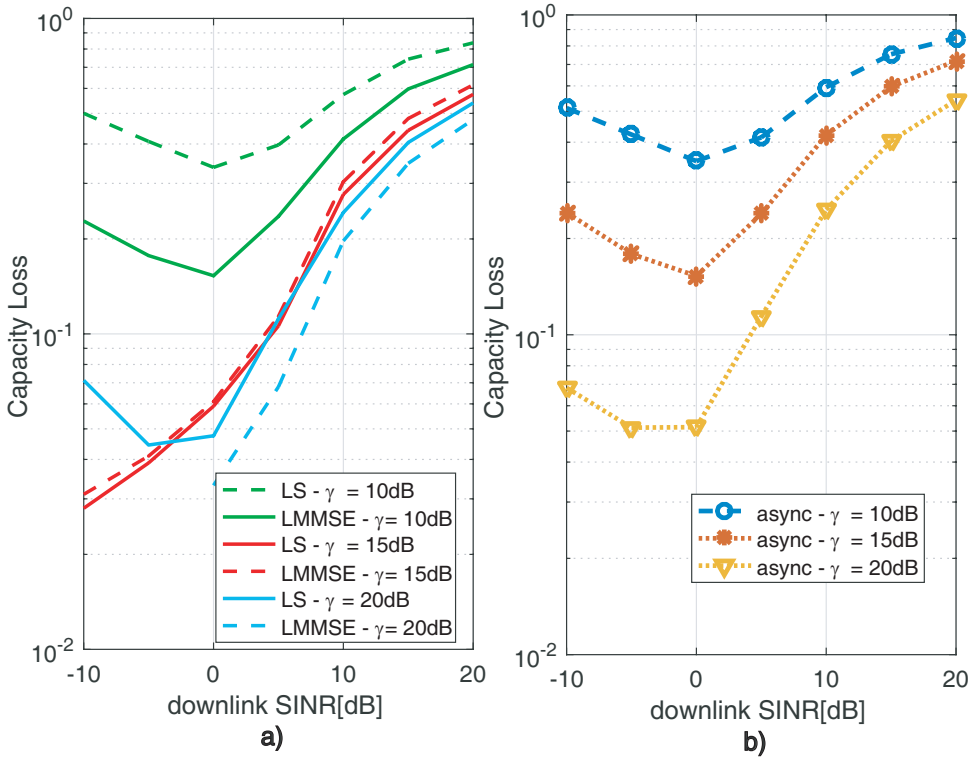

5 Conclusion

The first part of this Dissertation analyses the main single band spectrum sensing technologies. Many characteristics of all detectors are brought together and an up to date and detailed description of the state-of-art of SS in CRN is created. As observed during simulations, each sensor has a specific parameter that dramatically affects its performance. Results of Chapter 2 demonstrate the non-robustness of EnS for noisy environments, mainly because this sensor relies on the energy of a received signal. Results also demonstrated that MfS is the one which presents better performance between all studied detectors. However, knowledge of a pilot sequence is necessary, which is not always available. The comparison presented in Chapter 2 gives an overview about the detectors and opens possibility for a designer to analyze the one that most suits the application scenario.

Also in Chapter 2, a promising SS has been chosen to be applied into more complex scenarios. The HrS is a complex, but efficient likelihood-based spectrum sensor and deserves closer attention. Simulations showed that HrS is robust to multipath fading, once minimal degradation due to multiplicative effect of Rayleigh fading has been observed on performance figures. Additionally, even though a considerable difference between slow and fast fading scenarios, the results are still promising presenting high detection probabilities for low false alarm rates. The most interesting fact comes from observation of the necessary number of samples. For scenarios with $-3 \leq \gamma \leq 0$dB, HrS achieves $P_d \geq 0.95$ for $P_f = 0.1$ with a considerably low number of samples: $120 \leq N \leq 1024$.

The second area of this study consisted of an optimization technique to maximize sum capacity of a MISO-CRN. Chapter 3 presents a consistent mathematical description of the convexity analysis of SR in broadcast underlay MISO-CRN. This problem was sub-optimally solved via a classical interference zeroing technique known as Zero Forcing, which cancel both SU-PU and inter SUs interference and gives space for the optimal power allocation water filling algorithm. Another important achievement in this study was the linear dependence between k and n_{BS} to achieve maximum sum rate. Finally, an approximation to find the optimum

number of secondary users was obtained with $K^*(n_{\text{BS}}, \gamma)$.

A full duplex MISO-CRN wireless transmission has been studied in Chapter 4, where channel estimation are proceeded at the uplink in order to offer means for accurate precoding design at the downlink side. As observed, the precoder performance is directly related to the channel estimative accuracy; this makes a reliable channel estimation process indispensable for CR communications. Numerical simulation results demonstrated that the estimation process must be done under high values of uplink SINR in order to offer means for an accurate estimation. This is seen from the difference on capacity loss for cases with $\gamma = 10$dB and $\gamma = 20$dB, where the lower SINR case resulted over 20% of capacity loss.

The theory beyond LMMSE has been firstly adapted in such way to show that any cognitive device that wishes to make use of ZFWF precoder proposed in (CLAUDINO; ABRAO, 2017) must know primary and secondary pilot sequences and its statistics. This finding has been proved to happen when orthogonal code sequences and synchronous transmitters are deployed; However, numerical results proved that case with asynchronous transmitters and Gold sequence sets do not offer great deterioration on the sum capacity.

To sum up, this Master project has studied many different aspects of CRN. The SS research has showed some positive and negative points of each sensing technique, while the SR optimization has presented significant results and techniques to enhance the transmission of SUs. Finally, the impact of channel estimation error has been studied in order to show that accurate training process is essential to design optimum precoders.

Appendix A – Developed researches

This Appendix presents all publications related to this Master's research. A review of SS techniques was firstly published and gave space to a more complex analysis of SS techniques, which was published in a conference paper. The third publication is result of the studied non-linear optimization techniques applied to CRN in order to maximize the sum capacity of a MISO-CRN.

The following three sections present all published papers and developed works.

[A] Full paper - review: Claudino, L.; Abrão, T. Spectrum Sensing Methods for Cognitive Radio Networks - A Review. *Wireless Personal Communications*, v. 95, p.5003-50037, August 2017. ISSN 0929-6212.

[B] Conference paper: Claudino, L.; Kobayashi, R.; Abrão, T. Hadamard Ratio Sensor in Realistic CRN Scenarios. *XXXIV Simpósio Brasileiro de Telecomunicações e Processamento de Sinais*, Set. 2016.

[C] Conference paper: Kobayashi, R.; Claudino, L.; Hernandes,A.; Abrão, T. Multiband Spectrum Sensing via Edge Detection Using a Wavelet Approach. *XXXIV Simpósio Brasileiro de Telecomunicações e Processamento de Sinais*, Set. 2016.

[D] Full paper: Claudino, L.; Abrão, T. Efficient ZF-WF Strategy for Sum-Rate Maximization of MU-MISO Cognitive Radio Networks. *International Journal of Electronics and Communications*, v. 84, p.366-374, February 2018. ISSN 1434-8411.

[E] Full paper: Claudino, L.; Abrão, T. Linear MMSE Channel Estimation for Underlay Cognitive Radio Networks. *AeU - International Journal of Electronics and Communications* (submitted, Feb. 05th 2018).

A.1 Tutorial on Spectrum Sensing in Cognitive Radio Networks

Title:	*Spectrum Sensing Methods for Cognitive Radio Networks - A Review*
Authors:	Lucas Claudino and Taufik Abrão
Category:	*Tutorial*
Publication:	Published online in 21 April 2017
	Wireless Personal Communications
DOI:	10.1007/s11277-017-4143-1

Main contributions: this article is a great contribution to the cognitive radio state of art, once is tries to bring together the main spectrum sensing techniques and also compares them. Various performance metrics are used to evaluate the effectiveness of all detectors and to point out its strengths and weakness. This article not only presents various detectors, but also they are all extensively studied. Results of this article try to cover all parameters that can affect detector's performance and finally, the 3D surfaces give the reader an option to compactly understand each sensor.

Wireless Pers Commun (2017) 95:5003–5037
DOI 10.1007/s11277-017-4143-1

Spectrum Sensing Methods for Cognitive Radio Networks: A Review

Lucas Claudino[1] · **Taufik Abrão**[1]

Published online: 21 April 2017

Abstract The main spectrum sensing (SS) techniques suitable for cognitive radio networks (CRNs) such as energy, matched filter, covariance and Hadamard ratio-based detectors are analyzed. Principal methods and concepts associated with SS-CRNs are explored while numerical simulation experiments and comparison analysis are interpreted aiming to corroborate those concepts and demonstrate the effectiveness and drawbacks of those well-established SS-CRN techniques and methods.

Keywords Spectrum sensing · Cognitive radio network · Energy detector · Matched filter · Covariance detector · Hadamard ratio-based detector · Underlay CRN mode · Overlay CRN mode

1 Introduction

In order to optimize the spectrum utilization, cognitive radio (CR) principles establish for a secondary user (SU) a methodology of co-transmitting with primary users via either *spectrum hole access* or *low power transmission* over used frequencies. Spectrum hole is defined as an unused spectrum band that can be used by unlicensed user; spectrum holes are basic resource for cognitive radio systems. Most of existing contributions detect spectrum opportunities by sensing whether a primary signal is present or not and then try to access them so that CRs and primary users use the spectrum band either at different time

✉ Taufik Abrão
taufik@uel.br; abrao@ieee.org; taufik.abrao@gmail.com;
http://www.uel.br/pessoal/taufik

Lucas Claudino
lsclaudino@gmail.com

[1] Electrical Engineering Department, State University of Londrina (DEEL-UEL), Rod. Celso Garcia Cid - PR445, s/n, Campus Universitário, Po. Box 10.011, Londrina, PR 86057-970, Brazil

slots or in different geographic locations [43]. Specifically, a CR system has a high-level of environmental awareness so that it is able to recognize available band and to adapt its transmission (frequency, waveform and protocols) to achieve a better performance within a certain quality of service (QoS) [5, 42].

A CR has to constantly monitor the spectrum and look for opportunities either in bands or channels and investigate interference levels. This monitoring stage is not only important for CRs to detect white spaces in spectrum, but also to keep control of all interference which may harm any primary transmission [31].

Based on the above characteristics, cognitive radio operation is basically divided in three ways: underlay, overlay or hybrid modes. The underlay method for spectrum sharing allows the secondary user to transmit over all primary frequencies, as long as all interferences caused by this transmission do not harm the primary system's performance. In overlay approach, secondary users must use spectrum sensing (SS) techniques to detect unused frequencies; then, the unlicensed user access these frequencies to transmit its data without interfering PU's transmission. Additionally, hybrid CR mixes both underlay and overlay approaches. Spectrum sensing is also performed in hybrid access; however, when a PU is detected, underlay constraints for transmission power and interference levels are taken into consideration [9, 27, 33].

Figure 1 shows basic operation modes for a CR system. Basically, for every scenario, there will be N available channels to be sensed and shared between PUs and SUs. When transmitting with underlay access strategies, channel status is not required, but transmission power upper limits must be respected, so all interference levels are kept under a certain threshold over all transmission time. A SU transmission without SS is depicted in Fig. 1a, where unlicensed user is transmitting over all the time T without impinging interference to PU's signal. Differently, in overlay access mode, Fig. 1b, SU firstly divides the available time-slot T in a sensing part (τ) and a transmission part ($T - \tau$). Then, every channel is sensed; in case of absence of primary signals, SU is allowed to transmit with its full power; however, in case of presence of a PU, this channel must be left free to all

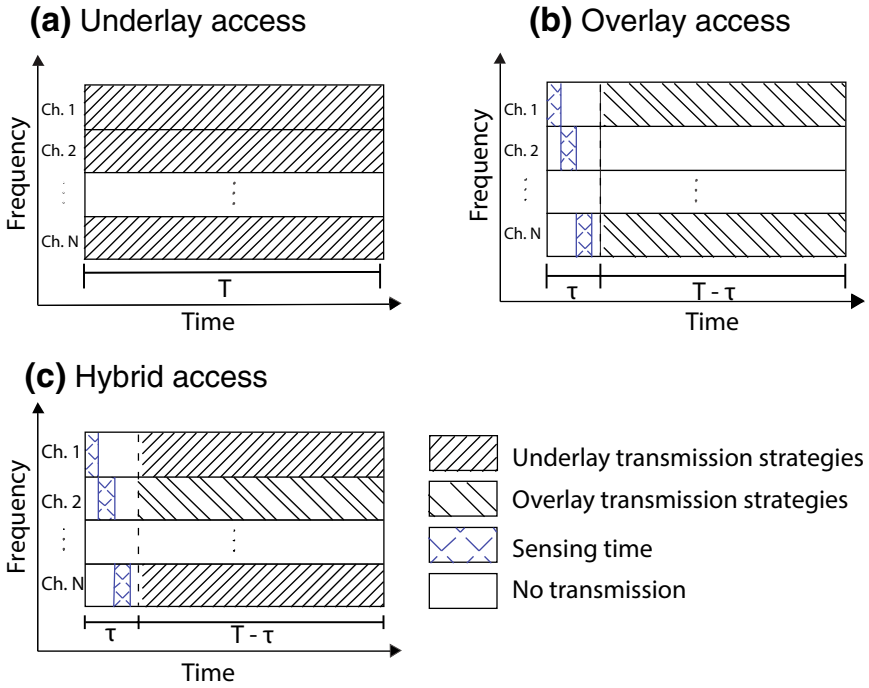

Fig. 1 Access strategies in cognitive radio networks

current primary transmissions. Finally, a hybrid access strategy mixes both underlay and overlay modes. The hybrid sensing is depicted in Fig. 1c, where SU also divides the available time into two parts, i.e., τ and $(T - \tau)$; when a PU is not detected in that specific channel, the secondary transmitter adapts its technique to transmit over the channel with a maximum power P_m that does not harm the licensed signal. In case of a free channel, full power is used for secondary transmissions.

A chronological perspective for representative spectrum sensing methods applied to CRNs is presented in Table 1. This is a sample for the state-of-art in SS-CRNs, covering from spectrum sensing detectors to capacity aspects, single-band and multi-band power spectral density (PSD) estimation scenarios, compressive sub-Nyquist sensing methods, as well as cooperative SS applied to CRNs.

This paper is divided as follows: Sect. 2 explains all basic access methods for CR, its characteristics and operation. Basic processes of spectrum sensing and how each access method uses them are shown in Sect. 3. Section 4 studies the four main methods for sensing primary signals. An important performance metric, namely SNR Wall, is explained and applied to SS-CR methods in Sect. 5. Finally, representative numerical results are analyzed in Sect. 6, whereas main conclusions and final remarks are offered in Sect. 7.

2 Access Methods for Cognitive Radio

As stated before, there are three basic ways a CR can operate: underlay, overlay and hybrid modes. The next subsections are devoted to explain each of them.

2.1 Underlay CR Networks

In underlay mode, the whole available spectrum is shared by primary and secondary users. From the primary user's point of view, any secondary signal is seen as a kind of interference. Hence, when measuring the primary's signal-to-interference plus noise ratio (SINR), the interference level must be less than a pre-determined value. This interference constraint means that total power of any secondary signal must respect a spectral mask bounded by the power spectral density (PSD) interference over all frequencies under the sensing band. Alternatively, for low variant interference constraints scenarios, the threshold might be simply set according to an average value of the PSD interference taken across all licensed frequencies [5].

Considering x_i as channel input for a secondary user instant i, y_i is the correspondent channel output at the primary user. Hence, the average interference power due to secondary users at primary receiver under underlay mode is limited by a threshold γ:

$$\frac{1}{n}\sum_{i=1}^{n}\mathbb{E}\left[|y_i|^2|x_i\right] \leq \gamma \tag{1}$$

where $\mathbb{E}[\cdot]$ is the expectation operator. Equation 1 means that the interference's average power is given by the conditional expectation function of all received interference at PU receiver in relation to transmitted secondary signal.

In order to quantize how harmful the interference is in a certain transmission, the Federal Communications Community (FCC) established a metric to measure interference caused by SUs in a primary transmission, named Interference Temperature (IT) [12], which is defined as:

Table 1 Contributions in spectrum sensing methods for CRNs

Year	References	Description
2004	[6]	Matched filtering, energy detection and cyclostationary feature detectors in CR are investigated; the goal is to evaluate the ability to sense the spectral environment and the flexibility to adapt transmission parameters aiming to maximize system capacity while coexisting with legacy wireless networks. Cyclostationary detection has advantages due to its ability to differentiate modulated signals, interference and noise in low SNRs
2006	[36]	Wideband spectrum sensing via wavelet transform (WT) approach is studied. WT is used to identify spectrum irregularities and characterize frequency bounds of each subband, and also estimate the spectrum mask, which defines used subbands and white spaces. The proposed PSD estimation scheme showed to be simple and efficient while is able to detect white spaces in wideband scenarios. However, when noise floor increases, multiscale product method is required to increase accuracy and consequently, computational complexity is also increased
2007	[21]	CR Capacity is defined when transmitter and receiver have different, but correlated, spectrum hole estimations. An analysis on the distributed and dynamic nature of CR channels is made aiming to evaluate all channel availability uncertainties. Using derived capacity expressions and results about the effect of correlation of spectral activity, the authors analyze how important is/isn't to add overhead of periodic feedforward and/or feedback about spectrum occupancy on secondary transmissions
2007	[37]	Authors propose a sub-Nyquist sampled compressed sensing technique based on wavelet edge detection. White space detection is performed by: (1) compressing random sub-Nyquist sampling of the spectrum, (2) linear PSD reconstruction via Basis Pursuit technique, (3) number and width of subbands and spectrum spaces; (4) estimation of the amplitude of each subband and classification in black, gray or white spaces. A technique to directly estimate each suband's characteristics (location, width and amplitude) directly from the compressed sampled data is proposed
2008	[28]	Overview about existing challenges and possible solutions for collaborative wideband SS in CR networks, including a SS techniques review and the main challenges, i.e., SS reliability and high-resolution requirement for wideband sensing. A methodology of combining SS of distributed nodes operating over narrowbands is proposed and two fusion schemes are analyzed: hard decision fusion and summary statistics combination. Also, a multiband joint detection is studied, where the wideband SS jointly optimizes a group of narrowband sensors. A few considerations on physical layer issues that emerge while designing a wideband CR network are made
2008	[8]	Security aspects os SS: this contribution investigates the effect of primary user emulation (PUE) attack, which is when a certain secondary user tries to copy PU's transmissions in order to confuse other SUs. Numerical results demonstrate how harmful this action is and quantizes its influence on SS. A solution called *LocDef* (location-based defense) is formulated to estimate location and other characteristics of the transmitted signal while identify whether it is a legitimate PU or not
2008	[14]	A SS methodology based on filter banks is proposed. Authors formulate a PSD estimation technique for multiband CR using filter banks and compare its performance with other former SS known as Thomson's multipaper method (MPM). Even though MTM has shown better performance and less signal's samples are needed, it has a very high computational burden. On the other hand, filter bank has presented very accurate results for higher number of samples and presents much lower computational complexity
2009	[29]	A technique to jointly detect PUs over multiple bands is proposed. Differently from other methods, authors formulate the SS problem as aggregate opportunistic throughput maximization problem and use the interference limit to PUs as a constraint of the main problem. Additionally, exploitation of spatial diversity is used to propose a cooperative wideband SS to enhance detection rates when single SUs are not able to reliably detect white spaces due to channel uncertainties (fading/shadowing).

Table 1 continued

Year	References	Description
2009	[18]	Multipaper method and cyclostationarity are investigated as strategies to enhance spectrum sensing. MPM is theoretically studied and proved, via numerical results, to be real-time computationally feasible, able to process multiband cases and present cyclostationarity features that provide effective white space detection. Additionally, it was proved that MPM may be formulated based on filter banks, which is a possible solution to reduce complexity while preserve high detection rates
2010	[3]	A joint cooperative multiband SS method to estimate the PSD at different locations is proposed. This joint estimation allows SUs to have an overview about white spaces at arbitrary locations, what may ease the spectrum management in CRNs. Indeed, CRs cooperatively estimate the PSD and locate positions of different transmitters. This architecture is useful in large CR areas, where an arbitrary PU signal does not reaches all SUs. Results showed that implementation of an online D-Lasso cooperation scheme stabilizes the PSD estimative over the entire network; as a consequece, each SU is able to obtain a reliable PSD estimation. The overhead for implementation of the D-Lasso procedure and its effect over the SU's capacity have not been considerered
2011	[40]	Challenges in wideband cooperative SS-CRNs are discussed. Given the wideband structure, compressive sensing is applied to reduce the necessary sampling rate. Collaborative SS among spatially distributed CRs is exploited in order to make use of spatial diversity principles. A decentralized decision algorithm is proposed to manage all individual CR's and obtain high performance with low computational complexity or power overhead. Simulations are proceeded for cases with and without channel knowledge
2012	[2]	Overview on CRN structure and principles is carried out. Basic theory of energy detection, feature detection, second order statistics-based, cyclostationarity-based, covariance-based, filter bank-based and blind detectors is explained and a few comparison points are enumerated. Authors also study wideband SS, compressive and cooperative sensing
2013	[32]	Analyses on various wideband SS methods, including Standard ADC (Analog-to-Digital Conversion), Sweep-tune/filter bank sampling, Compressive sensing and Multichannel sub-Nyquist sampling. Further discussion on the sub-Nyquist methods as a solution to attend all necessary sampling rates of wideband CR networks. Also, challenges of implementing feasible wideband SS for CR networks are addressed. All analysis aim to explain, categorize and compare wideband SS methods. No simulation or test results are provided to illustrate and quantify the comparisons
2014	[11]	A detection scheme based on reconstruction of power spectrum of sub-Nyquist sampled signals is proposed. Both sparse and non-sparse signals are considered as well as, for the case of sparse signal, blind and non-blind detection schemes. For each case, a minimal sampling rate and PSD reconstruction technique are proposed (for noise-free environments). Numerical results, in therms of reliable (or not) PSD reconstruction and ROC for each case are presented. Also, influence of SNR, number of samples and number of frames is analyzed for different cases. Results demonstrate that all sub-Nyquist PSD reconstruction proposed schemes are reliable solutions and have similar performance, under a certain limit of SNR, if compared to detectors implemented with Nyquist sampled signals
2015	[13]	Wideband multichannel SS methods via FFT or filter-bank-based methods for spectrum analysis are investigated under fine-grained spectrum analysis facilitating the optimal energy detection in practical scenarios (non-flat spectrum). Such sensing schemes can be tuned to the spectral characteristics of the target primary user signals, allowing simultaneous sensing of multiple target primary signals with low additional complexity. Model extension includes: specific scenario of detecting a reappearing PU during secondary transmission, as well as in SS scenarios where the frequency range of a primary user is unknown. The concept of *area under the receiver operating characteristics* (RoC) curve is introduced for evaluating the overall performance of the SS algorithms and scenarios

Table 1 continued

Year	References	Description
2016	[23]	Smart grids (SGs) require reliable, intelligent and energy/spectrum efficient communications network; indeed, SGs are a very promising scenario for CR technologies. CR should be able to provide reliable communication over all frequency bands available for SG. This paper provides an extensive discussion about SG architecture, communication network requirements and possible solutions/implementations of CR for this scenario. Additionally, a study of SS methods (energy detection, feature detection) and management architectures for SS is done. Authors also explain possible solutions to integrate CR and SG, summarize IEEE.802.22 standard and relate it to SG architectures. Also, a study on interference mitigation for CR-based SG is showed and possible solutions are proposed

$$T_I = \frac{P_I}{\kappa W} \tag{2}$$

where P_I is the average interfering power, W is the bandwidth and $\kappa = 1.38 \times 10^{-23}$ J/K is the Boltzmann's constant. Specially, if a system allows a certain interference limit T_L, SU is allowed to generate a maximum interference power of $\kappa W T_L$.

Section 3 discusses more specifically about how a CR system senses the interference temperature level and decides whether the transmission is within the acceptable limit or not.

2.2 Overlay CR Networks

The overlay CRN is a method where secondary users are known as opportunistic users. Unlicensed users are constantly monitoring the spectrum in order to detect any PU occupancy in frequency, space or time dimensions. Once a temporary white space is detected, SUs opportunistically communicate over it via orthogonal dimensions with minimum interference [5].

The main constraint of overlay CR protocols is that all unlicensed users must accurately detect a white space, otherwise its transmission power will harm the PU's signal. It means that the SU's spectrum sensing phase has to be able to always keep a very low miss-detection rate. These factors are well discussed in spectrum sensing techniques, once the user has to develop a reasonable method to correctly identify spectrum holes.

Another important factor is to identify the maximum capacity for an overlay transmission. Considering a network with one primary Tx–Rx pair and one secondary Tx–Rx pair; the capacity for each channel is dictated by the Shannon capacity equation. Thus, C_p is the primary user's Shannon capacity (for a transmission where SUs are in silent) and C_s is the associated SU's capacity, considering a transmission with silent primary user.

Now, supposing both primary and secondary users sharing the same spectrum bandwidth; each one has its own fraction of time for transmitting. Hence, α is the PU's transmission time. Indeed, primary channel's capacity is given by αC_p, whereas SU's capacity is given by $(1-\alpha)C_s$. Then, the rate region for this time sharing strategy is defined by the 2-tuple:

$$[R_p, R_s] = [\alpha C_p, (1-\alpha)C_s]$$

Expanding the system for K_p primary users and K_s secondary users ($K_p + K_s = K$), Shannon capacity for the i-th PU is C_i, while C_j is the j-th SU's capacity with associated

time slots α_i^p and α_j^s respectively. Furthermore, the capacity region is the union over all α_i^p and α_j^s:

$$\bigcup \{R_1 = \alpha_1 C_{p_1}, \ldots, R_{K_p} = \alpha_{K_p} C_{K_p}, \; R_{K_{p+1}} = \alpha_{s_1} C_{s_1}, \; R_K = \alpha_{sK_s} C_{sK_s}\} \tag{3}$$

where $\sum_{i=1}^{K_p} \alpha_{p_i} + \sum_{j=1}^{K_s} \alpha_{s_j} \leq 1$ guarantees the spectrum sharing between secondary and primary users.

3 Spectrum Sensing in CRNs: Basic Principles

Spectrum sensing is one of the necessary steps of cognitive radio networking. SS is responsible for analyzing the medium and giving an overview about the spectrum scenario, so the CR will be able to deploy these informations and adapt its techniques to co-transmit with a primary user. Hence, understanding how SS works will be very useful for a more accurate analysis of CR networks. Next, general spectrum sensing formulation in CRNs is explored [7].

The spectrum sensing is based on signal detection techniques, which can be simply stated by the following hypothesis test:

$$y(k) = \begin{cases} \eta(k) & : \mathrm{H}_0 \\ s(k) + \eta(k) & : \mathrm{H}_1 \end{cases} \tag{4}$$

where $y(k)$ is the sample to be analyzed at each instant k; $\eta(k)$ is additive noise and $s(k)$ is the transmitted signal. H_0 and H_1 are the two possible hypothesis: noise-only and signal-plus-noise. In a more developed and realistic form, it can be re-written considering fading and shadowing wireless channel effects, given by the complex random variable h:

$$y(k) = \begin{cases} \eta(k) & : \mathrm{H}_0 \\ h \cdot s(k) + \eta(k) & : \mathrm{H}_1 \end{cases} \tag{5}$$

Figure 2 depicts all four possible cases of signal detection:

1. Declaring H_0 when H_0 is true $(\mathrm{H}_0|\mathrm{H}_0)$
2. Declaring H_1 when H_1 is true $(\mathrm{H}_1|\mathrm{H}_1)$
3. Declaring H_0 when H_1 is true $(\mathrm{H}_0|\mathrm{H}_1)$
4. Declaring H_1 when H_0 is true $(\mathrm{H}_1|\mathrm{H}_0)$

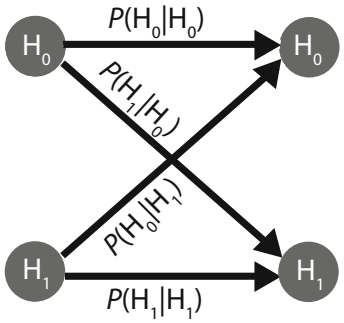

Fig. 2 Hypothesis tests and possible solutions for detection problems

Case 3 is known as the *missed detection*, while case 4 is the *false alarm*, and cases 1 and 2 are *correct detection*. Basically, a detector targets a high number of correct detections while keeping false alarm and the missed detection rates as low as possible.

3.1 SS in Underlay CR

A method of measuring the spectrum for cognitive underlaying mode is related to Sect. 2.1. In this technique, the CR device has to be able to select a bandwidth and a power level for transmitting its data without violating the interference temperature constraints. Hence, the goal is to monitor transmission power levels in order to keep them under a predefined limit and hence follow all interference temperature constraints [10]. Furthermore, the work in [10] explores spectrum sensing models for underlay CR networks leading with interference temperature.

3.2 SS in Overlay CR

According to Sect. 2.2, for overlay CR networks, the cognitive radio has to sense a white-space in the spectrum and then use it for a secondary transmission. Hence, the sensing systems must be able to do it without any help of the primary user, since in this work relying on cooperative networks has not been considered. Many different techniques for signal detection have been studies in CR context, i.e. energy detection (ED) sensing (EnS), coherent sensing, cyclostationary-based sensing, matched filter sensing (MfS) [5] [7], Hadamard ratio-based spectrum sensing (HrS) [20, 38], among others.

3.3 SS in Hybrid CR

Hybrid networks are a mix of underlay and overlay networks. Once SS is also necessary for hybrid networks, all SS techniques studied for overlay CR will also be applied to hybrid CR. The only difference is that, if no white space are detected, the CR transceiver may adapt its transmission strategies to remain within a certain interference limit (underlay CR mode).

4 Spectrum Sensing Methods

Correct detection of (un)occupied spectrum bands is extremely important in CR, once all secondary transmission strategies are based on outcomes of this stage. Indeed, SS must overcome all challenges and uncertainties like noise, channel effects and multipath fading [15]. Several methods can be used for sensing those white-spaces, such as energy detection (ED) sensing (EnS), coherent sensing (CS), cyclostationary-based sensing (CsS), matched filter sensing (MfS) [5, 7, 19], Hadamard ratio-based spectrum sensing (HrS) [20, 38], combined sensors like energy-based maximum likelihood [24] among others. Each one has its own characteristics, complexity and accuracy of detection. A brief comparison of basic sensors in terms of accuracy and complexity is depicted in Fig. 3.

In this section, the main methods commonly deployed to sensing CRNs are explained and analyzed in order to give theoretical base for results obtained in Sect. 6.

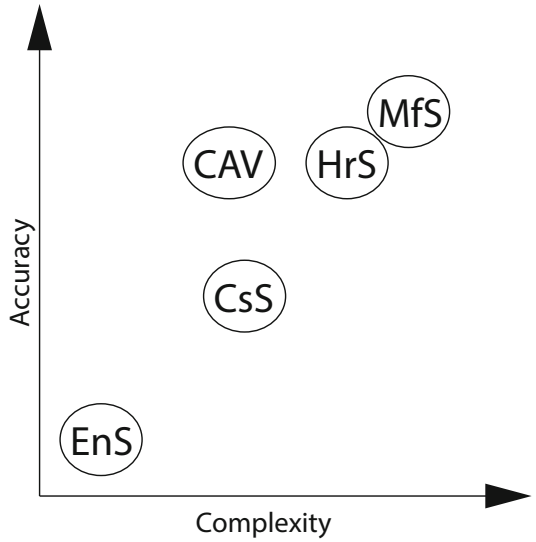

Fig. 3 Comparison of SS methods in therms of complexity × accuracy

4.1 Energy Detection Method

An Energy Detector has to basically measure the energy of all signals present on the medium and than compare it with a suitable threshold. The decision metric ξ_{ED} for this sensor is formulated as:

$$\xi_{\mathrm{ED}} = \frac{1}{N}\sum_{k=0}^{N-1} |y(k)|^2 \tag{6}$$

Or, using the definition of signal energy:

$$\xi_{\mathrm{ED}} = \int |y(t)|^2 dt, \tag{7}$$

where N is the total number of samples and $y(n)$ is the sampled received signal, as formulated in (5). Thus, the calculated signal energy is compared to a threshold γ_{ED} and finally hypothesis are chosen as H_0 if $\xi_{\mathrm{ED}} < \gamma_{\mathrm{ED}}$ and H_1 when $\xi_{\mathrm{ED}} \geq \gamma_{\mathrm{ED}}$ð.

Energy detector method is a very simple and easy to implement, if compared to other sensors; however, it may be very susceptible to noise floor, presence of interferences in the band, presence of frequency-selective fading and also its performance is very dependent on the sample rate.

Once the sensor has already estimated the decision metric ξ_{ED}, it has to compare it with an optimized threshold and evaluate if the transmission is within the interference levels or not.

The performance of a detector can be analyzed via probabilities of false alarm and missed detection. A simple model for ED without high noise effects is formulated in [5]. Indeed, the probability of false alarm (P_f) is given by:

$$\begin{aligned} P_f^{\mathrm{ED}} &= \mathbb{E}[\xi_{\mathrm{ED}}] P\left(\frac{1}{N}\sum_{n=0}^{N-1} |y_n|^2 > \gamma_{\mathrm{ED}} \;\middle|\; H_0 \right) \\ &= \mathbb{E}[\xi_{\mathrm{ED}}] P\left(\frac{2}{\sigma_y^2}\sum_{n=0}^{N-1} |y_n|^2 > \frac{2N\gamma_{\mathrm{ED}}}{\sigma_y^2} \;\middle|\; H_0 \right) \end{aligned} \tag{8}$$

where the random variable (r.v.) $\xi_{\mathrm{ED}} \sim \mathcal{N}_c(0, \sigma_\xi^2)$ and $P(\cdot|\cdot)$ is the conditional probability; consequently, the total sum in the conditional probability's argument results in a chi-squared distribution with $2N$ degrees of freedom.

Additionally, Eq. (8) can be re-written using a few notations:

$$P_f^{\mathrm{ED}} = Q(N, N\gamma_{\mathrm{ED}}/\sigma_y^2) \tag{9}$$

where $Q_(\cdot,\cdot)$ denotes the generalized Marcumm Q-function.

Similarly, the probability of detection is given by:

$$P_d^{\mathrm{ED}} = Q\left(\sqrt{\lambda}, \sqrt{2N\gamma_{\mathrm{ED}}/\sigma_y^2}\right), \tag{10}$$

where

$$\lambda \triangleq \frac{2}{\sigma_x^2} \sum_{n=0}^{N-1} |x_n|^2 \tag{11}$$

4.1.1 Energy Detection in AWGN Channels

There are three important measurements for a EnS model: probability of false alarm P_f^{ED}, probability of detection P_d^{ED} and threshold of detection γ_{ED}, defined as:

$$\gamma_{\mathrm{ED}} = Q^{-1}\left(P_f^{\mathrm{ED}}\right)\sigma_0^2 + \sigma_\eta^2 \tag{12}$$

$$P_f^{\mathrm{ED}} = Q\left(\frac{\gamma_{\mathrm{ED}} - \sigma_\eta^2}{\sigma_0^2}\right) \tag{13}$$

$$P_d^{\mathrm{ED}} = Q\left(\frac{\gamma_{\mathrm{ED}} - \mu_1}{\sigma_1^2}\right) \tag{14}$$

where $\sigma_0^2 = \dfrac{\sigma_\eta^2}{\sqrt{N}}$, $\mu_1 = \sigma_n^2(1 + \mathrm{SNR})$ and $\sigma_1^2 = \sigma_0^2\sqrt{2 \cdot \mathrm{SNR} + 1}$.

Majority of researches on energy detection in CR apply uniform sampling; however, random sampling was proved to be a good alternative to channel uncertainties and forbidden band restriction [30]. Herein, even though random sampling has been proven to enhance performance, it will be focused on using uniform sampling of signals due to ease on implementation and mathematical analysis.

4.2 Matched Filter Detection

In scenarios where there is a previous knowledge about some information of the primary users transmission, MfS can enhance the sensing process. Basically, a prior knowledge regarding some PU's information is needed, usually a pilot sequence. This received signal is then correlated with a pilot sequence at SU's receiver device and a channel status response is generated based on a certain preset threshold. An important point, which is considered in this work, is the formulation of a threshold level that maximizes probabilities of detection. Hence, the MfS uses this threshold value to decide between hypothesis H_0 and H_1.

In a continuous form, the statistical test comes from the correlation between received signal $y(t)$ and a replica of pilot sequence $x(t)$; hence, the signal to be compared with a threshold [26] is given by:

$$\widehat{s}(t) = \int_0^T x^*(t-\tau)y(\tau)d\tau \tag{15}$$

Or, in discrete time [7]:

$$\widehat{s}[n] = \sum_{k=1}^{N} x^*[n-k] \cdot y[k] \tag{16}$$

where $N = \frac{T}{T_s}$, with T_s being the sampling period and T the total sensing time.

Figure 4 shows an example of MF-based spectrum sensing signals to be compared with a threshold. In Fig. 4a PU's transmitted pilot pulse can be identified, while in Fig. 4b an usual replica of pilot pulse in the MF filter, which is a mirrored version of the transmitted pilot pulse. Graphic in Fig. 4c is a delayed version of this signal, while Fig. 4d is the received signal (pilot pulse plus the additive noise), typically at low SNR. After a convolution operation step, the MF output signal identified by plot in Fig. 4e shows a peak of energy, which is supposed to be at least the pilot signal replica's energy.

Indeed, MF's decision region is given by:

$$\text{Decidefor} = \begin{cases} \text{H}_0, & \text{if} \quad \widehat{\text{s}} < \gamma_{\text{MF}}, \\ \text{H}_1, & \text{if} \quad \widehat{\text{s}} \geq \gamma_{\text{MF}}. \end{cases} \tag{17}$$

where γ_{MF} is the threshold energy of detection in for MfS devices.

Furthermore, the probabilities of detection and false alarm for a MF spectrum sensing detector are given by [4, 26]:

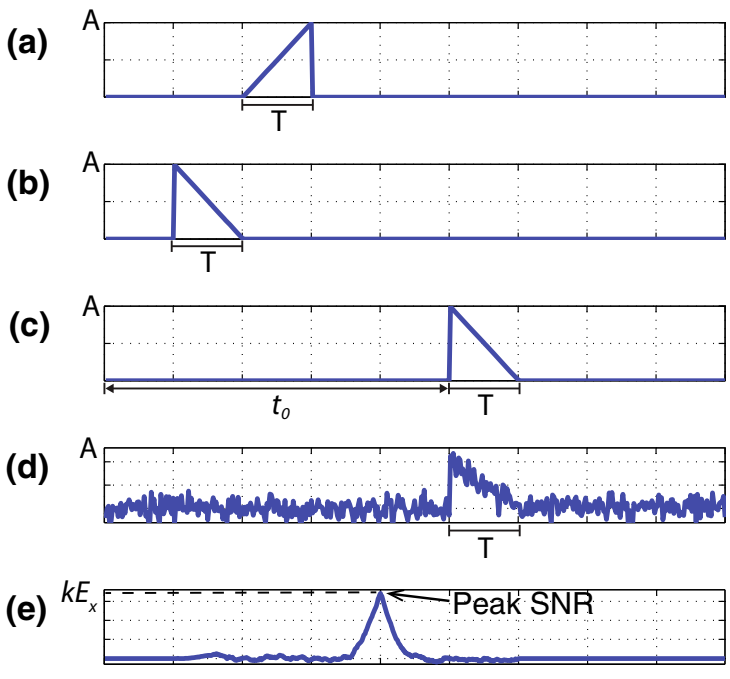

Fig. 4 Example of a MF detection signals

$$P_f^{\text{mf}} = P\{\widehat{s} > \gamma_{\text{MF}} | \text{H}_0\} = Q\left(\frac{\gamma_{\text{MF}}}{\sqrt{\varepsilon\sigma_\eta^2}}\right) \tag{18}$$

$$P_d^{\text{MF}} = P\{\widehat{s} > \gamma_{\text{MF}} | \text{H}_1\} = Q\left(\frac{\gamma_{\text{MF}} - \varepsilon}{\sqrt{\varepsilon\sigma_\eta^2}}\right) \tag{19}$$

where $\varepsilon = \sum_{k=1}^{N} x^2[k]$ and σ_η^2 is the additive noise's variance.

4.3 Covariance Absolute Value

The covariance absolute value (CAV) spectrum sensing detector is based on second order statistics of received signal samples. Considering L consecutive samples, the received signal, data and noise vectors can be defined, respectively, as:

$$\mathbf{y}(k) = [y(k) \quad y(k-1) \quad \cdots \quad y(k-L+1)]^T \tag{20}$$

$$\mathbf{s}(k) = [s(k) \quad s(k-1) \quad \cdots \quad s(k-L+1)]^T \tag{21}$$

$$\boldsymbol{\eta}(k) = [\eta(k) \quad \eta(k-1) \quad \cdots \quad \eta(k-L+1)]^T \tag{22}$$

where L is known as *smoothing factor* length. Additionally, received and transmitted signals covariance matrices are obtained as the expected values:

$$\mathbf{R}_y = \mathbb{E}\left[\mathbf{y}(k)\mathbf{y}^T(k)\right] \tag{23}$$

$$\mathbf{R}_s = \mathbb{E}\left[\mathbf{s}(k)\mathbf{s}^T(k)\right] \tag{24}$$

while the following equality holds:

$$\mathbf{R}_y = \mathbf{R}_s + \sigma_\eta^2 \mathbf{I}_L \tag{25}$$

If there is a signal, and its samples are sort of correlated, some of the off-diagonal elements of $\mathbf{R}_y$ are non-zero. In contrast, if the signal is absent, then $\mathbf{R}_s = 0$; hence, $\mathbf{R}_y$ has all the off-diagonal elements equals to zero. With this understanding, it is possible to create two tests aiming to define presence or absence of signal. Denoting r_{ij} as the ith row and jth column element of $\mathbf{R}_y$, the following test metric can be deployed:

$$T_1 = \frac{1}{L}\sum_{i=1}^{L}\sum_{j=1}^{L}|r_{ij}| \tag{26}$$

$$T_2 = \frac{1}{L}\sum_{\ell=1}^{L}|r_{\ell\ell}| = \frac{\text{tr}[\mathbf{R}_\text{y}]}{L} \tag{27}$$

where $\text{tr}[\cdot]$ is the trace matrix operator; indeed, T_1 metric has all the elements of $\mathbf{R}_y$, while T_2 presents only the diagonal ones. Thus, if there is no signal, the ratio $\frac{T_1}{T_2} = 1$. However, if the signal is present, $\frac{T_1}{T_2} > 1$.

In practice, N samples are received, but the system is usually limited to work with L samples. The covariance matrix $\mathbf{R}_y$ can be estimated via the sample covariance matrix:

$$\widehat{\mathbf{R}}_{\boldsymbol{y}} = \begin{bmatrix} \boldsymbol{\beta}(\boldsymbol{0}) & \boldsymbol{\beta}(\boldsymbol{1}) & \cdots & \boldsymbol{\beta}(\boldsymbol{L-1}) \\ \boldsymbol{\beta}(\boldsymbol{1}) & \boldsymbol{\beta}(\boldsymbol{0}) & \cdots & \boldsymbol{\beta}(\boldsymbol{L-2}) \\ \vdots & \vdots & \ddots & \vdots \\ \boldsymbol{\beta}(\boldsymbol{L-1}) & \boldsymbol{\beta}(\boldsymbol{L-2}) & \cdots & \boldsymbol{\beta}(\boldsymbol{0}) \end{bmatrix} \tag{28}$$

$$\text{where} \quad \beta(\ell) = \frac{1}{N}\sum_{n=0}^{N-1} y(n)y(n-\ell), \qquad \ell = 0, 1, \ldots, L-1 \tag{29}$$

Also, the statistics T_1 and T_2 can be adjusted according to $\widehat{\mathbf{R}}_y(N)$ [16]:

$$\widehat{T}_1 = \frac{1}{L}\sum_{i=1}^{L}\sum_{j=1}^{L} |\widehat{r}_{ij}| \tag{30}$$

$$\widehat{T}_2 = \frac{1}{L}\sum_{i=1}^{L} |\widehat{r}_{ii}| \tag{31}$$

where $\widehat{r}_{ij}$ is the ijth element of the sample covariance matrix, $\widehat{\mathbf{R}}_y$.

In order to analyze the efficiency of a CAV detector, probabilities of detection and false alarm have to be calculated [17, 41]:

$$\begin{aligned} P_f^{\text{CAV}} &= P\left(\frac{\widehat{T}_1}{\widehat{T}_2} > \gamma_{\text{CAV}} \middle| \text{H}_0\right) \\ &= 1 - Q\left(\frac{\frac{L-1}{\gamma_{\text{CAV}}}\sqrt{\frac{2}{N\pi}} - 1}{\sqrt{2/N}}\right) \end{aligned} \tag{32}$$

$$\begin{aligned} P_d^{\text{CAV}} &= P\left(\frac{\widehat{T}_1}{\widehat{T}_2} > \gamma_{\text{CAV}} \middle| \text{H}_1\right) \\ &= 1 - Q\left(\frac{\frac{1}{\gamma_{\text{CAV}}} + \frac{\Upsilon_L SNR}{\gamma_{\text{CAV}}(SNR+1)} - 1}{\sqrt{2/N}}\right) \end{aligned} \tag{33}$$

where Υ_L is the overall correlation strength:

$$\Upsilon_L \triangleq \frac{2}{L}\sum_{\ell=1}^{L-1}(L-\ell)|\alpha_\ell| \tag{34}$$

and the normalized form of (34), namely *normalized correlation coefficient*, is given by

$$\widehat{\Upsilon}_L = \frac{\Upsilon_L}{\sigma_s^2\sigma_\eta^2} \tag{35}$$

and

$$\alpha_\ell = \frac{\mathbb{E}[s(n)s(n-\ell)]}{\sigma_s^2} = \frac{R_s(\ell)}{\sigma_s^2} \tag{36}$$

Applying the inverse Q function, the value of the threshold γ_{CAV} is found based on an estimation of P_f^{CAV}:

$$\gamma_{\text{CAV}} = \frac{1 + (L-1)\sqrt{\frac{2}{N\pi}}}{1 - Q^{-1}(P_f^{\text{CAV}})\sqrt{2/N}} \tag{37}$$

4.4 Hadamard Ratio-Based Robust Spectrum Sensing

Hadamard ratio (HR) test is a robust method to provide signal detection in multivariate analysis which is able to deal with non-independent and identically distributed (IID) noise [20]. Recently, the HR test has been exploited for robust spectrum sensing in CR [38]. This subsection is devoted to analyze Hadamard ratio method for robust spectrum sensing purpose. By computing the first and second exact negative moments for the signal-presence hypothesis along with employing Beta distribution approximation, authors of [20] derived accurate analytical expression for detection probability, enabling to theoretically evaluate the detection behavior of the Hadamard ratio test. The analytic formula for the detection probability of the Hadamard ratio test derived in [20] allows us to theoretically evaluate the HrS performance.

Remembering that, according to (5), a received signal at instant k is $y(k)$, $s(k)$ is the transmitted symbol and $\eta(k)$ is a zero mean complex Gaussian noise. Aiming to decide between the two main hypothesis H_0 and H_1 the HrS detection method starts with a *general likelihood ratio test* (GLRT) derivation.

For this purpose, a MIMO (Multiple Input Multiple Output) CR network where the SU is equipped with n_R antennas has been considering sensing the data from n_T PUs; hence, a hypothesis test has to be adjusted in (5), where now the observation vectors are given by:

$$\mathbf{s}(k) = \begin{bmatrix} s_1(k) & s_2(k) & \cdots & s_{n_T}(k) \end{bmatrix}^T \tag{38}$$

$$\boldsymbol{\eta}(n) = \begin{bmatrix} \eta_1(k) & \eta_2(k) & \cdots & \eta_{n_R}(k) \end{bmatrix}^T \tag{39}$$

$$\mathbf{y}(k) = \begin{bmatrix} y_1(k) & y_2(k) & \cdots & y_{n_R}(k) \end{bmatrix}^T \tag{40}$$

while the channel matrix established between SU and PUs is denoted by $\mathbf{H} \in \mathbb{C}^{n_R \times n_T}$. Besides, we have assumed that elements of vector $\mathbf{s}(k)$ are Gaussian-distributed values with $s_i(k) \sim \mathcal{N}(0, \sigma_{s_i}^2)$, $i = 1, \ldots, n_T$ and $\eta_i(k) \sim \mathcal{N}(0, \sigma_{\eta_i}^2)$ for $i = 1, \ldots, n_R$. Indeed, the binary hypothesis can be re-written as:

$$\mathbf{y}(k) = \begin{cases} \boldsymbol{\eta}(k) & : \text{H}_0 \\ \mathbf{H}\mathbf{s}(k) + \boldsymbol{\eta}(k) & : \text{H}_1 \end{cases} \tag{41}$$

Assuming that the observation vector follows a Gaussian distribution $\mathbf{y}|H_i \sim \mathcal{N}\left(0, \Sigma^{(i)}\right)$, $i = 0, 1$, where $\Sigma^{(i)}$ is the covariance matrix. The covariance matrix under H_0 becomes $\Sigma^{(0)} = \text{diag}(\sigma_{v_1}, .., \sigma_{v_m})$, while under H_1 is given by $\Sigma^{(1)} \triangleq (\sigma_{ij})_{n_R \times n_R}$. According to these

assumptions, the likelihood function under a general hypothesis H_i is expressed by [20, 25]:

$$\mathbb{L}\left(\mathbf{Y}|\boldsymbol{\Sigma}^{(i)}\right) = \frac{1}{|\boldsymbol{\Sigma}^{(i)}|^N} \exp\left(-N \cdot \mathrm{tr}\left[\boldsymbol{\Sigma}^{(i)}\right]^{-1} \widehat{\boldsymbol{\Sigma}}\right) \tag{42}$$

Or even the log-likelihood function (LLF) of $\mathbf{Y}$:

$$\mathcal{L}\left(\mathbf{Y}|\boldsymbol{\Sigma}^{(i)}\right) = N \log\left|\boldsymbol{\Sigma}^{(i)}\right| + N \cdot \mathrm{tr}\left(\left[\boldsymbol{\Sigma}^{(i)}\right]^{-} \widehat{\boldsymbol{\Sigma}}\right) \tag{43}$$

where $\widehat{\boldsymbol{\Sigma}} = \frac{1}{N}\mathbf{Y}\mathbf{Y}^{\boldsymbol{H}}$ is the sample covariance matrix and $\mathbf{Y} = [\mathbf{y}_1, \ldots, \mathbf{y}_N]$ with N being the number of samples. Note that, under hypothesis H_0, $\widehat{\Sigma}^{(0)} = \mathrm{diag}(\widehat{\boldsymbol{\Sigma}})$, and under H_1 becomes $\widehat{\Sigma}^{(1)} = \widehat{\boldsymbol{\Sigma}}$. Moreover, the GLRT, which takes into account the relationship between probabilities of the two hypothesis, is computed and compared it with a preset threshold in order to determine presence or absence of a PU, which is expressed by:

$$\frac{\mathcal{L}\left(\mathbf{Y}|\Sigma^{(0)}\right)}{\mathcal{L}\left(\mathbf{Y}|\Sigma^{(1)}\right)} \tag{44}$$

The Hadamard Ratio is now obtained substituting (43) into (44):

$$\xi_{\mathrm{HR}} = \frac{\left|\widehat{\Sigma}^{(1)}\right|}{\left|\widehat{\Sigma}^{(0)}\right|} \underset{\mathrm{H}_1}{\overset{\mathrm{H}_0}{\gtrless}} \gamma_{\mathrm{HR}} \tag{45}$$

The exact distribution for this GLRT may assume complex values; however, its moments can be easily expressed. Also, values for GLRT are always between 0 and 1, what allows us to adopt a Beta distribution to approximate the test probabilities [25]. For this solution, a moment determination for ξ_{HR} is needed. Indeed, first and second exact negative moments are computed and detection probability is obtained by matching these moments with the Beta distribution ones. Hence, let's firstly define the PDF of a Beta distribution with parameters α and β [39]:

$$f_Z(\theta) \simeq \begin{cases} \dfrac{\theta^{\alpha-1}(1-\theta)^{\beta-1}}{B(\alpha,\beta)}, & 0 \le \theta \le 1 \\ 0, & \text{otherwise} \end{cases} \tag{46}$$

where $B(\alpha,\beta) = \dfrac{\Gamma(\alpha)\Gamma(\beta)}{\Gamma(\alpha+\beta)}$ is the Beta Function.

Given the k-th negative moment of a random variable Z defined as $\mathcal{M}_{-k} \triangleq \mathbb{E}[Z^{-k}]$, the first two negative moments of a Beta-distributed r.v. are defined as [22]:

$$\mathcal{M}_{-1} = \frac{\alpha+\beta-1}{\alpha-1} \tag{47}$$

$$\mathcal{M}_{-2} = \frac{(\alpha+\beta-1)(\alpha+\beta-2)}{(\alpha-1)(\alpha-2)} \tag{48}$$

Now, solving (47) and (48) for α and β:

$$\alpha = \frac{\mathcal{M}_{-1} - \frac{2\mathcal{M}_{-2}}{\mathcal{M}_{-1}} + 1}{\mathcal{M}_{-1} - \frac{\mathcal{M}_{-2}}{\mathcal{M}_{-1}}} \tag{49}$$

$$\beta = (1 - \mathcal{M}_{-1})(1 - \alpha) \tag{50}$$

$$F(x) = \frac{1}{B(\alpha, \beta)} \int_0^x \theta^{\alpha-1}(1-\theta)^{\beta-1} d\theta = \frac{B_x(\alpha, \beta)}{B(\alpha, \beta)} \tag{51}$$

where $B_x(\alpha, \beta) = \int_0^x \theta^{\alpha-1}(1-\theta)^{\beta-1} d\theta$ is the incomplete Beta function.

Hence, whenever the moments of the test statistic in (45) be matched to the ones of the Beta distribution, the behaviour of ξ_{HR} can be then be approximated by the Beta distribution, as discussed in [20].

Finally, probability of detection for a Hadamard ratio-based spectrum sensor is expressed as:

$$P_d^{\mathrm{HR}} \triangleq P(\xi_{\mathrm{HR}} < \gamma_{\mathrm{HR}} | \mathrm{H}_1) = F(\gamma_{\mathrm{HR}}) \tag{52}$$

The next step is to define the probability of false alarm for the Hadamard Ratio-based sensor. For this case, [25] studies the first two positive moments of (45) and proceeds similarly to the abode mathematical methods. For this case, the two variables α_2 and β_2 are given as a function of two positive moments of a beta distributed random variable:

$$\alpha_2 = \frac{\mathcal{M}_1(\mathcal{M}_2 - \mathcal{M}_1)}{\mathcal{M}_1^2 - \mathcal{M}_2} \tag{53}$$

$$\beta_2 = \frac{(1 - \mathcal{M}_1)(\mathcal{M}_2 - \mathcal{M}_1)}{\mathcal{M}_1^2 - \mathcal{M}_2} \tag{54}$$

Indeed, given the definition of a probability of false alarm $P_{FA} \triangleq \Pr\{\xi_{\mathrm{HR}} < \gamma_{\mathrm{HR}} | \mathrm{H}_0\}$ and using (46), we have:

$$\begin{aligned} P_{FA} &\simeq \int_0^{\gamma_{\mathrm{HR}}} \frac{1}{B(\alpha_2, \beta_2)} t^{\alpha_2 - 1}(1-t)^{\beta_2 - 1} dt \\ &= \tilde{B}(\alpha_2, \beta_2, \gamma_{\mathrm{HR}}) = \frac{B_\gamma(\alpha_2, \beta_2)}{B(\alpha_2, \beta_2)} \end{aligned} \tag{55}$$

5 Performance Metric: SNR Walls

In order to properly sense a frequency channel, the sensor has to lead with a tradeoff between prior knowledge of the signal, sensibility and computational complexity [35]. In CR, system performance is usually evaluated via *receiver operating characteristics* (ROC) analysis, which plots the dependency between probability of detection and false alarm. Real-world scenarios need the highest P_d possible for a given P_f (usually $P_f = 0.1$). Figure 5 shows a region that every CR sensor should target. Moreover, [1] and [35]

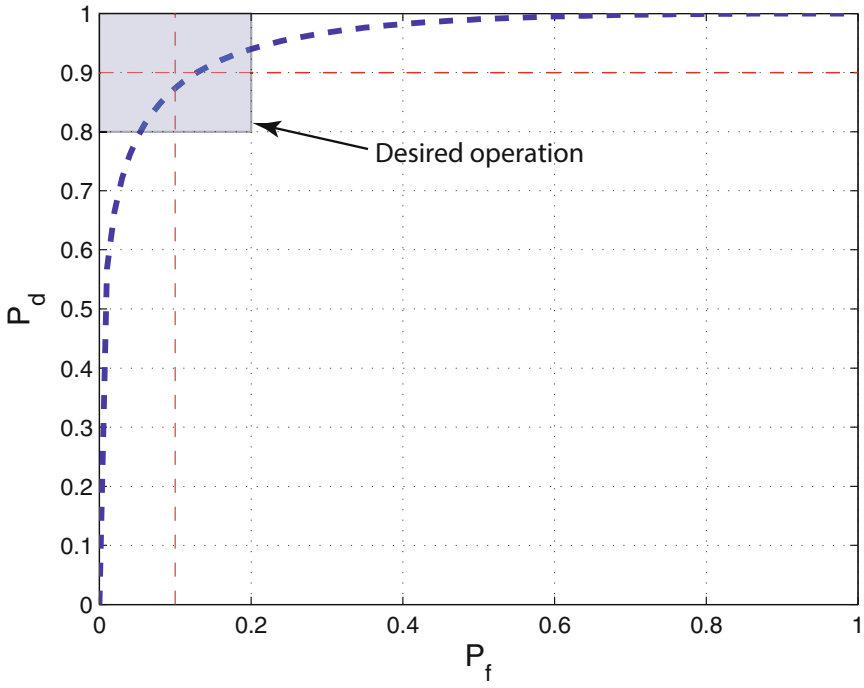

Fig. 5 Desired operation for a CR sensor

analyze a few ways of increasing performance in CR sensing; however, due to real case uncertainties, a new effect turns in when looking at the sample complexity. At some limit point, the "sample complexity blows up to infinity as the detector sensitivity approaches certain critical values" [1]. This phenomenon is known as *SNR Wall*. Figure 6 illustrates a generic sensor with a SNR wall located at −46 dB; the black dashed line indicates how this sensor should hypothetically behave.[1] Figure 6 also leads to an interpretation that a sensor with SNR wall is non-robust to noise, once it needs an infinity number of samples to achieve a desirable performance for SNRs below the wall.

It is also possible to quantize this sample complexity by isolating the number of samples in function of the usual variables of a CR spectrum sensing, including P_f, P_d, SNR and σ_η. Herein, we are going to apply the SNR wall metric for EnS, MfS and CAV; however, the Hadamard Ratio sensor, as seen in Sect. 4.4, does not have a closed expression for P_d and P_f as a function of the number of samples, which precludes us to plot it together with the other spectrum sensors.

5.1 SNR Wall for EnS

Given probabilities (13) and (14), the goal is to eliminate γ_{ED} and find the value for N. Authors in [35] also insert a factor $\rho = 10^{x/10}$, which quantifies the level of uncertainty in the noise power, scaling σ_η in an interval $[\sigma_\eta/\rho,\ \rho\sigma_\eta]$, where noise variance is allowed to have x dB of uncertainty. The uncertainty modeling of a noise is used to give an idea of approximated Gaussian noise (and not a precise one). The approximation consists in distributing the White noise (η_a) moments over a closed interval $\mathbb{E}\left[\eta_a^{2i}\right] \in \left[\frac{1}{\rho^i}\mathbb{E}\left[\eta^{2i}\right],\ \rho^i\mathbb{E}\left[\eta^{2i}\right]\right],\ \forall i = 1, 2, \ldots,$ with $\eta \sim \mathcal{N}(0, \sigma_\eta^2)$, such approximated

[1] In terms of linear dependence of the number of samples (log scale) increasing with the SNR (in dB) decreasing.

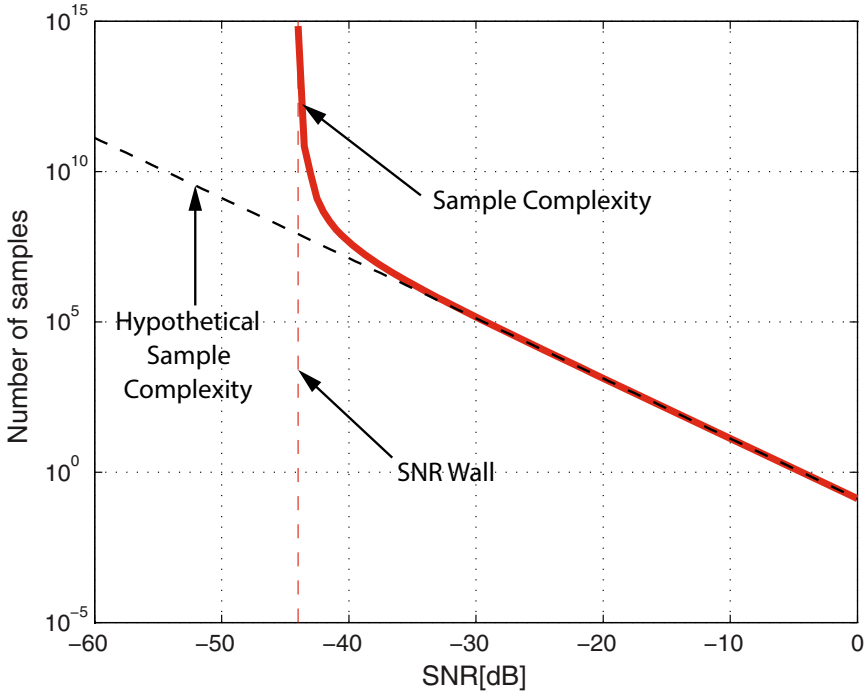

Fig. 6 SNR Wall characteristics

moments are close enough to nominal moments.[2] Hence, the following modified version of the probabilities emerge from this approximation:

$$P_f^{\mathrm{ED}} = Q\left(\frac{\gamma_{\mathrm{ED}} - \rho\sigma_\eta^2}{\sqrt{\frac{2}{N}}\rho\sigma_\eta^2}\right) \tag{56}$$

$$P_d^{\mathrm{ED}} = Q\left(\frac{\gamma_{\mathrm{ED}} - (SNR + \sigma_\eta^2/\rho)}{\sqrt{\frac{2}{N} - (SNR + \sigma_\eta^2/\rho)}}\right) \tag{57}$$

From (56), $\gamma_{\mathrm{ED}} = \rho\sigma_\eta\left(1 + \sqrt{2/N}Q^{-1}(P_f^{\mathrm{ED}})\right)$, and from the false alarm probability Eq. (57), $\gamma_{\mathrm{ED}} = \left(P + \sigma_\eta^2/\rho\right)\left(1 + Q^{-1}(P_d^{\mathrm{ED}}\sqrt{2/N})\right)$.

Eliminating γ_{ED}, by assuming that in the interest region $(1 + SNR) \approx 1$, we finally get the *Sample Complexity* for an Energy Detector:

$$N^{\mathrm{ED}} = \frac{2\left[Q^{-1}(P_f^{\mathrm{ED}}) - Q^{-1}(P_d^{\mathrm{ED}})\right]^2}{\left[SNR - \left(\frac{\rho^2 - 1}{\rho^2}\right)\right]^2} \tag{58}$$

which grows with the inverse of SNR. Notice that the denominator of (58) is fixed; however, at some point it goes to zero (depending on SNR and ρ values) and the number of

[2] For a better detailed description of the noise model and uncertainty models used in this work, please refer to [35].

samples tends to infinity. This simple mathematical analysis shows that, for SNR values around and below this discontinuity the EnS is unrealizable.

In order to find the exact point of discontinuity, we have to set the denominator of (58) to zero:

$$\left[SNR - \left(\frac{\rho^2 - 1}{\rho^2}\right)\right]^2 = 0 \qquad \Rightarrow \qquad \therefore \quad \mathrm{SNR}_{\mathrm{wall}}^{\mathrm{ED}} = \frac{\rho^2 - 1}{\rho^2} \tag{59}$$

5.2 SNR Wall for MfS

Similar to Sect. 5.1, a formula relating sample complexity and usual parameters is obtained for a matched filter-based CR sensor. In this case, one more parameter may influence the necessary number of samples, which is the percentage (θ) of total power present in the pilot tone. It is worth noting that SNR wall is an effect related to real world scenarios; hence, [35] suggests that, in many cases, PU's signal is multiplexed in time, what strongly limits the coherence time. Also, [34] says that MfS should be divided in coherence blocks, each one with N_c samples. So, when analyzing the sample complexity of a MfS, it is fair enough to divide it into two steps: firstly the signal is coherently sensed within each coherence time (it keeps the noise uncertainty and boosts signal power by N_c). Secondly, the boosted signal is detected via an Energy sensor.

A modification of (58) comes from the addition of variables θ representing the fraction of pilot tone power and N_c corresponding to the influence of coherence time:

$$N^{\mathrm{MF}} = \frac{2N_c\left[Q^{-1}(P_f^{\mathrm{ED}}) - Q^{-1}(P_d^{\mathrm{ED}})\right]^2}{\left[\theta \cdot N_c \cdot SNR - \left(\frac{\rho^2 - 1}{\rho^2}\right)\right]^2} \tag{60}$$

A simple analysis of MfS states the "Energy Sensor" part still non-robust to noise uncertainty; however, the coherent part boosts performance by a factor of $N_c \cdot \theta$, where $\{\theta \in \mathbb{R} | 0 \leq \theta \leq 1\}$ is a fraction of the pilot tone's total power. Similarly to the EnS case, (60) also has a discontinuity where the number of samples tends to infinity, but this value is also dependent on N_c and θ. This dependence shifts the limit SNR to the left, meaning an improvement of MfS detector performance regarding the ED.

To find the exact point of discontinuity, the denominator of (60) has been set to zero:

$$\left[\theta N_c SNR - \left(\frac{\rho^2 - 1}{\rho^2}\right)\right]^2 = 0 \qquad \Rightarrow \qquad \therefore \quad \mathrm{SNR}_{\mathrm{wall}}^{\mathrm{MF}} = \frac{\rho^2 - 1}{\theta \mathrm{N_c} \rho^2} \tag{61}$$

5.3 SNR Wall for CAV

For the covariance absolute value spectrum sensing detector, probabilities of detection and false alarm are given by (33) and (32), respectively. Firstly, isolating γ_{CAV} in both equations:

$$\gamma_{\mathrm{CAV}} = \frac{1 + (L-1)\sqrt{\frac{2}{N\pi}}}{1 - Q^{-1}\left(P_f^{\mathrm{CAV}}\right)\sqrt{2/N}} \tag{62}$$

$$\gamma_{\text{CAV}} = \frac{1 + \dfrac{\Upsilon_L SNR}{1 + SNR}}{1 + \sqrt{2/N} Q^{-1}\left(1 - P_d^{\text{CAV}}\right)} \tag{63}$$

Now, both equations are combines and a closed expression for sample complexity of a CAV spectrum sensor is obtained:

$$N^{\text{CAV}} = \frac{2\phi^2}{\left(\delta - \sqrt{\delta^2 - 2\Delta \cdot \phi}\right)^2} \tag{64}$$

where:

$$\begin{aligned} \delta =& Q^{-1}\left(1 - P_d^{\text{CAV}}\right) + \frac{(L-1)}{\sqrt{\pi}} + Q^{-1}(P_f)\left[1 + \frac{\Upsilon_L SNR}{1 + SNR}\right] \\ \phi =& \frac{2(L-1)}{\sqrt{\pi}} Q^{-1}\left(1 - P_d^{\text{CAV}}\right) \qquad \text{and} \qquad \Delta = -\frac{\Upsilon_{\text{L}} \text{SNR}}{1 + \text{SNR}} \end{aligned}$$

The exact point of discontinuity is obtained when the denominator of (64) is set to zero:

$$\begin{aligned} &\left(\delta - \sqrt{\delta^2 - 2\Delta\phi}\right)^2 = 0 \qquad \Rightarrow \qquad \therefore \quad 2\Delta\phi = 0 \\ &2\left(\frac{\Upsilon_L SNR}{1 + SNR}\right) \cdot \left(\frac{1(L-1)}{\sqrt{\pi}} Q^{-1}(1 - P_d)\right) = 0 \end{aligned} \tag{65}$$

There are two possibilities for the denominator to be set to zero: a) $L = 1$; b) $\Upsilon_L = 0$. This shows that, for fixed and valid values of L and Υ_L, the sample complexity for a CAV detector will not present a discontinuity point in terms of SNR.

Authors of [35] and [34] extended their investigation on SNR wall optimization in and showed that, for flat fading channels,[3] feature detectors are robust to noise uncertainty and don't have a SNR wall.

It is worth noting that Eq. (64) is proposed herein for first time; the numerical results discussed in Sect. 6.5 demonstrate accuracy with the above analysis, once there is no abrupt asymptotic behavior in sample complexity. This means that for our case of study, the CAV does not present a SNR wall.

6 Numerical Results

This section firstly brings an individual analysis for representative spectrum sensing detection schemes. Performance versus complexity analysis is carried out starting with ROC graphics, i.e. detection × false alarm probabilities, as well as detection probability × threshold, considering specific AWGN scenarios. The advantages and disadvantages or each one method have been highlighted. For every realization, a zero-mean Gaussian distributed data sequence is generated and its variance is chosen to be σ_x^2. In order to simulate a simple channel, AWGN is added to transmitted data sequence and then all analysis are evaluated using the received signal.

[3] The channel scenario case studied herein for the CAV detector.

Additionally, as more realistic representation of real world scenarios, multipath Rayleigh channels have been introduced and SS detection schemes such as HrS and EnS are compared in term of ROC and computational complexity.

Firstly, individual results for each sensor are comprehensively discussed. Subsequently, a broad comparison with all sensor is done under AWGN effect. Finally, HrS and EnS are analysed and compared considering more realistic Rayleigh channels.

6.1 Energy Detector

Detection probability dependence is given by Eq. (14). Indeed, the most significant parameters are threshold and SNR. Figure 7 shows that SNR is an extremely important factor, once for lower SNR values the probability of detection reaches 1 only when P_f^{ED} is close to 1. Therefore, higher system effectiveness is achieved for better values of SNR, because for low P_f the detector has already achieved $P_d^{\mathrm{ED}} \approx 1$.

Equation (14) firstly shows that somehow the threshold affects probabilities of detection and false alarm. A basic understanding is that μ_1 and σ_1^2 are constants dependent on noise and γ_{ED} is varying; hence, as γ_{ED} increases, P_d^{ED} decreases. The relationship on these variables is depicted in Fig. 8. Therefore, a correct threshold is set based on test statistics and correct estimation of the SNR. From this graph, it is observed that if the threshold is too high and transmitted signals have not enough energy to overcome this value, the spectrum sensor will identify every signal as a noise; consequently, the channel will always be sensed as idle.

Variation of P_d^{ED} according to values of SNR is shown in Fig. 9. For this simulation a target $P_f^{\mathrm{ED}} = 0.1$ has been set in order to find an adequate value for γ_{ED} and assumed a sensing period with $N = 2000$ samples. Threshold levels for EnS are directly related to noise variance and consequently the actual SNR value. Indeed, each SNR value sets a γ_{ED} aiming to establish a suitable detection probability for the system. Also, under the system

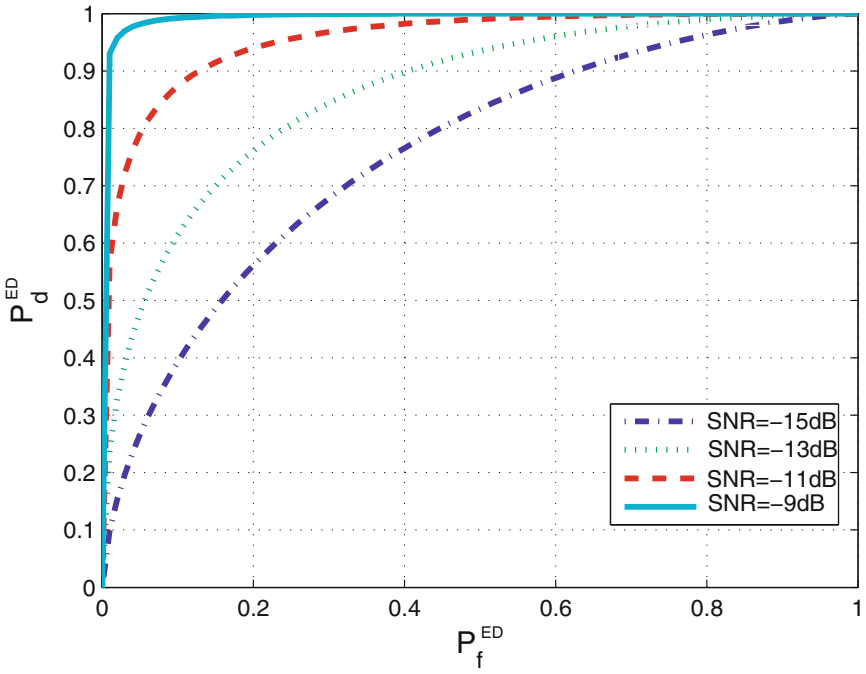

Fig. 7 ROC for an Energy detector with N = 1000 samples

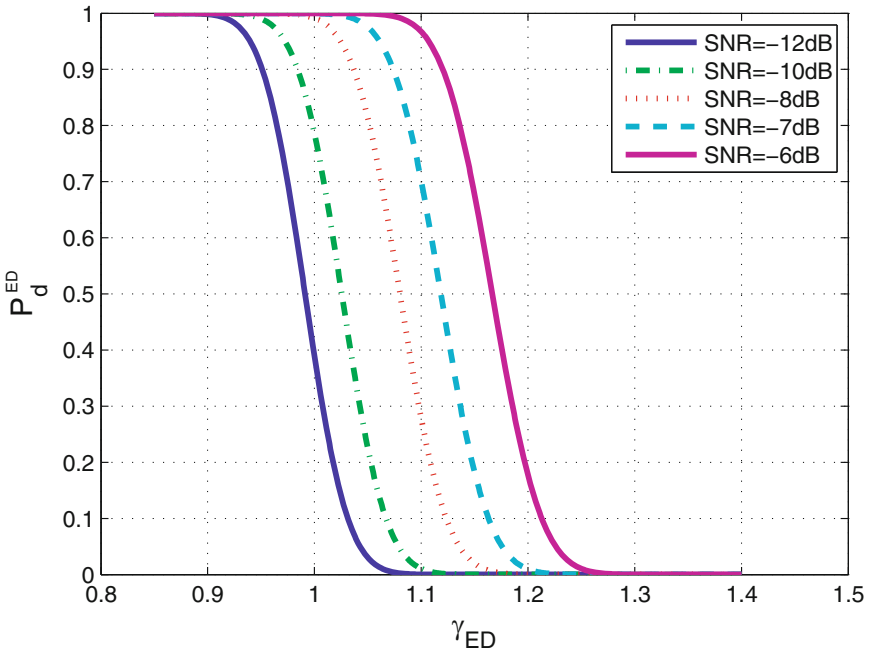

Fig. 8 Relationship between threshold and probability of detection

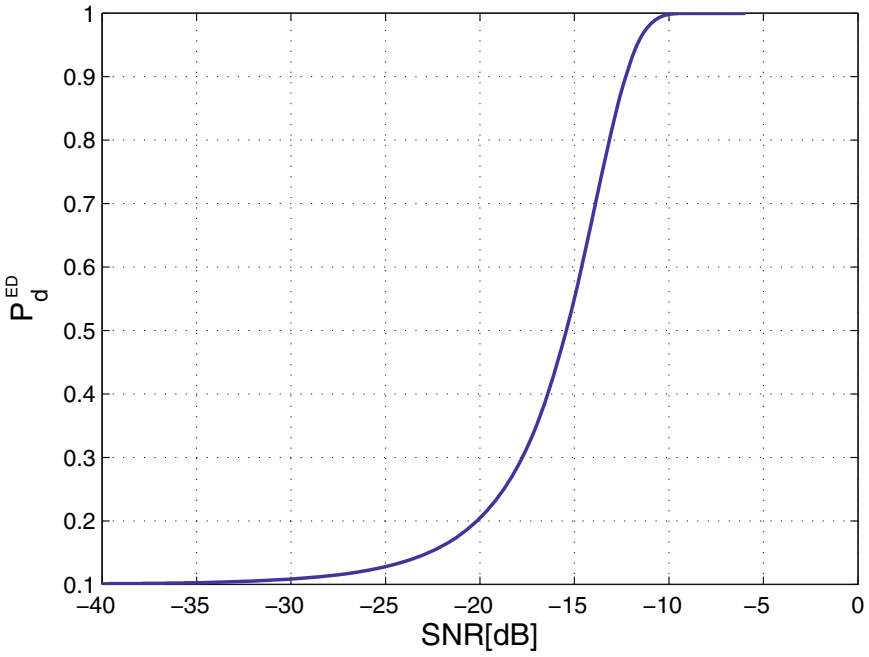

Fig. 9 P_d^{ED} dependency on SNR and set threshold for $N = 2000$ and $P_f^{\mathrm{ED}} = 0.1$

configuration of Fig. 9 (number of samples and false alarm probability), one can conclude that ED is not recommended for scenarios where the SNR is less than -15 dB, once the probability of detection is lower than 0.5.

Finally, in order to have a broad view about the behavior of P_d^{ED}, all main variables are related in a single 3-D surface on Fig. 10. The simulation has been done for a target probability of false alarm $P_f^{\mathrm{ED}} = 0.1$. For an EnS detector, a reasonable number of samples ranges from 500 to 1500, but also SNR has a strong effect on P_d^{ED}. For instance, if the CR is working in a -10 dB scenario, a sensing with $N = 1000$ samples should result in

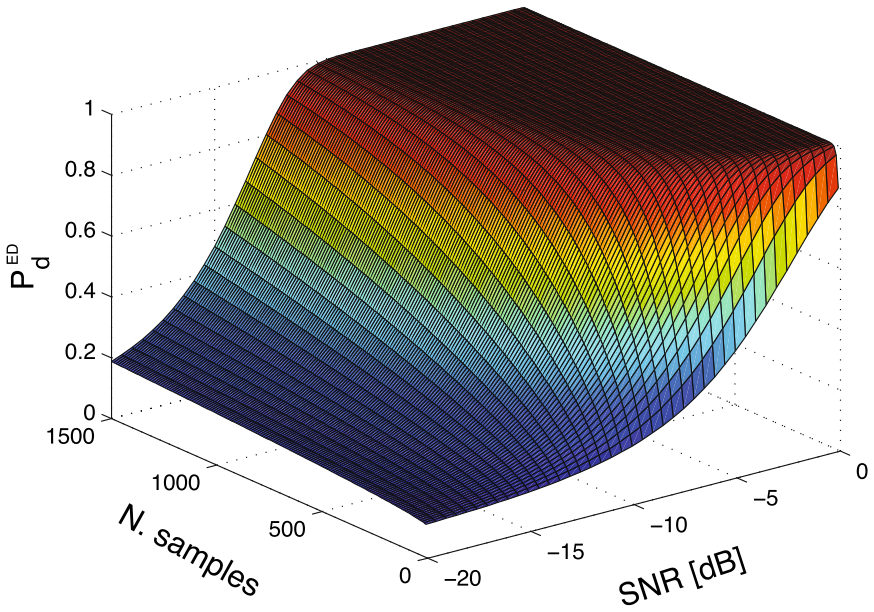

Fig. 10 Probability of detection for EnS considering dependency on number of samples N and SNR and fixed $P_f^{\mathrm{ED}} = 0.1$

$P_d^{\mathrm{ED}} \approx 0.6$; however, it is desirable a greater rate of detection. So, a sensing phase with 1500 samples could achieve $P_d^{\mathrm{ED}} \approx 0.1$.

6.2 Matched Filter

Similarly to EnS, behavior of MfS and its various parameters have been analyzed in order to identify their influence on sensor's performance. Firstly, probabilities of detection and false alarm for AWGN channels have been evaluated in terms of ROC. Figure 11 offers an overall performance idea of a MfS. A first comparison already pointed out that MfS can easily operate in much lower SNR scenarios than a EnS, once MfS ranges from SNR $= -30$ dB to -20 dB, while EnS results in the same characteristics for $-15 <$ SNR < -9 dB. Corroborating this found, [4] states that an energy sensor is much more degraded due to noise uncertainty than a traditional matched filter.

Figure 12 relates probability of detection and SNR for a MfS. From (18), γ_{MF} is directly related to probability of false alarm and noise variance. So, in a real scenario, for an optimal detection, the threshold has to be recalculated at each sensing process, once it is a function of the noise strength at (SNR $= \frac{\sigma_x^2}{\sigma_n^2}$), which may have an instantaneous fluctuation. Hence, for this simulation, at each new SNR value, a γ_{MF} is calculated and then inserted into (19), generating the performance curve of Fig. 12.

Figure 13 depicts how P_d^{MF} behaves with changes in number of samples and SNR. Comparing to EnS case, the MfS is able to work satisfactorily under low SNR scenarios (-30 dB). Indeed, for the same $N = 1500$ samples needed for EnS, MfS is able to provide a good performance under a -20 dB scenario. As a conclusion, matched filter spectrum sensing presents a working margin 10 dB greater than EnS.

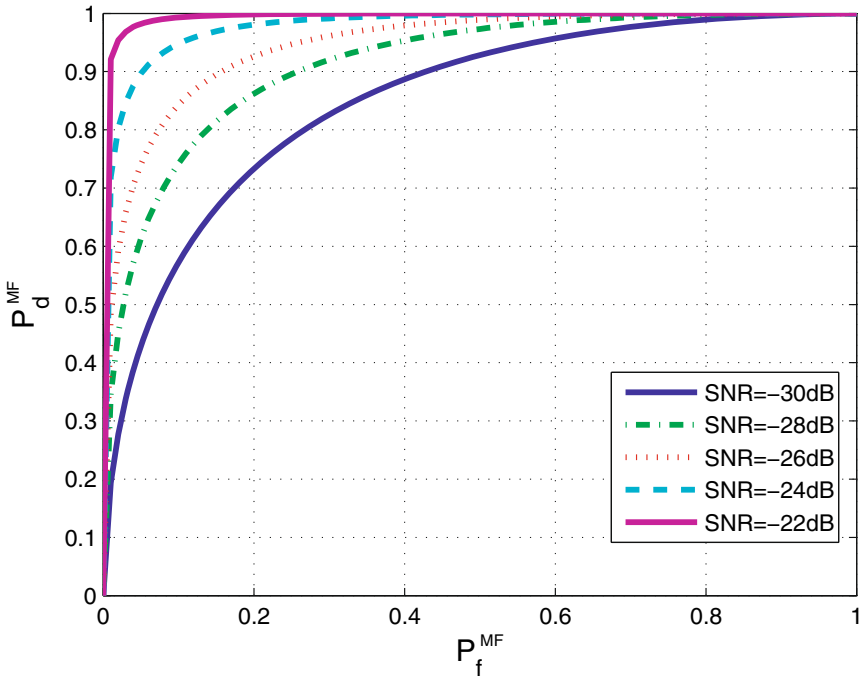

Fig. 11 ROC for a MF detector

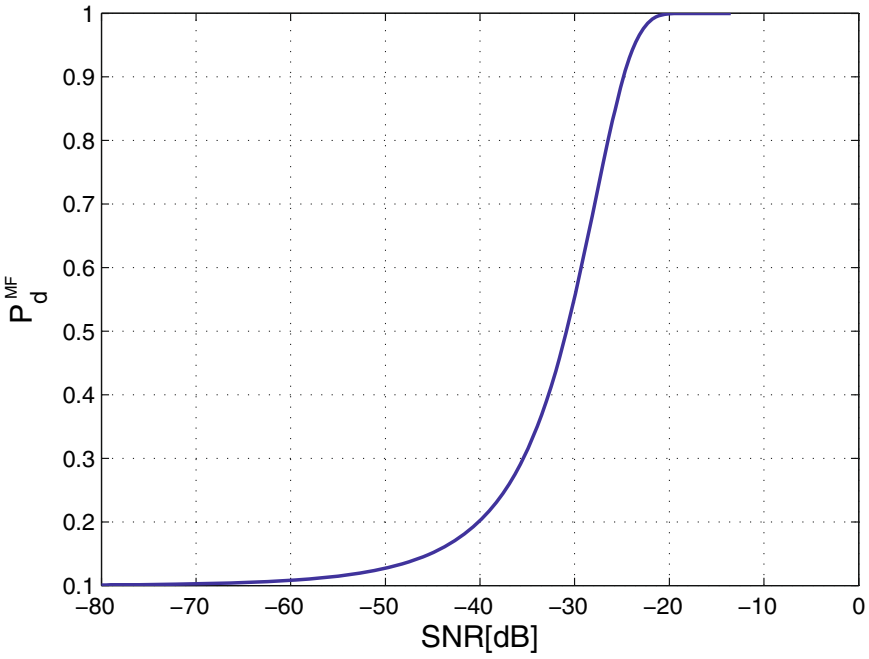

Fig. 12 Probability of detection analysis for different values of threshold and SNR with $N = 2000$ samples and $P_f^{\text{MF}} = 0.1$

6.3 Covariance Absolute Value Sensor

The CAV detection presented in Sect. 4.3 has its own probabilities of detection and false alarm. Equations (32) and (33) show explicitly that system's performance is highly related to threshold, number of samples, SNR and also the correlation coefficient of received samples. Hence, it is important to analyze how these factors affect the quality of spectrum sensing.

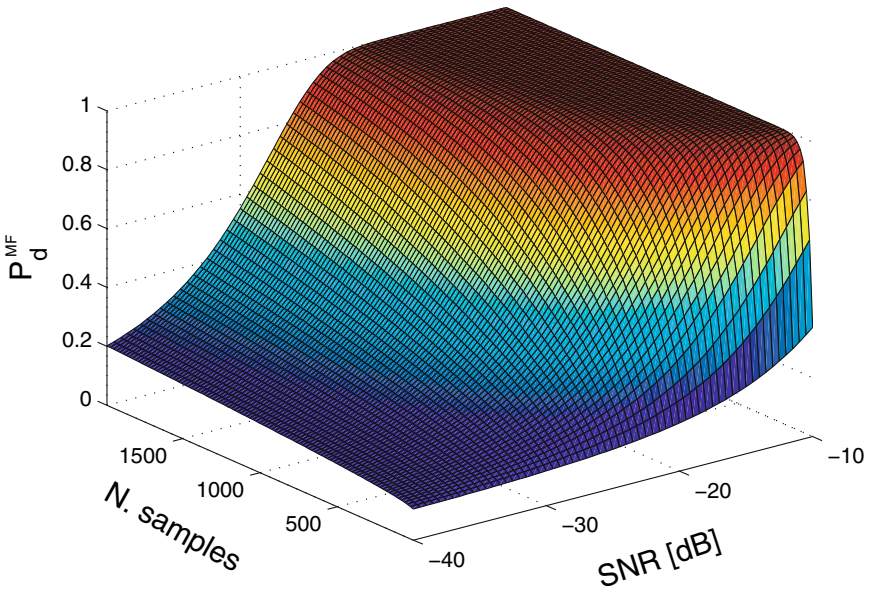

Fig. 13 Probability of detection for a MfS

Influence of SNR on ROC curves is presente in Fig. 14. Indeed, for values of SNR around -13.5 dB, CAV sensing method almost reaches an ideal detection, with $P_f^{\text{CAV}} = 0$ and $P_d^{\text{CAV}} = 1$. Additionally, comparing Figs. 7 and 14, one can identify which system has better ROC performance. An EnS reaches an excellent performance under SNR $= -9$ dB, while a CAV sensor does it with much less energy, as indicated in Fig. 15, i.e., under SNR $= -13.5$ dB.

Notice that not only SNR affects CAV spectral sensing detector. Also smoothing factor and the preset threshold do it. A CAV sensor is based on how strong correlated the samples are. Hence, if there is a scenario with a fixed SNR, the higher Υ_L is, the more efficient the

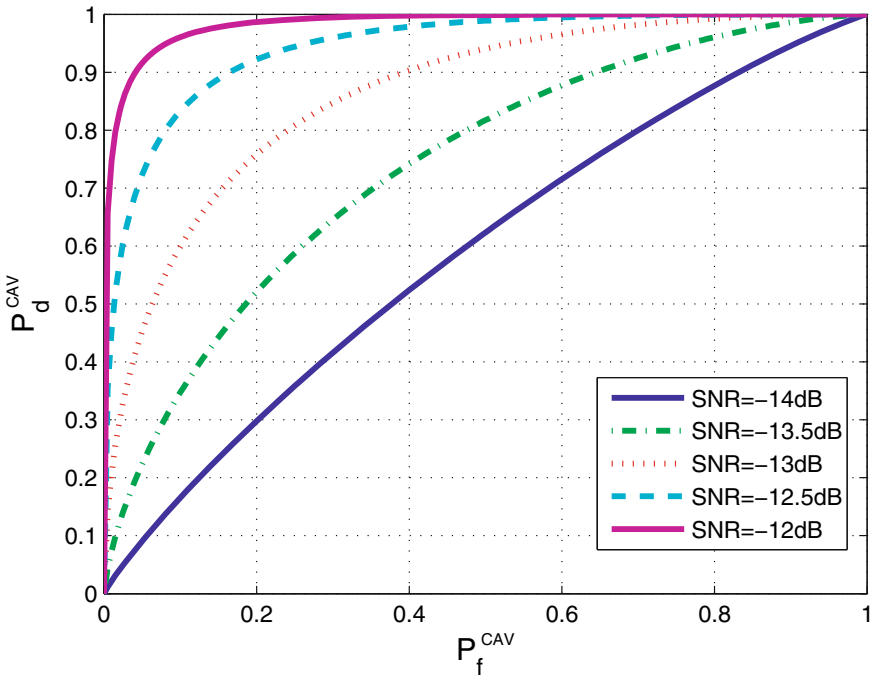

Fig. 14 ROC for a CAV detector with $L = 10$, $\Upsilon_L = 2$ and $N = 10{,}000$

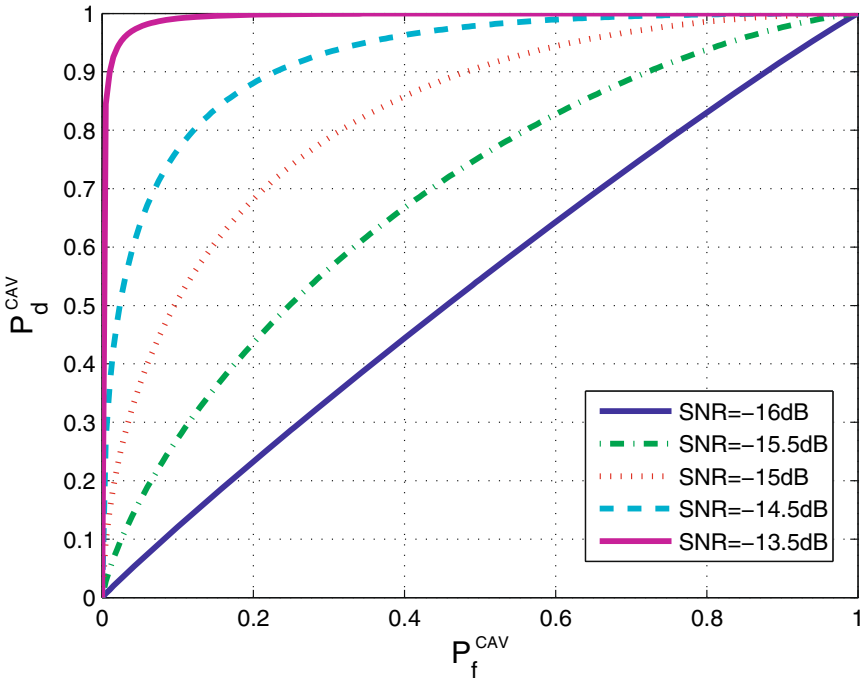

Fig. 15 ROC for a CAV detector with $L = 10$, $\Upsilon_L = 3$ and $N = 10,000$

detection will be. Figure 16 illustrates it. With a graph of $P_d^{\text{CAV}} \times$ SNR and different values for the overall correlation strength Υ_L , for example, if SNR $= -16$ dB a system with a correlation strength of 2 has $P_d^{\text{CAV}} = 0.1$, while the detector with $\Upsilon_L = 4$ has $P_d \simeq 1$.

Previous results in the literature have already pointed out that CAV spectrum sensing detectors need much higher number of samples when compared to EnS and MfS. Aiming to corroborate it, Fig. 17 relates the main factor that may influence CAV performance in terms of P_d^{CAV}. This numerical result has been obtained for middle correlated AWGN channels, i.e., $\Upsilon_L = 3$, while the normalized correlation coefficient $\widehat{\Upsilon}_L$ changes according to the SNR level. Indeed, from Fig. 17, given SNR $= -14$ one can identify the CAV sensor needs at least 9 times more samples than EnS and MfS. If SNR increases 2 dB, around -12 dB, <6000 samples would satisfy a $P_d^{\text{CAV}} > 0.8$; however, it still a huge number of samples, which may exceed the sensing time and consequently shorten the transmission phase.

6.4 Hadamard Ratio Test

Literature for Hadamard ratio spectrum sensing is yet very limited; performance results for this sensor are different from the ones present on previous sessions. A HrS performance for a system with one primary signal operating under SNR $= [-15, -8]$ dB, $n_R = 4$ SUs and $N = [1000]$ samples is presented in Fig. 18.

In order to compare the ROC with all previous cases d has been set to 1 in Fig. 19a. As analyzed in Sect. 4.4, performance of this sensor is enhanced according to number of PUs and SUs present in the system. Hence, an analysis with $n_T = 1$ will not make use of HrS' full performance. Figure 19b shows how a simple increase in the number of PUs $n_T = 3$ may enhance overall sensor's performance.

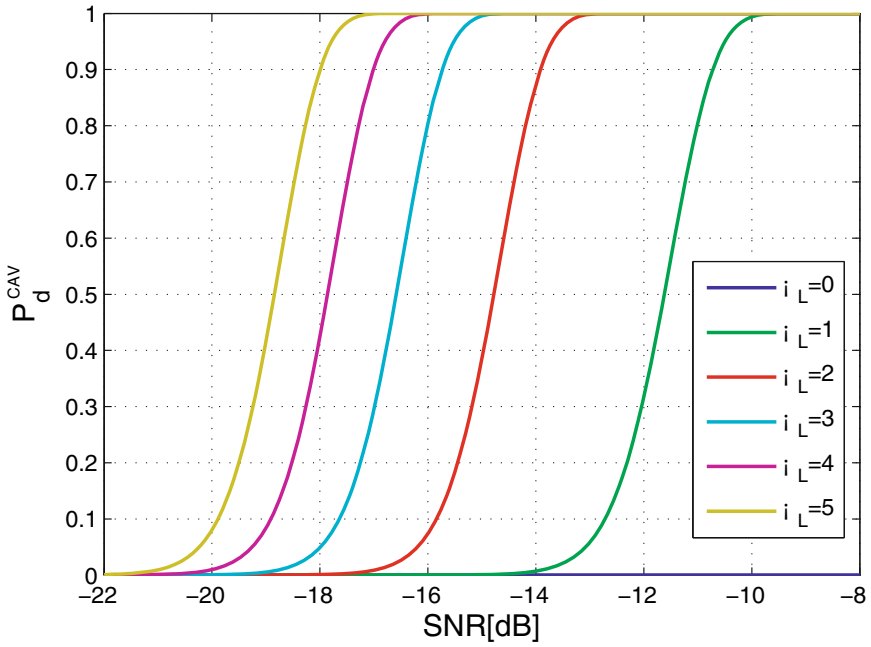

Fig. 16 Probability of detection versus SNR for different values of correlation strength

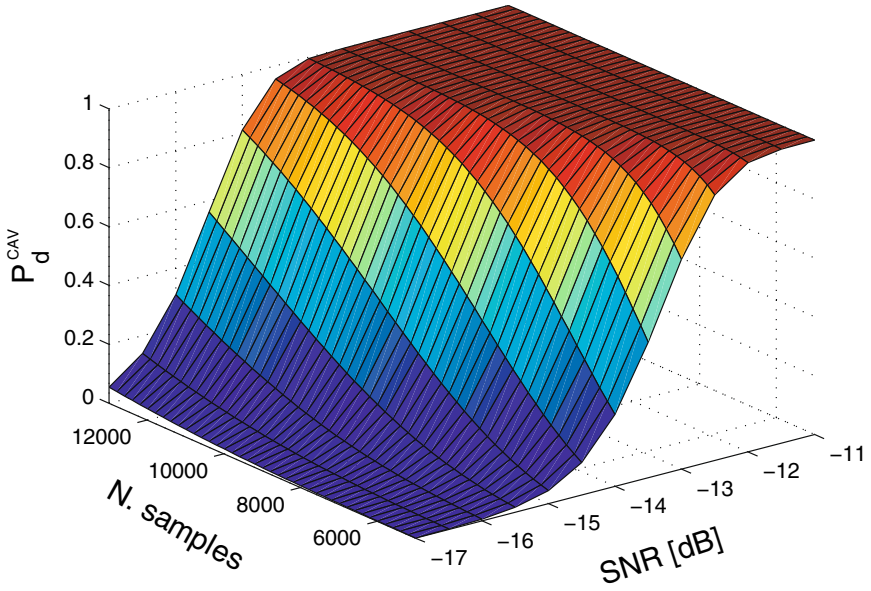

Fig. 17 Probability of detection for a CAV detector

6.5 SNR Walls in Cognitive Radio Sensors

At this point, seen each sensor characteristics and ROCs curves have already been studied, what gives an overview about its performance in scenarios of interest. Now, the next step is to analyze the sample complexity for each sensor via *SNR wall* graphs and study which presents better performance in a specific scenario. From the definition, a SNR wall is the SNR limit for which each analyzed spectrum sensing detector is able to perform without the necessity of using a number of sample tending to infinity. Figure 20 depicts the SNR walls for three sensors: EnS, MfS and CAV. A SNR wall for HrS is impractical because a few approximation have been done; hence, there is no theoretical expression relating number of samples and SNR.

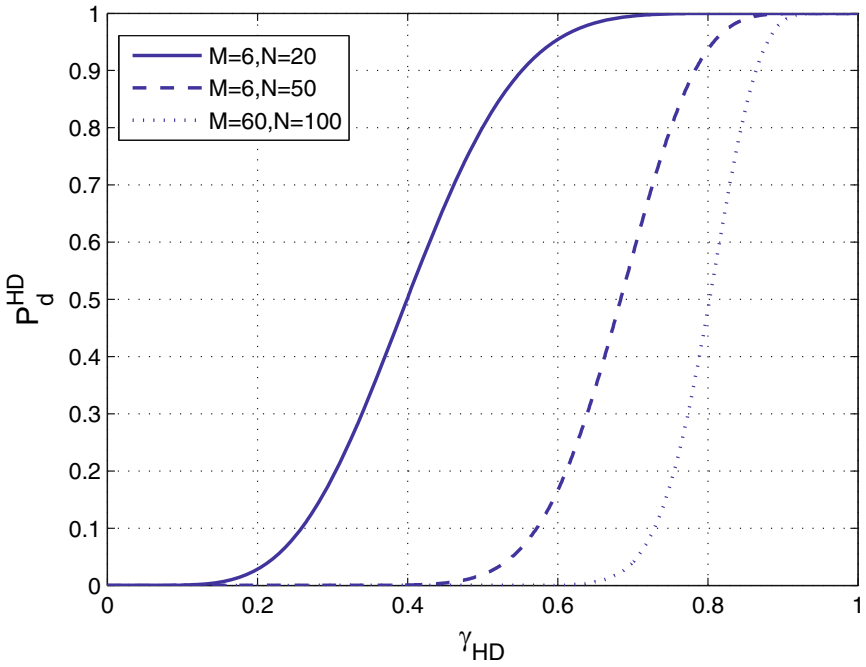

Fig. 18 Probability of detection versus threshold of a HrS for a MIMO system with uncalibrated receivers; Rayleigh channels

Firstly, a greater susceptibility to noise interference is observed in the EnS case, once its SNR wall is located at around -13.5 dB and it has to use an extremely high number of samples to keep its characteristics within an acceptable limit.

On the other hand, MfS' characteristics shows that the sample complexity boost of the coherent stage shifts SNR wall by around -30 dB, what gives an expressive working margin before sample complexity tends to infinity. For example, in very low-SNR sensing scenarios, i.e., $[-30;\ -25]$ dB, MfS is a suitable choice if a number of samples as large as 100,000 or 10,000 is available inside the sensing time period.

Finally and differently from the other cases, CAV sensor does not have a SNR wall; however, more samples are needed than MfS for low-SNR sensing scenarios. Another important analysis similarly presented in is that the EnS does not require any assumptions of the signal; consequently, the SNR wall is located at higher SNR. In contrast, MfS needs several assumptions[4] of the signals under spectrum sensing; however, it presents a SNR wall much lower than EnS. Presenting an intermediate sample complexity, CAV spectrum sensor only makes structural assumption of the signal (medium/high correlated signals), what may be the best choice as CRN Spectrum sensor in several practical scenarios of interest.

Next Sect. 6.6 provides numerical analysis for four sensors applied to some real case constraint scenarios.

6.6 Performance Analysis of ED, MF CAV and HR Sensors

A spectrum sensing system is usually applied to a real CRNs. Indeed, performance of SS methods under some specific constraints is one of the most important points while designing a CR network. In order to fairly compare previous analyzed sensors, optimal parameter values for each sensor have been selected and compared. The adopted system

[4] Actually MfS needs an entire pilot sequence.

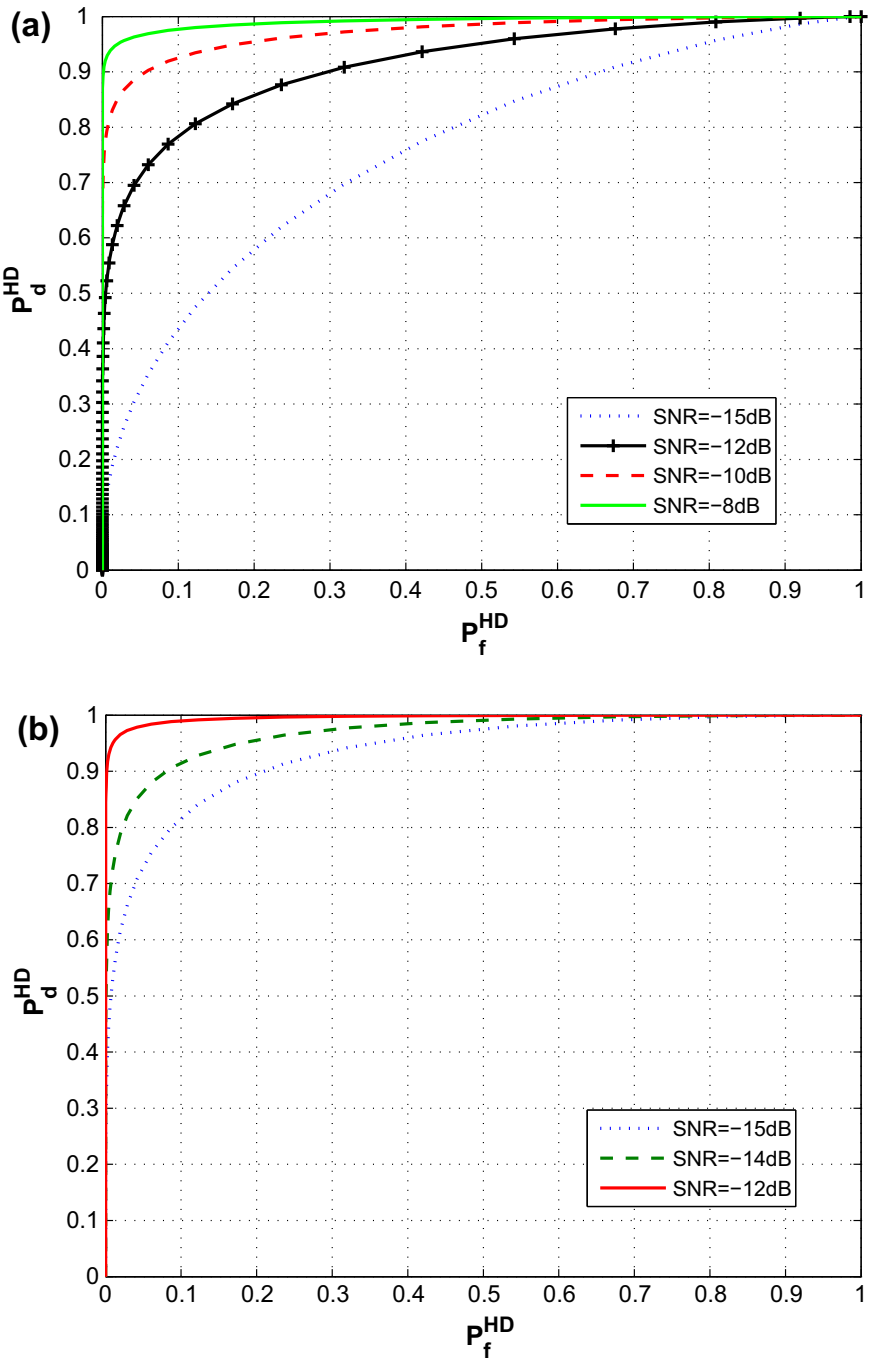

Fig. 19 ROC for a HrS with $N = 1000$ and $n_R = 4$: **a** $n_T = 1$; **b** $n_T = 3$

and channel configuration are described according to the values depicted in Table 2. The simulation trial has considered a LOS (line of sight) AWGN channel transmission of a microphone signal operating in a TV band with a power of 50 mW and bandwidth of 200 kHz. For this system configuration, the CAV correlation coefficient is then normalized by the signal and noise variances, as defined in Eq. (35), so it ranges between $|\widehat{\Upsilon}_L| \leq 1$. Performance analysis for SS detectors operating under realistic mobile NLOS channels, such as Rayleigh fading are discussed in Sect. 6.7.

Figure 21 depicts the spectrum sensing performance for several sensors under AWGN interference hypothesis. The correlation coefficient is set to $0.09 < \widehat{\Upsilon}_L < 0.15$. Again, notice that EnS is not efficient for low SNR scenarios, once it is based on an accurate

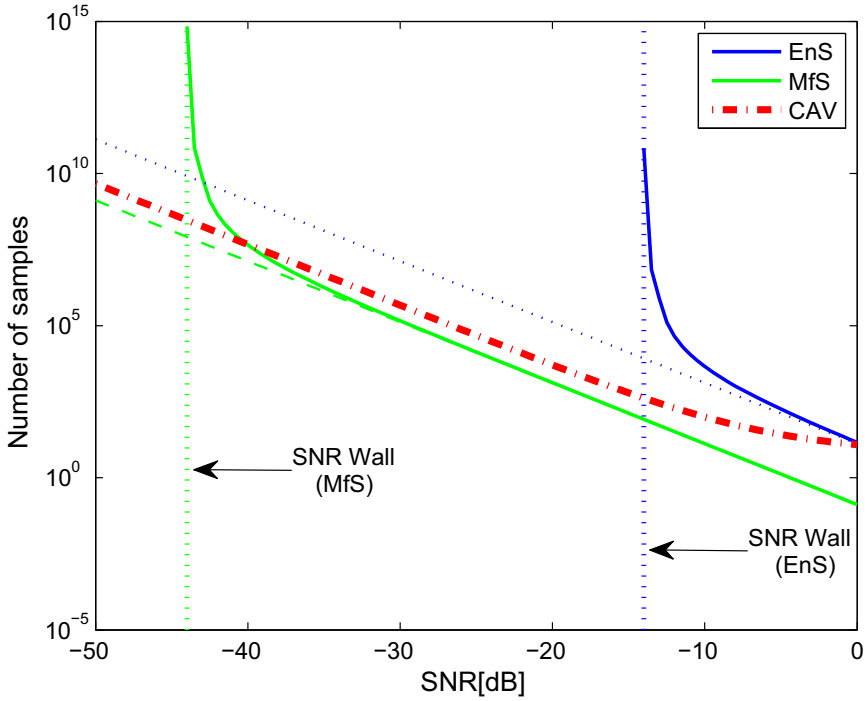

Fig. 20 Sample complexity for CRN sensors

Table 2 Adopted parameters values for the spectrum sensing system

Parameter	Adopted Value
SU: microphone signal	
Tx power	50 mW
Channel	AWGN, LOS
Frequency band	TV sub-band, $BW = 200$ KHz
General SS detector parameters	
Number of samples	$N \in [1, 10] \cdot 10^3$
SNR range	SNR $\in [-30, -10]$
Threshold	Varies for each sensor
Target P_f	0.1
CAV detector	
CAV correlation coefficient	$0.09 < \widehat{\Upsilon}_L < 0.15$
Smoothing factor length	$L = 10$
HrS detector	
n_T	$\{1, 3\}$
n_R	3

estimation of the noise power. On the other hand, CAV and MfS also depend on other characteristics of the received signal. MfS requires a pilot sequence given by PU, while CAV relies on sensing a correlated channel. The ROC performance curves demonstrated that for low SNR scenarios, MfS is much more efficient than CAV; however, for high/medium correlated channels, CAV is able to achieve higher probabilities of detection. For the HrS detector, the above graph shows that utilization of a MIMO CRN may enhance

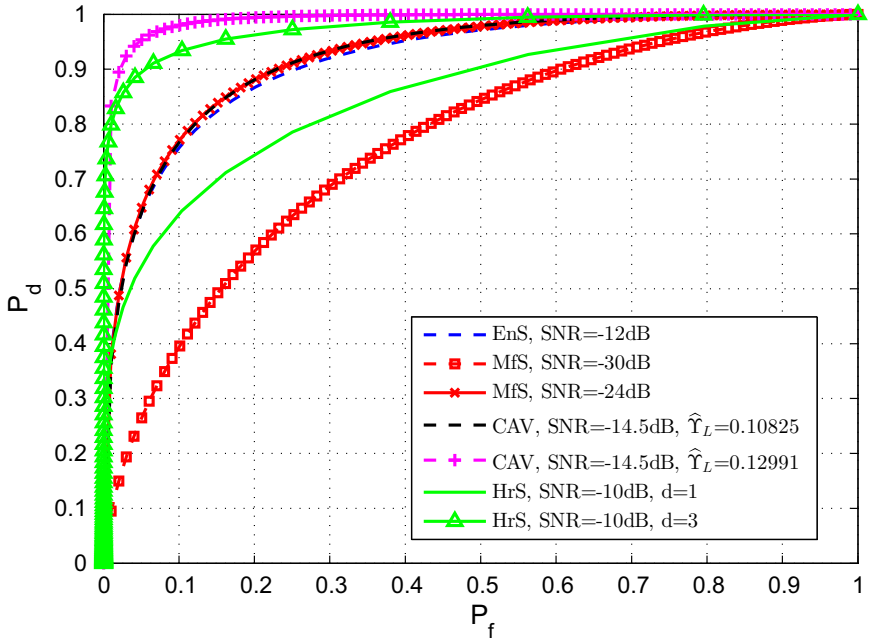

Fig. 21 ROC comparison for EnS, MfS, CAV and HrS

performance of spectrum sensing phase. For example, HrS with $n_T = 3$ presents a much higher performance than for the case with $n_T = 1$ and same SNR range.

To sum up, the graph shows that, for the proposed channel, the best detector is the Matched Filter Sensor, once the acceptable results of P_d and P_f are achieved under low ranges of SNR (around -24 dB).

6.7 Performance Comparison Under Realistic NLOS Channels

This section is devoted to compare two former sensors applied to realistic wireless channels. Section 6.6 has compared all previous studied sensors operating under AWGN channels, which is not the most accurate representation of real transmission channels for CRNs. For future 5G and CR systems, realistic MIMO channels must be studied in term of SS performance. In order to analyze it, this section includes Rayleigh multipath fading and AWGN noise in signal's formulation, which are known to represent a more accurate version of real scenarios. The path-loss influence can be overcome by increasing transmission power; hence will not be deeply considered in this article.

Two sensors have been chosen for this simulation. EnS due its low computational complexity and HrS because it is a robust sensor based on the accurate GLR theory, although it is more complex to implement. Other sensors present intermediate results either in terms of complexity or accuracy. All parameters necessary and respective values for this simulations are shown in Table 3.

Numerical results depicted in Fig. 22 demonstrate that HrS presents higher performance than EnS, in terms of detection probability. Considering the target P_f, EnS has not achieved $P_d \geq 0.8$ for SNR $= 12$ dB, while HrS presents $P_d \simeq 0.97$ for SNR $= 5$ dB. This fact shows that statistic test based on likelihood function is actually much more accurate than tests based only on signal's energy. As a disadvantage, the HrS is known to be more complex than EnS. Hence, the choice of which sensor should be used may depend not only on detection probabilities, but also considering other factors, such as the available transmission power and processing resources.

Table 3 SS system parameters values deployed in more realistic NLOS fading channels scenarios

Parameter	Adopted value
Number of samples	$N = 1024$
SNR range	SNR $\in [0, 12]$
Threshold	Varies for each sensor
Target P_f	0.1
AWGN noise	$\eta \sim \mathbb{C}\mathcal{N}(0, 1)$
PUs	$n_T = 3$
SUs	$n_R = 12$

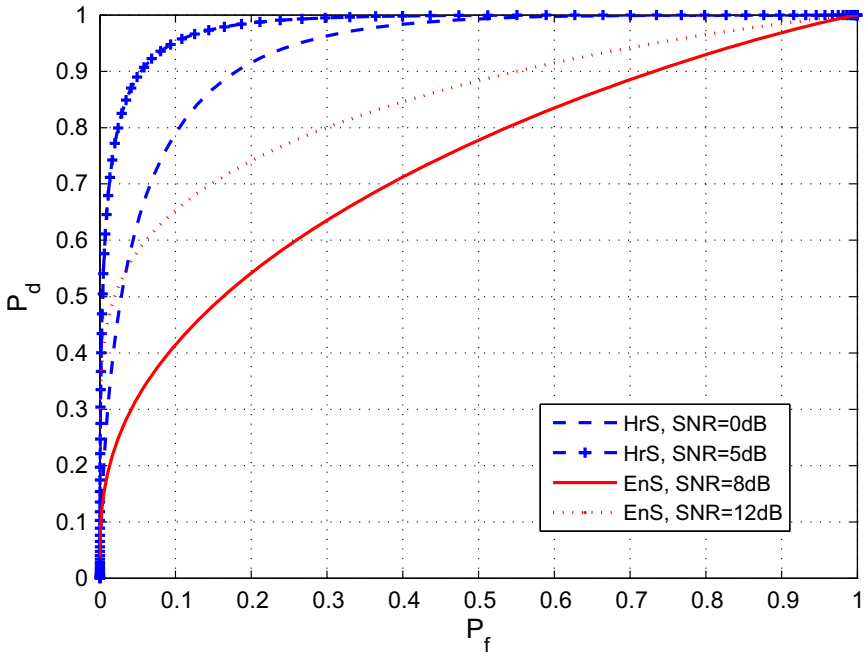

Fig. 22 ROC comparison for EnS and HrS over Rayleigh channel

7 Conclusion

This paper aims to analyze the spectrum sensing detectors available in the literature and further compare them for specific scenarios. Each sensor has a parameter that dramatically changes its performance. Numerical and analytical results demonstrate that EnS is not designed to work in low SNR scenarios, mainly because it is based on received signal's energy; therefore, if noise levels are too high at receiver, the sensor may look at it as an actual primary signal. On the other hand, CAV spectrum sensing detector is able to work in low SNR scenarios; however, correlated primary signals are needed. A significant increase in probabilities of detection for CAV is achieved by small gains in correlation $\widehat{\Upsilon}$, as seen in results of Sect. 6.6.

MfS, as discussed in Sects. 6.2 and 6.6, results in better performance if compared to EnS and CAV. The disadvantage of this SS technique is that a pilot sequence (or any known signal) is needed at the receiver, which is not often available in CR networks. Furthermore, one more factor to worry about is the *SNR wall* with results discussed in Sect. 6.5. Results have confirmed that, for high-SNR scenarios, the EnS may be an acceptable choice as a CRN spectrum sensor, once it has slightly higher sample complexity

but does not rely on any knowledge of the signal. However, for medium/low-SNR scenarios, the MfS performs better than all others and even lower sample complexity is needed.

If a MIMO CR network is suitable, the results from 6.6 have demonstrated that the more PUs and SUs are actually sensing the spectrum, the higher performance is achieved by HrS. Hence, for researches leading with MIMO systems, it is worth to have a close look at this promising spectrum sensing technique. In order to motivate this direction of investigation, realistic CRN scenarios have been analysed in Sect. 6.7. Numerical results indicated that HrS is able to perform more accurate spectrum sensing under low SNR scenarios; however, higher computational complexity is needed, if compared no EnS.

Acknowledgements This work was supported in part by the National Council for Scientific and Technological Development (CNPq) of Brazil under Grant 304066/2015-0, Fundação Araucária under Grant 302/2012, and in part by State University of Londrina—Paraná State Government (UEL), and CAPES/DS scholarship.

References

1. Anant Sahai, S. M. M., & Tandra, R. (2009). Spectrum sensing: Fundamental limits. Tech. rep., Berkeley University of California. http://www.eecs.berkeley.edu/∼sahai/Papers/SensingChapter.pdf.
2. Axell, E., Leus, G., Larsson, E. G., & Poor, H. V. (2012). Spectrum sensing for cognitive radio : State-of-the-art and recent advances. *IEEE Signal Processing Magazine*, *29*(3), 101–116. doi:10.1109/MSP.2012.2183771.
3. Bazerque, J. A., & Giannakis, G. B. (2010). Distributed spectrum sensing for cognitive radio networks by exploiting sparsity. *IEEE Transactions on Signal Processing*, *58*(3), 1847–1862. doi:10.1109/TSP.2009.2038417.
4. Bhargavi, D., & Murthy, C. (2010). Performance comparison of energy, matched-filter and cyclostationarity-based spectrum sensing. In *2010 IEEE eleventh international workshop on signal processing advances in wireless communications (SPAWC)* (pp. 1–5). doi:10.1109/SPAWC.2010.5670882.
5. Biglieri, E., Goldshimith, A. J., & Greenstein, L. J. (2012). *Principles of cognitive radio*. Cambridge: Cambridge University Press.
6. Cabric, D., Mishra, S. M., & Brodersen, R. W. (2004). Implementation issues in spectrum sensing for cognitive radios. In *Conference record of the thirty-eighth asilomar conference on signals, systems and computers, 2004* (Vol. 1, pp. 772–776) doi:10.1109/ACSSC.2004.1399240.
7. Cardoso, L., Debbah, M., Lasaulce, S., Kobayashi, M., & Palicot, J. (2010). Spectrum sensing in cognitive radio networks. In Y. Xiao & F. Hu (Eds.), *Cognitive radio networks*. Florida: CRC Press.
8. Chen, R., Park, J. M., & Reed, J. H. (2008). Defense against primary user emulation attacks in cognitive radio networks. *IEEE Journal on Selected Areas in Communications*, *26*(1), 25–37. doi:10.1109/JSAC.2008.080104.
9. Chung, G., Sridharan, S., Vishwanath, S., & Hwang, C. S. (2012). On the capacity of overlay cognitive radios with partial cognition. *IEEE Transacions on Information Theory*, *58*(5), 2935–2949.
10. Clancy, T. C. (2007). Formalizing the interference temperature model. *Wiley InterScience*, *7*, 1077–1086.
11. Cohen, D., & Eldar, Y. C. (2014). Sub-nyquist sampling for power spectrum sensing in cognitive radios: A unified approach. *IEEE Transactions on Signal Processing*, *62*(15), 3897–3910. doi:10.1109/TSP.2014.2331613.
12. Community, F. C. (2003). Establishment of an interference temperature metric to quantify and manage interference and to expand available unlicensed operation in certain fixed, mobile and satellite frequency bands. Tech. Rep. 03-237, ET Rocket.
13. Dikmese, S., Sofotasios, P. C., Ihalainen, T., Renfors, M., & Valkama, M. (2015). Efficient energy detection methods for spectrum sensing under non-flat spectral characteristics. *IEEE Journal on Selected Areas in Communications*, *33*(5), 755–770. doi:10.1109/JSAC.2014.2361074.
14. Farhang-Boroujeny, B. (2008). Filter bank spectrum sensing for cognitive radios. *IEEE Transactions on Signal Processing*, *56*(5), 1801–1811. doi:10.1109/TSP.2007.911490.

15. Gavrilovska, L., & Atanasovski, V. (2011). Spectrum sensing framework for cognitive radio networks. *Wireless Personal Communications*, *59*(3), 447–469. doi:10.1007/s11277-011-0239-1.
16. Geethu, S., & Narayanan, G. (2012). A novel selection based hybrid spectrum sensing technique for cognitive radios. In *2012 2nd international conference on power, control and embedded systems (ICPCES)* (pp. 1–6). doi:10.1109/ICPCES.2012.6508114.
17. Geethu, S., & Narayanan, G. (2013). A novel selection based hybrid spectrum sensing technique for cognitive radios. In *2013 International conference on emerging trends in computing, communication and nanotechnology (ICE-CCN)* (pp. 476–480).
18. Haykin, S., Thomson, D. J., & Reed, J. H. (2009). Spectrum sensing for cognitive radio. *Proceedings of the IEEE*, *97*(5), 849–877. doi:10.1109/JPROC.2009.2015711.
19. Hernandes, A. G., Kobayashi, R. T., & Abrao, T. (2016). *Introduction to cognitive radio newtorks and applications* (pp. 46–81). Boca Raton: CRC Press. (**chap. 4**).
20. Huang, L., Xiao, Y., So, H. C., & Fang, J. (2015). Accurate performance analysis of hadamard ratio test for robust spectrum sensing. *IEEE Transactions on Wireless Communications*, *14*(2), 750–758. doi:10.1109/TWC.2014.2359223.
21. Jafar, S. A., & Srinivasa, S. (2007). Capacity limits of cognitive radio with distributed and dynamic spectral activity. *IEEE Journal on Selected Areas in Communications*, *25*(3), 529–537. doi:10.1109/JSAC.2007.070403.
22. Johnson, N. L., Kotz, S., & Balakrishnan, N. (1995). *Continuous univariate distributions*. London: Wiley.
23. Khan, A. A., Rehmani, M. H., & Reisslein, M. (2016). Cognitive radio for smart grids: Survey of architectures, spectrum sensing mechanisms, and networking protocols. *IEEE Communications Surveys Tutorials*, *18*(1), 860–898. doi:10.1109/COMST.2015.2481722.
24. Li, C. M., & Lu, S. H. (2016). Energy-based maximum likelihood spectrum sensing method for the cognitive radio. *Wireless Personal Communications*, *89*(1), 289–302. doi:10.1007/s11277-016-3266-0.
25. Mariani, A., Giorgetti, A., & Chiani, M. (2012). Test of independence for cooperative spectrum sensing with uncalibrated receivers. In *Global communications conference (GLOBECOM), 2012 IEEE* (pp. 1374–1379). doi:10.1109/GLOCOM.2012.6503305.
26. McDonough, N. R., & Whalen, D. A. (1995). Detection of signals in noise (2nd ed.). Elsevier. http://app.knovel.com/hotlink/toc/id:kpDSNE000A/detection-signals-in/detection-signals-in
27. Naeem, M., Anpalagan, A., Jaseemudin, M., & Lee, D. C. (2014). Resource allocation techniques in cooperative cognitive radi networks. *IEEE Communications Suerveys and Tutorials*, *16*, 729–744.
28. Quan, Z., Cui, S., Poor, H. V., & Sayed, A. H. (2008). Collaborative wideband sensing for cognitive radios. *IEEE Signal Processing Magazine*, *25*(6), 60–73. doi:10.1109/MSP.2008.929296.
29. Quan, Z., Cui, S., Sayed, A. H., & Poor, H. V. (2009). Optimal multiband joint detection for spectrum sensing in cognitive radio networks. *IEEE Transactions on Signal Processing*, *57*(3), 1128–1140. doi:10.1109/TSP.2008.2008540.
30. Semlali, H., Boumaaz, N., Soulmani, A., Ghammaz, A., & Diouris, J. F. (2014). Energy detection approach for spectrum sensing in cognitive radio systems with the use of random sampling. *Wireless Personal Communications*, *79*(2), 1053–1061. doi:10.1007/s11277-014-1917-6.
31. Sridhara, K., Chandra, A., & Tripathi, P. S. M. (2008). Spectrum challenges and solutions by cognitive radio: An overview. *Wireless Personal Communications*, *45*(3), 281–291. doi:10.1007/s11277-008-9465-6.
32. Sun, H., Nallanathan, A., Wang, C. X., & Chen, Y. (2013). Wideband spectrum sensing for cognitive radio networks: A survey. *IEEE Wireless Communications*, *20*(2), 74–81. doi:10.1109/MWC.2013.6507397.
33. Sun, S., Ju, Y., & Yamao, Y. (2013). Overlay cognitive radio ofdm system for 4g cellular networks. *IEEE Wireless Communications, 20*(2), 68–73.
34. Tandra, R., & Sahai, A. (2007). Snr walls for feature detectors. In *2nd IEEE international symposium on new frontiers in dynamic spectrum access networks, 2007. DySPAN 2007* (pp. 559–570). doi:10.1109/DYSPAN.2007.79.
35. Tandra, R., & Sahai, A. (2008). Snr walls for signal detection. *IEEE Journal of Selected Topics in Signal Processing*, *2*(1), 4–17. doi:10.1109/JSTSP.2007.914879.
36. Tian, Z., & Giannakis, G. B. (2006). A wavelet approach to wideband spectrum sensing for cognitive radios. In *2006 1st international conference on cognitive radio Oriented wireless networks and communications* (pp. 1–5). doi:10.1109/CROWNCOM.2006.363459.
37. Tian, Z., & Giannakis, G. B. (2007). Compressed sensing for wideband cognitive radios. In *2007 IEEE international conference on acoustics, speech and signal processing-ICASSP '07* (Vol. 4, pp. IV-1357–IV-1360). doi:10.1109/ICASSP.2007.367330.

38. Tugnait, J. (2012). On multiple antenna spectrum sensing under noise variance uncertainty and flat fading. *IEEE Transactions on Signal Processing*, *60*(4), 1823–1832. doi:10.1109/TSP.2011.2180721.
39. Walck, C. (1998). Hand-book on statistical distributions for experimentalists. In *Internal report*.
40. Zeng, F., Li, C., & Tian, Z. (2011). Distributed compressive spectrum sensing in cooperative multihop cognitive networks. *IEEE Journal of Selected Topics in Signal Processing*, *5*(1), 37–48. doi:10.1109/JSTSP.2010.2055037.
41. Zeng, Y., & Liang, Y. C. (2009). Spectrum-sensing algorithms for cognitive radio based on statistical covariances. *IEEE Transactions on Vehicular Technology*, *58*(4), 1804–1815. doi:10.1109/TVT.2008.2005267.
42. Zhang, R., Liang, Y. C., & Cui, S. (2010). Dynamic resource allocation in cognitive networks. *IEEE Signal Processing Magazine*, *10*, 102–114.
43. Zhao, G., Ma, J., Li, G., Wu, T., Kwon, Y., Soong, A., et al. (2009). Spatial spectrum holes for cognitive radio with relay-assisted directional transmission. *IEEE Transactions on Wireless Communications*, *8*(10), 5270–5279. doi:10.1109/TWC.2009.081541.

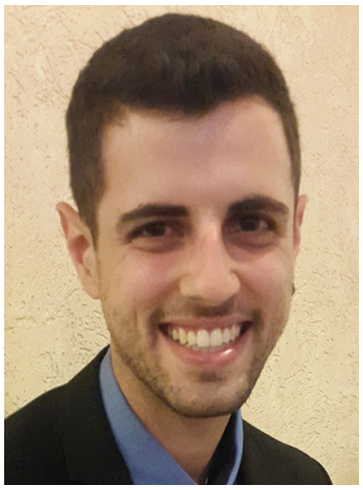

Lucas Claudino received his B.S. in Electrical Engineering from Londrina State University (UEL) in 2016. Since 2013, he has been engaged with telecommunication subjects at the Digital Signal Processing and Telecommunications Lab. (UEL) and has undertaken an internship at Swinburne University of Technology at the Centre for Advanced Internet Architectures (CAIA) in 2014. His interests lie in digital signal processing, internet architectures, cognitive radio, resource alloation, heuristic and convex optimization aspects of 3G and 4G systems, electronic systems and integrated circuit design.

Taufik Abrão (IEEE Senior Member'12; IEEE Member'97) received his B.S., M.Sc. and Ph.D., all in Electrical Engineering, from the Polytechnic School of the University of São Paulo (EPUSP), Brazil, in 1992, 1996, and 2001, respectively. Since March 1997, he has been with the Communications Group, Department of Electrical Engineering, Londrina State University (UEL), PR, Brazil, where he is currently an Associate Professor in communications engineering. In 2012 (2nd semester), he was an Academic Visitor at Communications, Signal Processing and Control Research Group, University of Southampton, UK. In 2007–2008, he was a postdoctoral researcher at the Department of Signal Theory and Communications of the Polytechnic University of Catalonia (TSC/UPC), Barcelona, Spain. Dr Abrao has participated in several projects funded by government agencies and industrial companies. He is involved in editorial board activities of three journals in the communication area and he has served as TPC member in several symposium and conferences in the field. Dr Abrao is a member of the IEEE and SBrT. His research interests lie in communications and signal processing, including multiuser detection and estimation, MC-CDMA and MIMO systems, cooperative communication and relaying, resource allocation, heuristic and convex optimization aspects of 3G and 4G systems. He is authored or coauthored of more than a 190 research papers published in specialized/international journals and conferences. For more information, please, see the author's personal HP: http://www.uel.br/pessoal/taufik/

A.2 Hadamard Ratio Sensor in Realistic CRN Scenarios

Title:	*Hadamard Ratio Spectrum Sensing in Realistic CRN Channels*
Authors:	Lucas Claudino, Ricardo Kobayashi and Taufik Abrão
Category:	*Symposium Paper*
Publication:	2016
Congress:	XXXIV Simpósio Brasileiro de Telecomunicações e Processamento de Sinais - SBrT'2016

Contributions: the main contribution of this works is on Section III, where the likelihood theory is applied to realistic cognitive radio scenarios and expressive results are obtained. We found out the this sensor is robust to fast fading, once the change in doppler frequency does not significantly affect its performance.

Hadamard Ratio Spectrum Sensing in Realistic CRN Channels

Lucas Claudino, Ricardo Kobayashi and Taufik Abrão

***Abstract*— Cognitive radio networks (CRN) are constantly in need for new technologies able to improve their performance. Hence, study of new spectrum sensing (SS) techniques and devices is extremely important for a development of more accurate and sensible devices. The Hadamard ratio-based spectrum sensor (HrS) is a robust method able to accurately sense the presence of a wireless signal by applying a statistic test based on maximum-likelihood (ML) of collected signal data. A further performance analysis of HrS techniques under realistic MIMO (Multiple-Input and Multiple-Output) fading channels is the contribution of this work. As a result, simulations aim to demonstrate its efficiency and how applicable would be a HrS procedure when inserted in real non-line-of-sight (NLOS) MIMO channel scenarios.**

***Keywords*— Cognitive Radio; Spectrum Sensing; Hadamard Ratio; Rayleigh fading; Path loss.**

I. INTRODUCTION

Cognitive radio (CR) technologies aim to optimize spectrum access by proposing methods for a licensed user (PU, primary user) to share the spectrum with a secondary user (SU). Many techniques try to detect white-spaces (in spectrum, time or space) sensing whether a primary signal is present or not and then try to access them so both CR and PU use the spectrum band either at different time or frequency slots or in different geographic regions [1]. Several methods can be used for sensing those white-spaces, such as energy detection sensing (EnS), coherent sensing, cyclostationary-based sensing, matched filter sensing [2], [3], among others.

A few authors [4]–[6] have devoted a long time to study, develop and prove statistical models for a new and promising technology based on generalized likelihood ratio test (GLRT), known as HrS applied to CR; however, the majority of results are valid for AWGN channels, which represents a simplified condition for real wireless channel scenarios. This article comes to contribute to SS in cognitive radio by analyzing the HrS under realistic wireless communication channels. The proposed HrS detector has been characterized by Monte-Carlo simulations considering Rayleigh fading and path-loss channels effects, as well as thermal interference, aiming to understand how this technology would behave if inserted in a real cognitive radio hardware.

This paper firstly formulates important signals of a typical HrS scenario, then basic HrS theory, operation and sensing methods and merit figures are properly calculated and explained. Section III analyses performance of a HrS under Rayleigh fading, path loss and AWGN channels via probabilities of detection (P_d) and false alarm (P_f) for different cases. A further extension of works in [5], [6] has been done. In order tho show the benefits of HrS, a comparison between HrS and other former sensors has been simulated based on an accurate estimation previously formulated. Additionally, differently from [5], a realistic channel has been considered. Also, a further analysis of sample complexity for HrS operating in fading channels has been considered as another point to confirm the sensor's robustness. Finally, results, future study possibilities and applications are discussed in section IV.

Notation: $\mathcal{L}(\cdot)$ denotes the likelihood function, P_d is probability of detection and P_f probability of false alarm. An scalar variable is denoted as x, while $\mathbf{x}$ is a vector and $\mathbf{X}$ represents a matrix form. $\Gamma(\cdot)$ is the gamma function.

II. HADAMARD RATIO-BASED ROBUST SPECTRUM SENSING

Hadamard ratio test is a robust method to provide signal detection in multivariate analysis which is able to deal with non-independent and identically distributed (non-*i.i.d.*) noise [5]. Recently, Hadamard Ratio test has been exploited for robust SS in CR [4], [6].

For the proposed problem, a transmission with n_T primary antennas not necessarily co-located is considered. At receiver's side, N samples are received by M SU's antennas under two circumstances: H_0 when PUs are absent and H_1 when they are active. Hence, a received

L. Claudino, R. Kobayashi and T. Abrão. Department of Electrical Engineering, Londrina State University, Londrina-PR, Brazil, E-mails: lsclaudino@gmail.com, taufik@uel.br, ricardokobayashi_5@hotmail.com.

signal can be written as:

$$\mathbf{x}[n] = \begin{cases} \boldsymbol{\eta}[n] & : \mathrm{H}_0 \\ \mathbf{H}\mathbf{s}[n] + \boldsymbol{\eta}[n] & : \mathrm{H}_1 \end{cases}. \quad (1)$$

Notice: $n = 1, 2, \ldots, N$ is the discrete-time index for all signals. Also, the received signal $\mathbf{x}[n]$ has M complex entries, one for each received antenna, i.e., $\mathbf{x}[n] \in \mathbb{C}^M$. Furthermore, $\mathbf{H} \in \mathbb{C}^{M \times n_T}$ is the MIMO channel matrix. Transmitting signals are denoted as $\mathbf{s}[n] \in \mathbb{C}^{n_T}$, where each entry stores a signal from one of the n_T users, considering $s_i \sim \mathcal{N}\left(0, \sigma^2_{s_i}\right)$. Finally, noise at receiver side is represented by $\boldsymbol{\eta}[n] \in \mathbb{C}^M$, where $\sigma^2_{\eta_i}$ is the unknown noise variance on each antenna, i.e., , $\eta_i[n] \sim \mathcal{N}\left(0, \sigma^2_{\eta_i}\right)$.

If radio frequency chains on receiver's side are uncalibrated, noise will be different at each antenna, consequently: $\sigma^2_{\eta_i} \neq \sigma^2_{\eta_j}$ for $i \neq j$. Thus, the sensing problem is to actually determine if $\mathbf{X} = [\mathbf{x}[1] \cdots \mathbf{x}[N]]$ is composed only by noise or both signal plus noise.

Fig. 1 depicts a block diagram for the proposed HrS. Firstly, a transmitter (PU) generates data string $\mathbf{s}[n]$ which is transmitted over a MIMO channel. At the SU, ML estimator is obtained by calculating the received signal's covariance matrix under both hypothesis H_0 and H_1, which allows the SS device to determine statistics of a test variable ξ. Finally, the spectrum status is determined based on a preset threshold: if $\xi < \gamma \rightarrow \mathrm{H}_1$ or if $\xi > \gamma \rightarrow \mathrm{H}_0$.

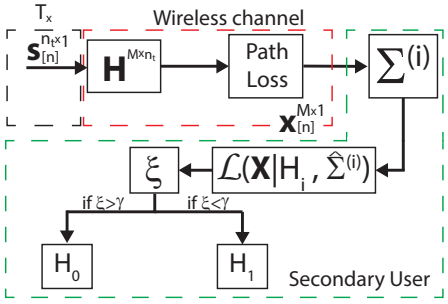

Fig. 1. Block diagram for a generic HrS.

1) GLRT Derivation: The observation set (1) is assumed to be Gaussian distributed and conditioned to the ith $(i = 0, 1)$ hypothesis test, $\mathbf{x}[n]|\mathrm{H}_i \sim \mathcal{N}\left(0, \boldsymbol{\Sigma}^{(i)}\right)$, with $\boldsymbol{\Sigma}^{(i)} \in \mathbb{C}^{M \times M}$ being the covariance matrix defined as:

$$\boldsymbol{\Sigma} = \mathbb{E}\left[\mathbf{X}\mathbf{X}^H\right] = \begin{bmatrix} \Sigma_{11} & \Sigma_{12} & \cdots & \Sigma_{1M} \\ \Sigma_{21} & \Sigma_{22} & \cdots & \Sigma_{2M} \\ \vdots & \vdots & \ddots & \vdots \\ \Sigma_{M1} & \Sigma_{M2} & \cdots & \Sigma_{MM} \end{bmatrix} \quad (2)$$

and $\Sigma_{ij} = \Sigma^H_{ij} = \mathbb{E}\left[\mathbf{x}^H_i \mathbf{x}_j\right]$. The matrix $\boldsymbol{\Sigma}$ expresses independence between every pair of channels [7].

Indeed, $\boldsymbol{\Sigma}^{(0)} = \mathrm{diag}(\sigma^2_{\eta_1}, \cdots, \sigma^2_{\eta_M})$ represents the noise-only observation hypothesis H_0 and $\boldsymbol{\Sigma}^{(1)}$ is a non-diagonal matrix representing covariance between every pair of secondary antennas under hypothesis H_1.

According to [7], the conditional likelihood function of $\mathbf{X}$ under H_i hypothesis may be defined as:

$$\mathcal{L}\left(\mathbf{X}\,|H_i\right) = \frac{\exp\left\{-N \cdot \mathrm{tr}\left[\left(\boldsymbol{\Sigma}^{(i)}\right)^{-1} \widehat{\boldsymbol{\Sigma}}\right]\right\}}{\pi^{MN}\left|\boldsymbol{\Sigma}^{(i)}\right|^N} \quad (3)$$

Using ML estimation procedure, the derivative of (3) is set to zero in order to find the ML estimator of $\boldsymbol{\Sigma}^{(0)}$ and $\boldsymbol{\Sigma}^{(1)}$ as $\widehat{\boldsymbol{\Sigma}}^{(0)} = \mathrm{diag}(\widehat{\boldsymbol{\Sigma}})$ and $\widehat{\boldsymbol{\Sigma}}^{(1)} = \widehat{\boldsymbol{\Sigma}}$, where $\widehat{\boldsymbol{\Sigma}} = (1/N)\sum_{n=1}^{N} \mathbf{x}[n]\mathbf{x}[n]^H$ is the sample covariance matrix. Finally, HrS's GLR for is written as:

$$\xi = \frac{\max\limits_{\boldsymbol{\Sigma} \in H_0} \mathcal{L}\left(\mathbf{X}|\mathrm{H}_0, \boldsymbol{\Sigma}^{(0)}\right)}{\max\limits_{\boldsymbol{\Sigma} \in H_1} \mathcal{L}\left(\mathbf{X}|\mathrm{H}_1, \boldsymbol{\Sigma}^{(1)}\right)} \quad (4)$$

Hence, the Hadamard Ratio is finally obtained by applying ML estimators and (3) into (4), i.e.:

$$\xi = \frac{\left|\widehat{\boldsymbol{\Sigma}}^{(1)}\right|}{\left|\widehat{\boldsymbol{\Sigma}}^{(0)}\right|} \quad (5)$$

which is bounded by $[0, 1]$, once $\left|\widehat{\boldsymbol{\Sigma}}\right|$ dramatically decreases in presence of primary signals and presents its maximum value of $\left|\mathrm{diag}(\widehat{\boldsymbol{\Sigma}})\right| = \left|\widehat{\boldsymbol{\Sigma}}^{(0)}\right|$ when under H_0. Hence, H_1 is sensed if ξ is smaller than a chosen threshold γ, otherwise, H_0 occurs:

$$\xi \underset{H_1}{\overset{H_0}{\gtrless}} \gamma \quad (6)$$

Exact distribution for this GLRT may assume complex values; however, its moments can be straightforwardly expressed using a moment approximation. The test statistic ξ can be approximated by a beta distributed random variable (*r.v.*) defined in $[\theta_1, \theta_2]$, with shaping parameters α and β and a probability density function *p.d.f.*:

$$f(x) \simeq \begin{cases} \dfrac{(x-\theta_1)^{\alpha-1}(\theta_2 - x)^{\beta-1}}{B(\alpha, \beta)}, & \theta_1 \leq x \leq \theta_2 \\ 0, & \text{otherwise,} \end{cases} \quad (7)$$

where $B(\alpha, \beta) = \dfrac{\Gamma(\alpha)\Gamma(\beta)}{\Gamma(\alpha + \beta)}$ is the Beta Function.

Based on methods of [8]–[10], first and second moments of ξ can be calculated. Beta distribution is then used to perform a moment matching, so probabilities of detection and false alarm are accurately estimated [5].

Indeed, authors of [5] and [6] have precisely derived exact moments of ξ in order to provide a more accurate approximation for the test's distribution. For simulation purposes, it is valid to numerically calculate moments from available signal samples and use them as a beta distributed *r.v.*

Probability of false alarm for ξ is defined as $P_f \triangleq \Pr\{\xi < \gamma \,|\mathrm{H}_0\}$ and, given the c.d.f. of a beta *r.v.* bounded by $[0,1]$, P_f is calculated as:

$$P_f \simeq \int_0^{\gamma} \frac{1}{B(\alpha_0,\beta_0)} z^{\alpha_0-1}(1-z)^{\beta_0-1}dz = \frac{B_x(\alpha_0,\beta_0)}{B(\alpha_0,\beta_0)} = F(\gamma) \quad (8)$$

where $B_x(\alpha_0,\beta_0) = \int_0^x z^{\alpha_0-1}(1-z)^{\beta_0-1}dz$ is the incomplete Beta function, α_0 and β_0 are shape parameters for H_1 approximated with the first two positive moments of ξ.

Similarly, probability of detection for ξ $\left(P_d \triangleq \Pr\{\xi < \gamma \,|\mathrm{H}_1\}\right)$ was derived in [5] via moment matching strategy:

$$P_d \triangleq Pr\{\xi < \gamma \,|\mathrm{H}_1\} = \frac{B_x(\alpha_1,\beta_1)}{B(\alpha_1,\beta_1)} = F(\gamma) \quad (9)$$

where shape parameters for hypothesis H_1, *i.e.*, α_1 and β_1 are obtained as function of the test statistic's first two negative moments.

III. Numerical Results

This section is devoted to compare and analyze performance of proposed HrS in realistic wireless channel scenarios. Most researches on HrS, have been done on performance analysis under AWGN channels [5], [6], [11], [12]; however, for future 5G networks and CR possibilities, SS performance must be analyzed in realistic MIMO channel scenarios, including path-loss influence, non-line-of-sight Rayleigh fading and shadowing effects.

Firstly, sensor's robustness must be tested and compared to other SS techniques. Indeed, based on results of [13], an Energy detector in realistic scenario has been considered as a comparison metric for analyzing HrS's performance.

AWGN channels represent a very simple and unrealistic approximation of real wireless channel scenarios. Hence, Clarke's fading model is deployed [14], [15] to create a Rayleigh fading channel matrix. This channel model not only is a more accurate representation of a wireless channel but also allows evaluation of user's mobility influence by inserting the maximum Doppler shift factor f_d. The constant f_d depends on user's velocity v and carrier frequency f_c, i.e., $f_d = \frac{v}{c} f_c$, where c is the light velocity. Hence, for slow fading channels, a pedestrian user with $f_d \approx 5$Hz has been considered, while for fast fading a vehicular user, $f_d \approx 100$Hz has been adopted.

TABLE I
Reference values used for simulations

Parameter	Value
Avg. PU power	$P_t \in [-100, -20]$dBm
PU-SU dist.	$d = 1000$m
Noise power	$P_{\text{noise}} = -100$dBm
SNR	SNR $\in [-3, 7]$dB
# samples	$N \in [32, 1024]$
# SU antennas	$M = 12$
# PU	$n_T = 5$
Doppler freq.	$f_d \in \{5, 200\}$Hz
Path-loss exponent	$\psi = 4$

Additionally, an average PU-SU separation d has been considered when calculating the path-loss effect, while the average transmitted power was set to operate in range $P_t \in [-100; -20]$ dBm. Table I contains reference values for channel and signal estimation used on simulations of this section. AWGN noise interference was modeled mainly as thermal effect with $P_{\text{noise}} = -100$dBm, which allows us to calculate the receiver's SNR dividing the received power by the noise power.

Fig. 2 compares the simulation results for both conventional EnS and Hadamard ratio SS techniques. All simulations have been done for $d = 1$km, fast fading $f_d = 200$Hz, $N = 128$, samples and other parameters according to Table I. In order to characterize the average CR system behavior, Monte-Carlo simulations with $\mathbf{10^6}$ realizations per performance point were proceeded, guaranteeing a confidence interval of 98% and maximum error of 5%.

Firstly, fig. 2 shows how harmful the channel is for an EnS detection. For an AWGN scenario, EnS has an expressive performance for $SNR = -3$dB; however, fading processes severely degrades its performance, once not even at $SNR = 7dB$ an acceptable detection rate is achieved. In contrast, proposed HrS has similar and satisfying performance under both AWGN and fading channels (red circled and blue dashed lines, respectively), which indicates a certain robustness to fading for HrS-based SS techniques.

Additionally, an analysis of user mobility effects on SS is also important. In this sense, a ROC (Receiver Operating Characteristics) comparison for transmissions under slow and fast fading illustrates this process of interference. A flat Rayleigh fading channel, i.e. $h_{ij} \sim$

$\mathcal{CN}(0,1)$[1], was considered. Also, channel matrix's elements were normalized not to affect signal's power, as it is the path loss task; thus, the constraint $\mathbb{E}\left[|h_{ij}|^2\right] = 1$ must be respected.

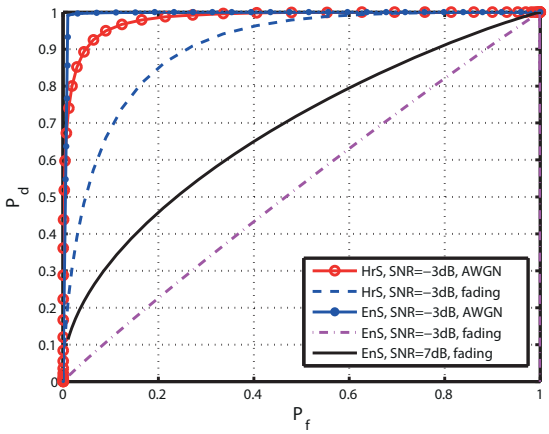

Fig. 2. ROC comparison for EnS and HrS.

For the next scenario, a wireless transmission under Rayleigh fading, path-loss and thermal noise effects will be considered as a scenario for analyzing influence of user's mobility and total number of samples used in SS. Two cases were considered: firstly a slow Rayleigh fading scenario and secondly a fast fading, where the channel is changing at every collected sample.

The performance of a HrS operating under different channel scenarios and a variable number of samples in range of $N \in [32, 1024]$ is presented on fig. 3. For this simulation experiment, the transmitting power was fixed to -20dBm, $M = 12$ antennas, $n_t = 5$ users and $d = 1000$m, which results in $SNR = 0$dB. The remaining parameters are set according to table I. Also, it is noteworthy mentioning that a *semilogx* scale has been used as an alternative to offer a better view of curves' behavior, once they would all be compacted at the upper left corner of a linear scale graphic.

Firstly, axes limits of fig. 3.a) show how HrS presents an excellent performance for slow fading cases. Additionally, the samples variation suggests the absence of an SNR wall for this case, once a small variation on sample complexity causes a minimal performance enhancement, but a double in sample complexity also doubles P_d.

A performance gap can be observed by comparing figs. 3.a) and 3.b). Despite performance degradations caused by fast fading, the HrS can still achieve a good performance even with a low number of samples. For example, at a 0dB SNR scenario, an acceptable performance for a SS device is already guaranteed with 1024

[1] $|h_{ij}|$ follows a Rayleigh distribution, while $\angle h_{ij}$ is uniformly distributed

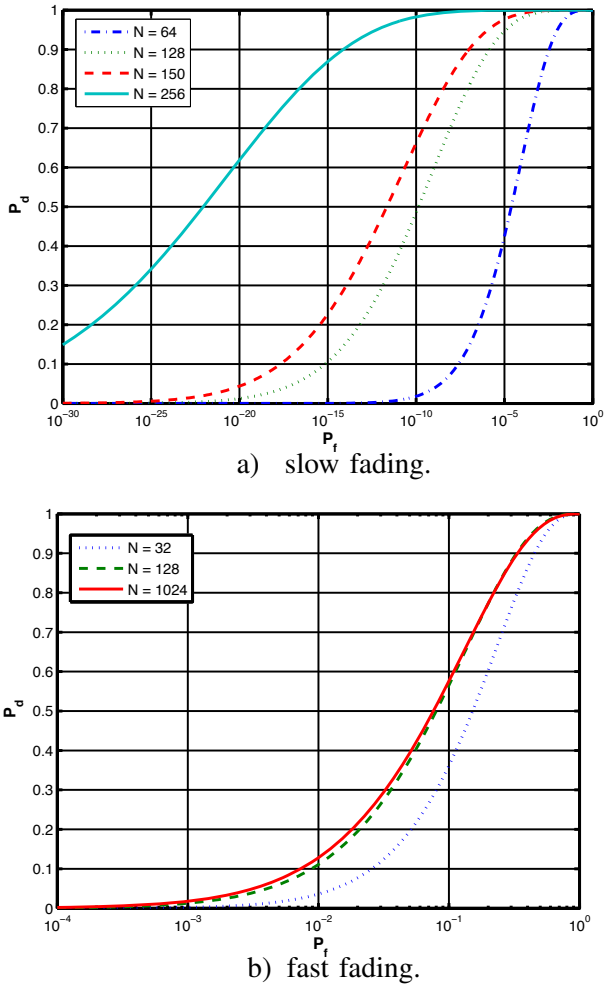

Fig. 3. ROC for a HrS with different sample complexities.

samples. Additionally, a closer look at fig. 3 suggests an SNR wall at $N \approx 128$ as performance improvements are negligible if more samples are used.

An average upper power limit of 10W for an urban cellular tower has been established by the Federal Communications Commission [16]. In case of a HrS, an average transmitting power of -10dBm was used for simulations of a sensor located 1km away; hence, HrS' performance under effect of fast fading channels, path-loss and AWGN noise interference is hold in strict accordance with requirements for realistic application scenarios, confirming the sensor's robustness for cognitive radio networks.

IV. Final Remarks

This paper aims to study a new and promising technology based on the well established likelihood theory for SS of cognitive radio networks: Hadamard ratio detector. Current literature for this technique is yet very limited, as it is based on studies of non-realistic AWGN scenarios. A few work on performance of HrS in realistic cases has

been done. Hence, an application of previous developed statistic theory was considered in this paper. Monte-Carlo simulations for HrS under Rayleigh multipath fading channels have been proceeded for wireless setups under effect of the path-loss.

Numerical results showed how basic detectors, such as EnS may de inefficient when operating in realistic scenarios. Additionally, HrS' robustness was proved via simulations of multipath fading channels, once a minimal degradation due to multiplicative effect of Rayleigh fading has been observed on performance figures of section III. Additionally, simulations considered Tx-Rx separation via inserting a model of path loss, so transmission power level limits could be tested for both EnS and HrS detectors.

A difference in performance of fast and slow fading channels was observed; however, both situations show an advantage of HrS: the low sample complexity. This first results strongly encourage us to believe HrS is prone to achieve high performance under real CRN channel scenarios. Indeed, considering realistic wireless channel scenarios (including path-loss effect with $\psi = 4$), HrS has demonstrated suitable performance in terms of ROC, achieving a $P_d \geq 0.95$ for a $P_f = 0.1$ under low number of samples in the range $128 \leq N \leq 1024$ and low signal-to-noise ratio, ranging $-3 \leq \text{SNR} \leq 0$ dB.

CR technology has been developed to allow systems to work with very low transmission power and achieve high performance levels. Even though path-loss effect showed to be harmful to CRs, power levels remain very low if compared to conventional cellular base stations and terminals. For example, according to the Federal Communications Commission, a transmission power operating with $P_t = 10\text{W}$ in urban regions is acceptable; our simulations showed that, if considering an average Tx-Rx separation $d = 1\text{km}$, spectral sensing device will operate with high level of SS detection $P_d \geq 0.9$ if PU is transmitting with $P_t \geq -20\text{dBm}$. Hence, the SS of CRs may be a technology able to significantly increase power efficiency of wireless transmissions.

Hence, this research enables many opportunities for further studies beyond optimization of cell configurations, performance of HrS in different and possibly even more realistic as well challenging CR scenarios and also identification of an optimal value of sample complexity and transmission power that enhances even more performance of CR networks.

REFERENCES

[1] G. Zhao, J. Ma, G. Li, T. Wu, Y. Kwon, A. Soong, and C. Yang, "Spatial spectrum holes for cognitive radio with relay-assisted directional transmission," *Wireless Communications, IEEE Transactions on*, vol. 8, no. 10, pp. 5270–5279, October 2009.

[2] E. Biglieri, A. Goldsmith, L. Greenstein, N. Mandayam, and H. V. Poor, *Principles of Cognitive Radio*. Cambridge, UK.: Cambridge University Press, 2012.

[3] A. G. Hernandes, R. T. Kobayashi, and T. Abrão, *Introduction to Cognitive Radio Networks and Applications*, 1st ed. Chapman and Hall/CRC Press, July 2016, ch. Spectrum Sensing Techniques in cognitive radio networks: Achievements and challenges, p. 42.

[4] J. Tugnait, "On multiple antenna spectrum sensing under noise variance uncertainty and flat fading," *Signal Processing, IEEE Transactions on*, vol. 60, no. 4, pp. 1823–1832, April 2012.

[5] L. Huang, Y. Xiao, H. C. So, and J. Fang, "Accurate performance analysis of hadamard ratio test for robust spectrum sensing," *Wireless Communications, IEEE Transactions on*, vol. 14, no. 2, pp. 750–758, Feb 2015.

[6] A. Mariani, A. Giorgetti, and M. Chiani, "Test of independence for cooperative spectrum sensing with uncalibrated receivers," in *Global Communications Conference (GLOBECOM), 2012 IEEE*, Dec 2012, pp. 1374–1379.

[7] N. Klausner, M. Azimi-Sadjadi, L. Scharf, and D. Cochran, "Space-time coherence and its exact null distribution," in *Acoustics, Speech and Signal Processing (ICASSP), 2013 IEEE International Conference on*, May 2013, pp. 3919–3923.

[8] A. Simaan M., H. Daniel W., and W. James R., "Fitting beta distributions based on sample data," in *Journal of Construction Engineering and Management*, vol. 120, no. 2, June 1994, pp. 288–305.

[9] N. L. Johnson, S. Kotz, and N. Balakrishnan, *Continuous Univariate Distributions*. Wiley-Interscience, 1995.

[10] M. T. Chao and W. E. Strawderman, "Negative moments of positive random variables," in *Journal of the American Statistical Association*, vol. 67, no. 338, June 1971, pp. 429–431.

[11] R. Lopez-Valcarce, G. Vazquez-Vilar, and J. Sala, "Multi-antenna spectrum sensing for cognitive radio: overcoming noise uncertainty," in *Cognitive Information Processing (CIP), 2010 2nd International Workshop on*, June 2010, pp. 310–315.

[12] D. Ramirez, G. Vazquez, R. Lopez Valcarce, J. Via, and I. Santamaria, "Detection of rank- p signals in cognitive radio networks with uncalibrated multiple antennas," *Signal Processing, IEEE Transactions on*, vol. 59, no. 8, pp. 3764–3774, Aug 2011.

[13] F. F. Digham, M. S. Alouini, and M. K. Simon, "On the energy detection of unknown signals over fading channels," in *Communications, 2003. ICC '03. IEEE International Conference on*, vol. 5, May 2003, pp. 3575–3579 vol.5.

[14] A. Goldsmith, *Wireless Communications*. New York, NY, USA: Cambridge University Press, 2005.

[15] G. L. Stuber, *Principles of Mobile Communication*. Springer, 2002.

[16] F. C. Commission, "Human exposure to radio frequency fields: Guidelines for cellular and pcs sites," Available at: http://transition.fcc.gov/cgb/consumerfacts/rfexposure.pdf, 2015.

A.3 Precoding Strategies in Cognitive Radio

Title:	*Efficient ZF-WF Strategy for Sum-Rate Maximization of MU-MISO Cognitive Radio Networks;*
Authors:	Lucas Claudino and Taufik Abrão;
Category:	*Full Paper*;
Publication:	submitted;

Contributions: This article brings use of optimization techniques to maximize the sum capacity of a MISO-CRN. The chosen technique is ZFWF strategy, which is already known and well studied. However, studies on cognitive radio technologies are yet recent. The main contribution of this work is not the application and development of ZFWF in this scenario. We have here developed a tool to accurately select the optimum number of secondary users to be allowed in a certain CRN in order to maximize the sum capacity. The choice of K^* is based only on the values of n_{BS} and SINR. All results showed to achieve maximum capacity using the approximations. This might be very useful when designing and controlling the network, once the BS can select the best quality links and discard the poor ones.

Int. J. Electron. Commun. (AEÜ) 84 (2018) 366–374

Contents lists available at ScienceDirect

Int. J. Electron. Commun. (AEÜ)

journal homepage: www.elsevier.com/locate/aeue

Regular paper

Efficient ZF-WF strategy for sum-rate maximization of MU-MISO cognitive radio networks

Lucas Claudino, Taufik Abrão*

Department of Electrical Engineering of Londrina State University, Paraná, Brazil

ARTICLE INFO

Keywords:
Cognitive radio
Beamforming
Precoding
Nonconvex optimization
Zero-forcing
Water filling

ABSTRACT

This article presents an efficient quasi-optimal sum rate (SR) maximization technique based on zero-forcing water-filling (ZFWF) algorithm directly applied to cognitive radio networks (CRNs). We have defined the non-convexity nature of the optimization problem in the context of CRNs while we have offered all necessary conditions to solve the related SR maximization problem, which considers power limit at cognitive transmitter and interference levels at primary users (PUs) and secondary users (SUs). A general expression capable to determine the optimal number of users as a function of the main system parameters, namely the signal-to-interference-plus-noise ratio (SINR) and the number of BS antennas is proposed. Our numerical results for the CRN performance are analyzed in terms of both BER and sum-capacity for the proposed ZF-WF precoding technique, and compared to the classical minimum mean square error (MMSE), corroborating the effectiveness of the proposed technique operating in multi user multiple input single output (MU-MISO) CRNs.

1. Introduction

The spectrum is a limited resource that, until nowadays, has been regulated in a *fixed spectrum access* form. This means that each sub-band of the total spectrum bandwidth is assigned to one specific owner (PU) who has paid for the right to transmit over these frequencies; indeed, no other user is allowed to exploit this preallocated spectrum, regardless if the PU is using it or not. The problem is that, in the past decades, wireless technologies have been significantly developed and these fixed frequency bandwidths are becoming scarce. In recent studies, regulatory commissions, such as Federal Communications Commission (FCC), have discovered that the spectrum is underutilized [1,2]. These studies reveal the need for new and more efficient schemes of spectrum management. Hence, researchers have been looking for strategies to enhance spectrum utilization efficiency. A recent technology, known as cognitive radio (CR) aims to solve the recurrent and critical spectrum scarcity problem via proposing a wireless transceiver able to interact with the environment and change its transmission parameters in order to achieve a better performance [3].

The concept of CR has been firstly introduced in [4], where the author stated that CR may be interpreted as an evolution of software defined radio (SDR), where the various SDRs present a high level of computational intelligence. Such intelligence makes them able to mimic some human cognitive behavior like observation, orientation, planning, decision and action, in order to derivate a broad view about the wireless scenario and provide appropriate wireless services.

The CR is basically a system with high environmental awareness able to dynamically access all available bandwidth. Therefore, a CR is a special radio system with two main abilities: the cognition capability and the reconfigurability [5]. Cognition of a CR is basically the ability to sense the environment and observe the spectral opportunities so the radio is able to identify the available spectrum bands. Reconfigurability is related to the fact that a CR, after estimating the bandwidth usage, is able to interactively adapt its transmissions values and plans in terms of power, bandwidth and time availability.

A typical CRN layout consists of a series of PUs coexisting harmoniously with the CR devices, namely secondary users. PUs are also known as licensed users, which are the ones who own the license to transmit over some specific bandwidth. CR basically proposes that SUs operate over the bandwidth, even though they do not hold a license. In order to do so, a series of constraints must be followed, *i.e.*, the SU may only operate when the PU is not transmitting or, in case of PU activity, the SU must not overcome an energy threshold in order not to affect the PU's transmission [5].

Some work has been done in CR scenarios regarding the SR maximization. This optimization problem is treated as a tradeoff between

* Corresponding author.
E-mail addresses: lsclaudino@gmail.com (L. Claudino), taufik@uel.br (T. Abrão).

https://doi.org/10.1016/j.aeue.2017.12.021
Received 8 August 2017; Accepted 18 December 2017

spatial multiplexing at SUs and interference avoidance at PUs in [6]. Also, authors in [6] propose sub-optimal SVD-based algorithms (Singular Value Decomposition) to maximize the sum capacity of secondary transmissions. The work in [7] proposes a weighted SR problem with solution based on iterative subgradient algorithms, once the resultant relaxed problem cannot be solved with traditional iterative water-filing techniques. Recently, a relaxed problem is proposed in [8], where all constraints are transformed into a nonnegative matrix spectral radius. This relaxation is then solved with polynomial-time iterative algorithms. Also, physical quantities are analyzed and taken into account, *i.e.* channel parameters, transmission power and achievable rates for SUs.

Recently, a linear precoder design for an underlay cognitive radio MIMO broadcast channel with multiuser interference elimination provided by zero-forcing is proposed in [9]. To develop an efficient precoder design for multiuser MIMO-CRN under interference constraints, the authors firstly apply a rank relaxation method to transform the problem into a convex problem, and then deploy a barrier interior-point method to solve the resulting saddle point problem. Solving a system of discrete-time Sylvester equations, authors demonstrated with numerical results a substantial complexity reduction compared to conventional methods. Considering the multiuser interference alignment (IA) technique, the work [10] analyses the problem of SINR decreasing due to channel conditions in IA-based CRNs, which reduce the quality of service (QoS) of PUs. In this context, the authors propose a multiuser-diversity-based IA scheme applicable to CRNs. Under small number of SUs, the authors have found that the IA network can accommodate all the users simultaneously without mutual interference; however, under large number of SUs, the IA-based CRN is not effective, being not able to accommodate all the PUs and SUs simultaneously with perfect elimination of interferences.

Recent work has dealt with MIMO-CR downlink architectures and developed a block matrix strategy to cancel interference between SUs and to PUs to keep all interference levels under a certain threshold [11]. The authors use the second order Karush-Kuhn-Tucker (KKT) conditions to design a precoder able to deal with this interference. Also, the sum rate maximization problem in CRN is examined when imperfect channel state information (CSI) is available, and come up with high computationally complex but optimal power distribution scheme.

The SR maximization problem of CRNs has been a classical problem in wireless system design [12,13]. Specifically, in [12] it was considered the weighted SR maximization problem for CRNs with multiple-SUs MIMO broadcast channel under sum power constraint and interference power constraints. Authors have shown that optimization problem is a nonconvex problem, but can be transformed into an equivalent convex MIMO multiple access channel problem. Moreover, the work in [13] deals with the optimal resource allocation problem in MIMO Adhoc CRNs; a semi distributed algorithm and a centralized algorithm based on geometric programming and network duality were introduced under the interference constraint at primary receivers, aiming obtaining a locally optimal linear precoder for the nonconvex weight SR maximization problem. It is worth to note that these SR maximization algorithms in CRNs generally result in excessive computational complexity combined to slow convergence.

This contribution is devoted to analyze an underlay MU-MISO CRN, where all SUs are equipped with a single antenna and communicate with a multiple-antenna base-station (BS). The goal is to design beamforming vectors aiming to maximize the SU's sum rate while reducing (or even avoiding) interference levels seen at all PUs. The *main contribution* of this paper consists in *combining low-complexity power allocation optimization design with a conventional precoding solution aiming to alleviate the constraints requirements* directly applicable to the maximization of CRNs SR capacity. We have provided a general fitting expression capable to determine the optimal number of users as a function of the main system parameters SINR and number of BS antennas.

The work is divided as follows. Section 2 models the CRN system scenarios, explaining basics of precoding techniques deployed in this contribution. Section 3 states the optimization problem and analyzes its convexity based on non-linear optimization theory and KKT necessary conditions. Section 4 uses the well-known zero-forcing (ZF) precoding technique to reduce the constraints and narrow down the problem to a power allocation optimization problem. For this combined strategy, we have provided a comprehensive analysis and details on the design when applied to the CRNs. Moreover, corroborative numerical results and respective analysis are presented in Section 5, demonstrating the improvement offered by the proposed combined optimization strategy in terms of sum capacity of an entire secondary network constrained by interference limits to PUs. Additionally, our numerical results also emphasize system capacity improvements upon other classical beamformer strategies, which are not designed to maximize capacity or do not intend to cancel (or alleviate) interference to PUs. Final remarks and future work are offered in Section 6.

To facilitate the readability of the paper, in the following we provide the notation and a list of symbols adopted in this work.

Notation: x represents a scalar variable, while $\mathbf{x}$ is a vector and $\mathbf{X}$ is a matrix. Hermitian matrix is denoted by $(\cdot)^H$. ∇f is the gradient of f and $\nabla^2 f$ is the respective Hessian matrix.

K	number of SUs
K^*	optimum number of SUs
$\mathscr{K}$	set of SUs
M	number of PUs
$\mathscr{M}$	set of PUs
$\mathscr{S}$	set of active SUs
n_{BS}	base station's number of antennas
I_m	interference limit to m-th PU
I_p	interference from PUs to SUs
P_{BS}	SU-BS's power constraint
$\mathscr{C}_k$	capacity of user k
φ,β	angular, linear coefficients of the linear fitting
y_k	received signal
η_k	AWGN noise
n_k	AWGN noise plus constant interference from PUs
x_k, $\mathbf{x}$	transmitted symbol (scalar) and signal vector
$\mathbf{z}_j$	PU's transmitted signal
$\mathbf{h}_k$,$\mathbf{g}_m$,$\mathbf{q}_{m,k}$	BS-SU, BS-PU, PU-SU link's channel vectors
$\mathbf{w}_k$,$\mathbf{t}_k$	general and ZF precoding vectors
$\mathbf{p}$	power allocation vector
$\mathbf{H}$,$\mathbf{G}$	SU and PU channel matrices
$\mathbf{W}$	precoding matrix
$\mathbf{F}_{-k}$	PU and SU channel matrices concatenated, except user k

2. System model

In this article a MU-MISO underlay[1] A CR system is considered, where K single antenna SUs are simultaneously transmitting with M single-antenna PUs over the same frequency bandwidth. As illustrated in Fig. 1, each k-th link between BS and k-th SU has a channel response $\mathbf{h}_k \in \mathbb{C}^{n_{\text{BS}}\times 1}$, $k \in \mathscr{K} = \{1,2,...,K\}$, $\mathbf{g}_m \in \mathbb{C}^{n_{\text{BS}}\times 1}$, $m \in \mathscr{M} = \{1,2,...,M\}$ is the channel matrix for the m-th BS-PU link, which is considered a form of interference for any PU. Also, and all PUs are considered to be constantly transmitting, their transmission signal is seen as interference at SUs; consequently, there is a channel vector $\mathbf{q}_{m,k}$ relating each m-th PU and k-th SU.

In such scenario, the secondary BS is responsible for choosing each k-th link's appropriate transmit power in order to keep all interference power under an upper limit I_m, which varies for each m-th PU. The goal

[1] Remember from the definition of underlay CR that any SINR measurement at PUs must be below a pre-determined threshold [14].

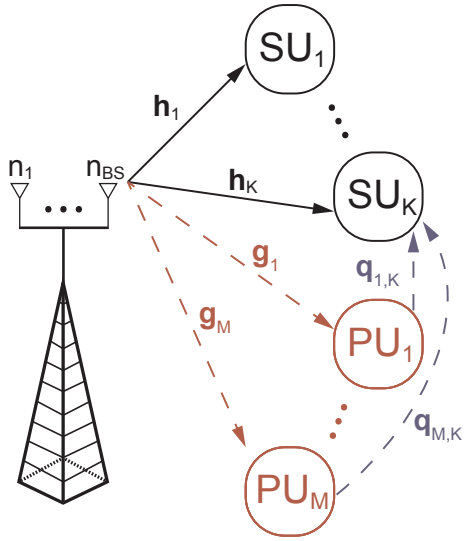

Fig. 1. Typical MISO CRN scenario.

is to maximize the sum capacity via designing an optimal SU precoding vector $\mathbf{w}_k$ attending to per-antenna and interference power constraints. Also, capacity depends on the interference level from PUs to SUs (related to channel vectors $\mathbf{q}_{\mathbf{m,k}}$), which will later be considered, for computational simplicity, a constant with average power denoted by I_p to be added to the denominator of the SINR expression.

Ideally, precoding relies on perfect CSI; hence, knowledge of $\mathbf{h}_k$ at BS is assumed. Even though this assumption is an ideal hypothesis, the problem of imperfect CSI can be neglected with the purpose of investigating the potential of new transmission schemes combining resource allocation and precoding techniques. The perfect CSI assumption has also been considered in recent contributions, including [7,9,15–17] in order to ease studies of beamforming design for CR-MU-MIMO networks.

A downlink (DL) transmission is considered, where a baseband signal $\mathbf{x}$ contains all transmitted symbols x_k and beamforming vector $\mathbf{w}_k \in \mathbb{C}^{n_{\mathrm{BS}}\times 1}$ associated to every $k \in \mathscr{K}$ SU user:

$$\mathbf{x} = \sum_{k\in\mathscr{K}} \mathbf{w}_k \mathrm{x}_k \tag{1}$$

Received signal y_k at k-th SU is then expressed as a function of the signal destined to user k plus an interference from another secondary transmissions and interference from PUs:

$$\mathrm{y}_k = \mathbf{h}_k^H \mathbf{w}_k \mathrm{x}_k + \sum_{i\in\mathscr{K},i\neq k} \mathbf{h}_k^H \mathbf{w}_i \mathrm{x}_i + \sum_{j=1}^{M} \mathbf{q}_{j,k}^H \mathbf{z}_j + \eta_k \tag{2}$$

where $\eta_k \sim \mathscr{CN}(0,\sigma_k^2)$ is the additive white Gaussian noise (AWGN) and transmitted symbols have normalized power $\mathrm{x}_k \sim \mathscr{CN}(0,1)$; so, transmitted power is set only by precoding vectors. Also, there is a transmitted signal $\mathbf{z}_j$ for all M PUs; however, SUs do not have any information about primary user characteristics or its transmitted symbols.

As mentioned before, all PUs are considered to be constantly transmitting. This is an unavoidable matter, once SUs do not have any power upon primary transmissions and must design strategies to lead with this interference. Considering that all M PUs transmit over the entire period of time, for sake of simplicity, an average interference power I_p can be used instead of calculating $\mathbb{E}\left[\sum_{j=1}^{M} (\mathbf{q}_{j,k}^H \mathbf{z}_j)^2\right]$. Hence, once this constant power interference has been considered, I_p can be incorporated into the noise term in (2) as n_k, such that $n_k \sim \mathscr{CN}(0,\sigma_k^2 + I_p)$. As a result, the received signal at k-th SU can be re-written as:

$$\mathrm{y}_k = \mathbf{h}_k^H \mathbf{w}_k \mathrm{x}_k + \sum_{i\in\mathscr{K},i\neq k} \mathbf{h}_k^H \mathbf{w}_i \mathrm{x}_i + n_k \tag{3}$$

Given the received signal in (3) and perfect channel knowledge at transmitter's side, it is possible to design a precoder to optimize the received signal in terms of power, signal integrity, QoS, bit error rate (BER) or capacity. The optimization metric chosen in this work is the sum capacity of the CRN. Indeed, the first part in this work focuses on the analysis and comparison of different precoders in terms of sum capacity.

3. Convexity analysis

The optimization problem consists of a SR maximization with respect to all SUs in the CRN, constrained by power limit at BS, P_{BS}, and a maximum interference to any PU transmission, I_m. For this case scenario, every k-th SU transmission is subject to interference from others SUs and additive noise. Hence, the SINR is defined as:

$$\gamma_k = \frac{\mathbf{h}_k \mathbf{w}_k \mathbf{w}_k^H \mathbf{h}_k^H}{\sum_{j\neq k}^{K} \mathbf{h}_k \mathbf{w}_j \mathbf{w}_j^H \mathbf{h}_k^H + \sigma_k^2 + I_p} \quad \forall\, k \in \mathscr{K} \tag{4}$$

The SR maximization problem subject to power and interference constraints is then defined as:

$$\max_{\{\mathbf{w}_1,\ldots,\mathbf{w}_K\}} \quad \sum_{k=1}^{K} \log_2(1+\gamma_k) \tag{5a}$$

$$\text{s.t:} \qquad \mathbf{w}_k^H \mathbf{w}_k \leqslant P_{\mathrm{BS}}\,, \quad \forall\, k \in \mathscr{K} \tag{5b}$$

$$\sum_{k\in\mathscr{K}} \mathbf{g}_m \mathbf{w}_k \mathbf{w}_k^H \mathbf{g}_m^H \leqslant I_m\,, \quad \forall\, m \in \mathscr{M} \tag{5c}$$

The problem in (5) is said to be convex if both cost function and inequalities constraints are convex. A few works say this is a non-convex optimization problem, however they do not prove it [16,17]. Constraints (5b) and (5c) are both quadratic functions with domain $\mathbb{R}^K \to \mathbb{R}$, which are known to be convex [18]. Hence, the problem is reduced to identifying whether (5a) is convex or not. Via composition property, given an arbitrary function $f(x) = h(g(x))$ is concave if $g(x)$ and $h(x)$ are concave and non-decreasing. Logarithmic functions are concave non-decreasing, which brings us to analyze the concavity of the γ_k expression.

A function is convex/concave if its Hessian matrix is positive/negative semidefinite. The multidimensional analysis of (5a) is quite complex; however, if the unidimensional case is proved to be non-concave, the cost function is non-concave for any dimension. In contrast, if the unidimensional case is concave, no further assumptions can be made about the multidimensional one. Let us assume:

$$f(w_k) = \frac{h_k w_k w_k^* h_k^*}{\sum_{j\neq k}^{K} h_k w_j w_j^* h_k^* + \sigma_k^2 + I_p} \tag{6}$$

then, $f(w_k)$ is concave if and only if the Hessian matrix $\mathbf{H}_f$ is negative semidefinite:

$$\mathbf{H}_f = \nabla^2 f \triangleq \begin{bmatrix} \frac{\partial^2 f}{\partial w_1^2} & \cdots & \frac{\partial^2 f}{\partial w_1 w_K} \\ \vdots & \ddots & \vdots \\ \frac{\partial^2 f}{\partial w_K w_1} & \cdots & \frac{\partial^2 f}{\partial w_K^2} \end{bmatrix} \preceq \mathbf{0} \tag{7}$$

The partial derivatives with respect to the main diagonal of $\mathbf{H}_f$ are:

$$\frac{\partial^2 f}{\partial w_k^2} = \frac{\partial}{\partial w_k}\left[\frac{2\,|\,h_k|^2 w_k}{\sum_{j\neq k}\,|\,h_k|^2\,|\,w_j|^2 + \sigma_k^2 + I_p}\right] = \frac{2\,|\,h_k|^2}{\sum_{j\neq k}\,|\,h_k|^2\,|\,w_j|^2 + \sigma_k^2 + I_p} \tag{8}$$

which are all non-negative values.

Additionally, the partial derivatives with respect to the off-diagonal elements are:

$$\frac{\partial^2 f}{\partial w_k w_j} = \frac{\partial}{\partial w_j}\left[\frac{2\,|h_k|^2 w_k}{\sum_{j\neq k}|h_k|^2|w_j|^2+\sigma_k^2+I_p}\right] = 2\,|h_k|^2 w_k \frac{-2\sum_{j\neq k} h_k w_j h_k}{\left(\sum_{j\neq k}|h_k|^2|w_j|^2+\sigma_k^2+I_p\right)^2} = -\frac{4\,|h_k|^4 w_k \sum_{j\neq k} w_j}{\left(\sum_{j\neq k}|h_k|^2|w_j|^2+\sigma_k^2+I_p\right)^2} \tag{9}$$

Analysis of (9) shows that the Hessian matrix is non symmetric:

$$\frac{\partial^2 f}{\partial w_1 w_2} = -\frac{4\,|h_1|^4 w_1 \sum_{j\neq 1} w_j}{\left(\sum_{j\neq 1}|h_1|^2|w_j|^2+\sigma_1^2+I_p\right)^2} \neq \frac{\partial^2 f}{\partial w_2 w_1} = -\frac{4\,|h_2|^4 w_2 \sum_{j\neq 2} w_j}{\left(\sum_{j\neq 2}|h_2|^2|w_j|^2+\sigma_2^2+I_p\right)^2} \tag{10}$$

A simple property is that, a negative semidefinite matrix has all its eigenvalues smaller or equal to zero. If a matrix is not symmetric, then its eigenvalues are not necessarily in $\mathbb{R}$; hence, this matrix is not negative semidefinite [19].

Additionally, numerical simulations aiming to corroborate this fact have been proceeded. A set of matrices with negative main diagonal and complex-normally distributed off-diagonal elements has been generated. Indeed, some of such matrices showed to have both positive and negative eigenvalues, which corroborates that the Hessian matrix of γ_k, Eq. (4), is not negative semidefinite.

3.1. KKT necessary conditions and absence of closed expression

Convex problems can be straightforwardly solved applying KKT necessary conditions. Indeed, a possible optimal point $\mathbf{w}_k^*$ would be found setting the derivative of the Lagrangian of the problem (5) to zero, where the Lagrangian is defined in Eq. (11).

$$\mathscr{L}(\mathbf{w}_k,\lambda_k,\mu_m) = \sum_{k=1}^{K}\log_2(1+\mathrm{SINR_k}) - \sum_{k=1}^{K}\lambda_k\left(\frac{\mathbf{w}_k\mathbf{w}_k^H}{P_{\mathrm{BS}}}-1\right) - \sum_{m=1}^{M}\frac{\mu_m}{I_m}\left(\sum_{k=1}^{K}\mathbf{g}_m\mathbf{w}_k\mathbf{g}_m^H\mathbf{w}_k^H-1\right) \tag{11}$$

Similar to [17], gradient of the Lagrangian can be set to zero as in Eq. (12), where λ_k and μ_m are the Lagrange multipliers. Inspection of (12) shows that all three terms depend on the optimization variable $\mathbf{w}$, which makes it impractical to find a close expression for the optimum precoding vector solution. Hence, herein we prefer to elaborate iterative methods to find near-optimum solutions.

$$\frac{\partial\mathscr{L}(\mathbf{w}_k,\lambda_k,\mu_m)}{\partial\mathbf{w}_k^*} = \frac{q_k^*\mathbf{h}_k^H}{\ln(2)} - \sum_{j\neq k}\frac{q_j\omega_j q_j^*\mathbf{h}_j^H\mathbf{h}_j\mathbf{w}_k}{\ln(2)} - \frac{\lambda_k\mathbf{w}_k}{P_{\mathrm{BS}}-\sum_{m=1}^{M}\frac{\mu_m}{I_m}\mathbf{g}_m^H\mathbf{g}_m\mathbf{w}_k} = \mathbf{0} \tag{12}$$

where $q_k = e_k d_k^{-1}\mathbf{w}_k^H\mathbf{h}_k^H$, $e_k = (1+\mathbf{h}_k\mathbf{w}_k\mathbf{w}_k^H\mathbf{h}_k^H d_k^{-1}) = \omega_k^{-1}$, $d_k = \sum_{j\neg k, j\in\mathscr{K}}\mathbf{h}_k\mathbf{w}_j\mathbf{w}_j^H\mathbf{h}_k^H$

4. Zero-forcing water filling precoding

It this section a mixed technique known as ZFWF precoding is analyzed for MU-MISO systems. ZF is largely applied to MU-MISO networks due to its facility of design beamforming vectors for the kth user, $\mathbf{t}_k$, such that users receive interference free signals due to orthogonality between beamforming vectors of different users. In CR scenarios, ZF is able to provide a design that eliminates interference between distinct SUs. Herein, a suboptimal ZF solution for problem (5) is considered as a strategy of interference canceling for both classes of users, SUs and PUs.

The beamforming vector is divided into power allocation (p_k) and interference cancellation ($\mathbf{t}_k$) parts:

$$\mathbf{w}_k = \sqrt{p_k}\mathbf{t}_k \tag{13}$$

Interference canceler vector $\mathbf{t}_k$ is designed such that it is simultaneously orthogonal to the ith SU and mth PU channel vectors:

$$\mathbf{h}_i^H\mathbf{t}_k = 0\,, \qquad \forall\, i,k\in\mathscr{K},\quad i\neq k \tag{14a}$$

$$\mathbf{g}_m^H\mathbf{t}_k = 0\,, \qquad \forall\, m\in\mathscr{M} \tag{14b}$$

Let us concatenate all SU and PU channel vectors, except the kth SU channel vector, as a matrix: $\mathbf{F}_{-k}\triangleq\{\mathbf{g}_1,\ldots,\mathbf{g}_M,\mathbf{h}_1,\ldots,\mathbf{h}_{k-1},\mathbf{h}_{k+1},\ldots,\mathbf{h}_K\}\in\mathbb{C}^{n_{\mathrm{BS}}\times(M+K-1)}$. The interference free constraint is then re-written as $\mathbf{F}_{-k}^H\mathbf{t}_k=\mathbf{0}$; indeed, $\mathbf{t}_k$ should be designed to lie on the null-space of $\mathbf{F}_{-k}$. This assumption will simplify the original problem in (5) such that (5c) is eliminated, once the beamforming vector design guarantees zero interference from SUs to PUs. Additionally, $\mathbf{p}=[p_1,\ldots,p_k]$ is solution to the simplified decoupled power allocation problem. Even though the original problem was proved to be non-convex, the interference-free constraint imposed by the ZFWF precoder simplifies the SINR expression and, from (9), setting the multiplication $w_j h_k = 0$,$\forall\, j\neq k$, all off-diagonal elements become zero. Indeed, the Hessian matrix has its main diagonal elements greater or equal zero and the off-diagonal equal zero, what is characteristic of a positive semidefinite matrix.

Under such assumptions, the optimization problem is simply re-written as:

$$\max_{\{\mathbf{t}_k\},\mathbf{p}} \quad \sum_{k=1}^{K}\log_2(1+\gamma_k) \tag{15a}$$

$$\text{s.t:} \quad \sum_{k=1}^{K} p_k\mathbf{t}_k^H\mathbf{t}_k \leqslant P_{\mathrm{BS}}\,, \quad \forall\, k\in\mathscr{K} \tag{15b}$$

$$\mathbf{F}_{-k}^H\mathbf{t}_k = \mathbf{0} \tag{15c}$$

(1) When $(M+K-1) < n_{\mathrm{BS}}$,$\mathrm{rank}(\mathbf{F}_{-k}) < n_{\mathrm{BS}}$; consequently, $\mathbf{F}_{-k}^H\mathbf{t}_k=\mathbf{0}$,$\forall\, k$ presents an infinite number of solutions, including the optimal $\mathbf{W}^*=\mathbf{T}\cdot\mathrm{diag}(\sqrt{\mathbf{p}^*})$, where $\mathbf{T}$ is the classical ZF solution: $\mathbf{T}^*=\mathbf{T}'(\mathbf{T}'\mathbf{T}'^H)^{-1}$, where $\mathbf{T}'=(\mathbf{I}-\mathbf{G}^H\mathbf{G})\mathbf{H}^H$ and $\mathbf{p}^*$ is an optimal power allocation. Note that is the collection of all downlink BS-SU channel vectors and $\mathbf{G}=[\mathbf{g}_1,\ldots,\mathbf{g}_M]$ refers to downlink BS-PU power linkage link.

(2) When $(M+K-1) > n_{\mathrm{BS}}$,$\mathrm{rank}(\mathbf{F}_{-k}) = n_{\mathrm{BS}}$ and $\mathbf{F}_{-k}\mathbf{t}_k=\mathbf{0}$ only has the trivial solution $\mathbf{t}_k^*=\mathbf{0}$, which implies that all SUs are deactivated. In order to avoid this effect, we will ensure that a subset $\mathscr{S}\subset\mathscr{K}$ of active SUs is used to keep $(M+K-1) < n_{\mathrm{BS}}$.

Once the maximum number of users is respected, the problem is further narrowed down to an optimal power allocation problem, based on the ZF solution given by the pseudo-inverse matrix of the channel matrix:

$$\max_{\mathbf{p}\geq 0} \quad \sum_{k\in\mathscr{S}}\log_2(1+\gamma_k) \tag{16a}$$

$$\text{s.t:} \quad \sum_{k\in\mathscr{S}} p_k\,|\mathbf{t}_k^*|^2 \leqslant P_{\mathrm{BS}} \tag{16b}$$

which solution is already known as WF solution:

$$p_k = \frac{1}{b_k}[\mu-b_k]^+, \quad \text{with } \mu \text{ such that } \sum_{k\in\mathscr{S}}[\mu-b_k]^+ = P_{\mathrm{BS}} \tag{17}$$

where μ is the water level, b_k denotes the k-th diagonal element of $(\mathbf{H}\mathbf{H}^H)^{-1}$, and the operator $[\cdot]^+=\max\{0,\cdot\}$.

5. Numerical results

Section 4 presented an alternative suboptimal solution to the sum capacity initial problem, where a ZFWF manipulation eliminates the

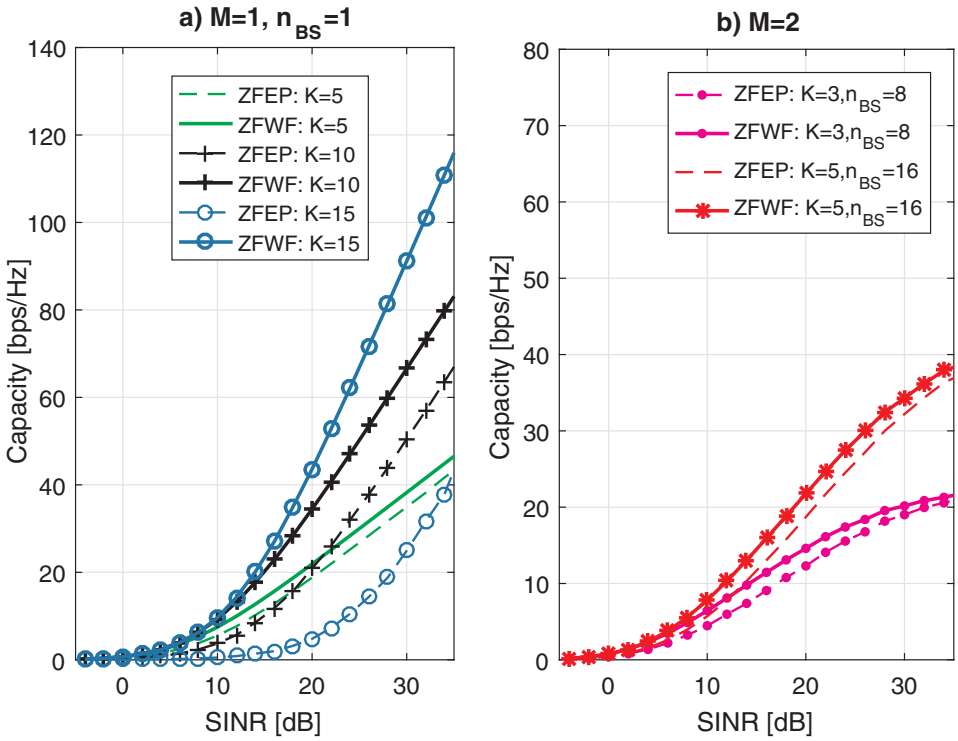

Fig. 2. Sum capacity for ZFWF and ZFEP power allocation schemes.

interference constraint inherent to the original optimization problem, while reducing the overall optimization problem to a power allocation strategy, which can be straightforwardly and optimally solved via water filling algorithm.

This section analyses numerical results comparing BER and sum capacity figures-of-merit taking into account different CRN configurations. In the numerical simulations we have considered 4-QAM transmission, varying the number of PUs, SUs and n_{BS}, short-term fading, while the interference from PUs to SUs was fixed to $I_p = 0$ dB. Monte Carlo simulations with 10^6 realizations were proceeded in order to guarantee a confidence interval of 98% and relative error of 5% [20].

5.1. Capacity comparison

The proposed precoding technique is intended to optimize the sum-capacity of the SUs class in a MISO-CRN subject to power and interference constraints. Numerical results in this subsection are devoted to demonstrate the efficiency and effectiveness of the proposed near-optimal ZFWF precoding-based transmission design. Fig. 2 compares the sum capacity of a CRN with different number of primary (M) and secondary (K) users and BS antennas for two power allocation strategies: the ZFWF proposed in Section 4 and a ZF with *equal power allocation* (ZFEP), where every antenna transmits with the same power, $P_{\text{BS}}/n_{\text{BS}}$. All network specifications are depicted in Table 1. In both cases the ZF strategy was used to eliminate interference from SU to others cognitive users and to PUs. Our numerical results corroborate that water filing power allocation strategy plays an important role in capacity enhancement of SUs. This fact is observed by the wide gap between ZFEP and ZFWF curves in all simulated scenarios. As expected, increasing the number of SUs or antennas at BS also reflects in sum-capacity grow, which is expected once the algorithm has optimized the sum capacity of a secondary network subject to the interference constraint.

Furthermore, increasing the number of PUs from $M = 1$ to $M = 2$ (Fig. 2b) will decrease the sum capacity of the secondary network, once SUs have to limit their transmission to avoid degrading all primary transmissions. It is observed in red and magenta curves, which didn't present the same slope as the other curves for high SINR values in Fig. 2a). This fact is also due to the interference I_p overall secondary transmission. Once there are more than one PU transmitting over the band, this fixed interference is also greater, and SUs do not have how to avoid it.

Table 1
Reference values used for simulation scenario 1.

Parameter	Value
SINR	$\gamma \in [-15, 35]$ dB
SUs	$K \in \{3, 5, 10, 15\}$
PUs	$M \in \{1, 2\}$
CR-BS antennas	$n_{\text{BS}} \in \{8, 16\}$
PU interference	$I_p = 0$ dB
Modulation	4-QAM

5.2. Optimum number of secondary users in a CRN

A CR network is unique in terms of spectrum management and interference limits. As seen before, an underlay CR has strict interference thresholds and scarce transmission power. As a consequence, these constraints pose an important role in capacity of CR scenarios. In order to achieve greater capacity, the SU has to increase power or spacial diversity (more users or antennas at the BS). However, the presence of PUs limits this capacity enhancement. Differently from conventional MIMO systems, a CRN does not presents an unlimited increase in capacity when more users/antennas are transmitting.

In order to illustrate this phenomenon, a simulation varying n_{BS} and number of single antenna SUs was carried out for different values of SINR. The result is plotted if Fig. 3 and clearly expresses the existence of an optimal point for the number of users according to each n_{BS} configuration. This effect is explained by two major factors. Firstly, as K and n_{bs} increase, the dimension of $\mathbf{F}_{-k}$ also increases; as a consequence, there exists fewer solutions that guarantee a precoding matrix lying in the null space of $\mathbf{F}_{-k}$ and the ZF algorithm is not able to completely null the interference. Secondly, as SUs are generally low-cost, low-power radios, when K increases, an unavailable amount of transmission power is

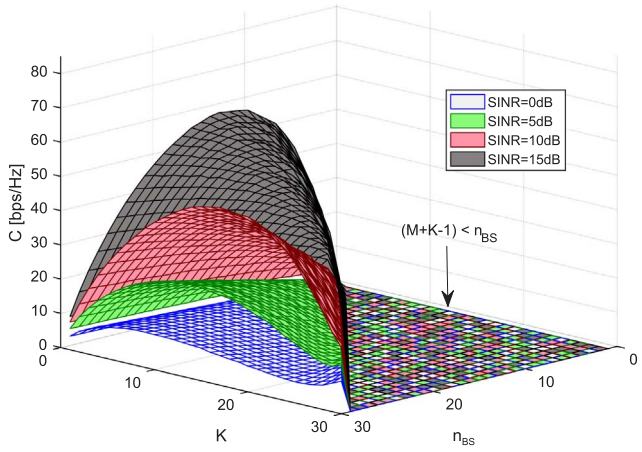

Fig. 3. Capacity dependency on K and n_{BS}.

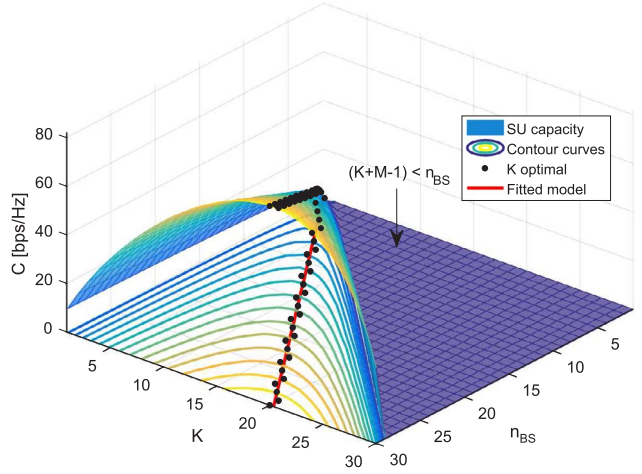

Fig. 4. Sum capacity for a CR network with varying K and n_{BS} and $\gamma = 15$ dB.

required to guarantee quality communication for all users, which ends up reducing the secondary sum capacity.

All cases in Fig. 3 presented a peak capacity dependent on K and n_{BS}. In real scenarios, the cognitive BS has a fixed number of transmitting antennas; however, it is possible to choose an adequate number of SUs aiming to maximize the sum capacity of the secondary network while guaranteeing the primary interference constraint. In order to do so, we have created a fitted model to approximate and ease the decision of how many SUs should be allowed to transmit in a certain CR network. The contour curves and maximum capacity points depicted in Fig. 4 confirms a linear dependence between K and n_{BS} to achieve the maximal sum-capacity of SUs network, $\mathscr{C}_{max}$. Hence, the fitted curve for the best number of users is obtained for a specific SINR:

$$K^* = 0.6712 \cdot n_{BS} + 0.2299, \qquad @\gamma = 15\ [\text{dB}] \tag{18}$$

where K^* is the number of SUs that maximizes sum capacity of a certain number of base station antennas, for an specific operating SINR network value.

Notice that all linear fittings of K^* are dependent on SINR; as a consequence, there will exist one different equation for every desired SINR, as follows:

$$\begin{aligned} K^* &= 0.3071 \cdot n_{BS} + 0.5429, \qquad @\gamma = 0\ [\text{dB}] \\ K^* &= 0.5357 \cdot n_{BS} + 0.3143, \qquad @\gamma = 8\ [\text{dB}] \\ K^* &= 0.6893 \cdot n_{BS} + 0.2190, \qquad @\gamma = 16\ [\text{dB}] \\ K^* &= 0.8143 \cdot n_{BS} - 0.0476, \qquad @\gamma = 24\ [\text{dB}] \end{aligned}$$

Our main goal is to identify a general equation relating K^*,n_{BS} and SINR. Once K^* is a linear equation regarding the number of antennas n_{BS}, we can write:

$$K^*(\gamma, n_{BS}) = \varphi(\gamma) \cdot n_{BS} + \beta(\gamma) \tag{19}$$

where the angular coefficient (φ) and the constant term β have to be estimated as a function of SINR and number of antennas. Fig. 5 illustrates the estimation method for φ and β.

As observed in Fig. 5 both coefficients behave log-exponentially according to SINR, which allows us to make use of an exponential fitting with SINR γ being the independent variable:

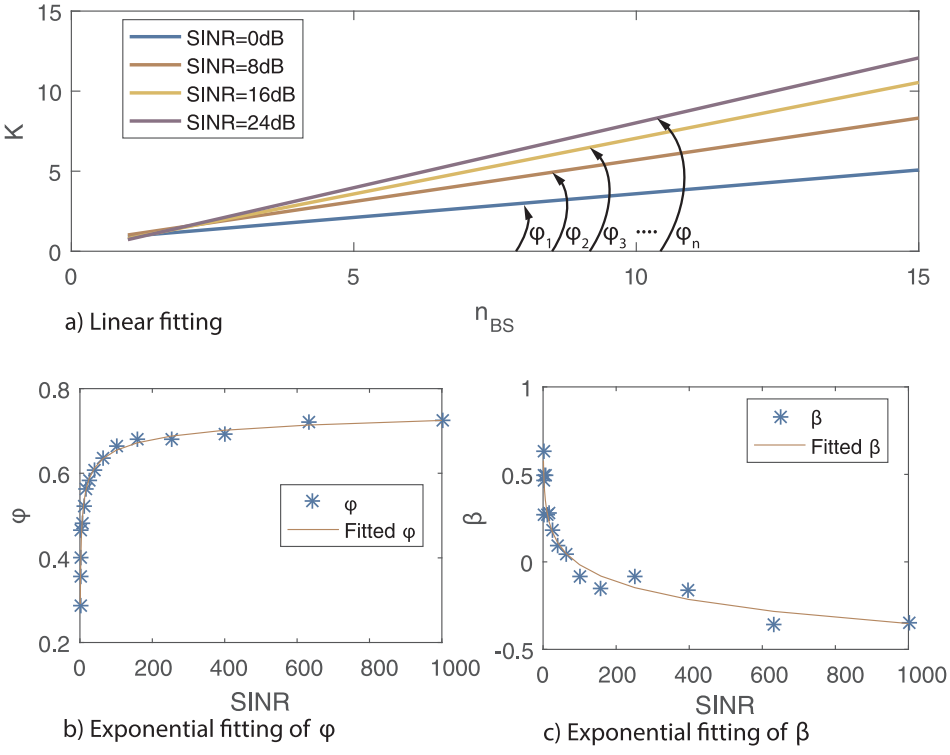

Fig. 5. Exponential fitting procedure to estimate parameters φ and β.

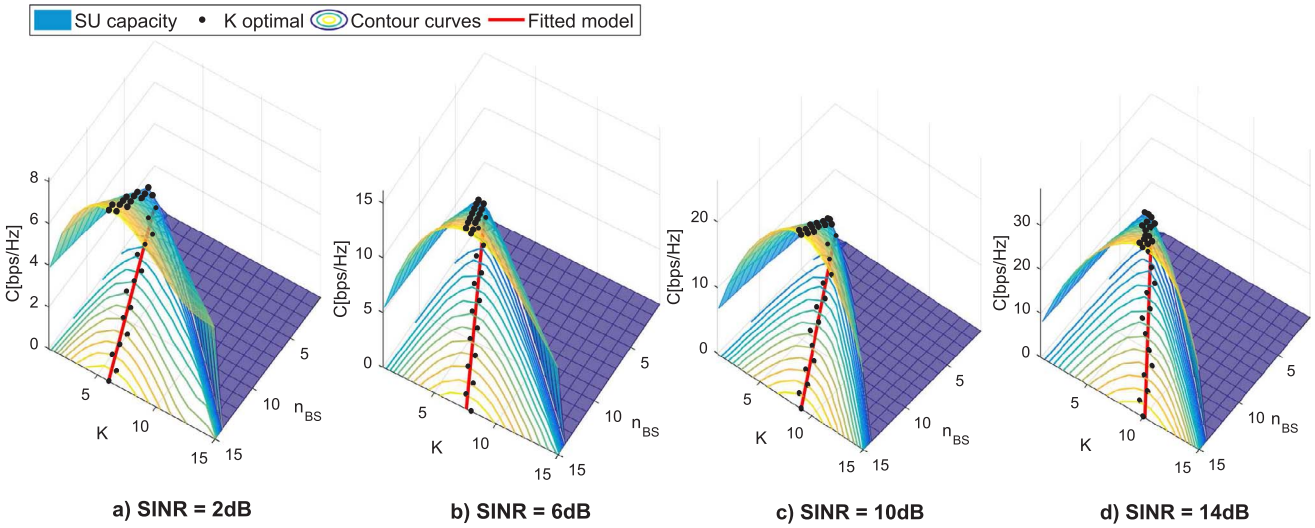

Fig. 6. Evaluating the consistence of the proposed fitting expression for K optimum.

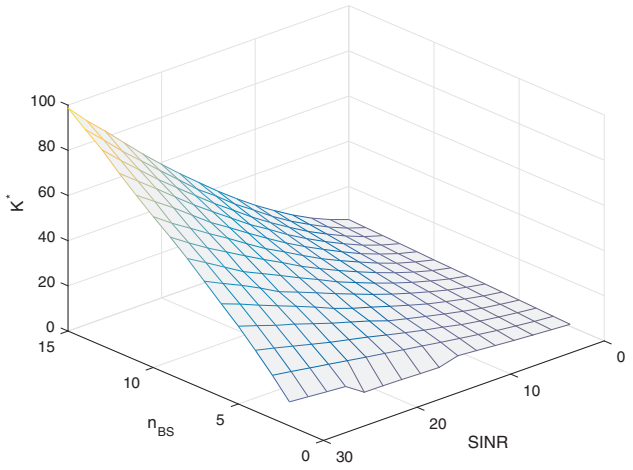

Fig. 7. Maximum SR capacity of a CRN is achieved with the optimum number of SUs, K^*.

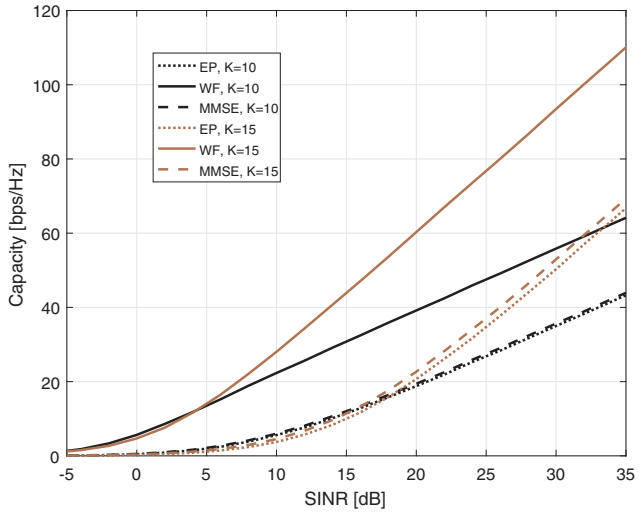

Fig. 8. Sum rate capacity for ZF and MMSE beamforming techniques. $K = 10$ and $K = 15$ SUs.

Table 2
Reference values used for simulation scenario 2.

Parameter	Value
SINR	$\gamma \in [-5, 35]$ dB
SUs	$K \in \{10, 15\}$
PUs	$M = 1$
CR-BS antennas	$n_{BS} = 16$
PU interference	$I_p = 0$ dB
Modulation	4-QAM

$$\varphi(\gamma) = a_1 \cdot \gamma^{b_1} + c_1 \tag{20}$$

$$\beta(\gamma) = a_2 \cdot \gamma^{b_2} + c_2 \tag{21}$$

By applying an exponential fitting procedure on the data of Fig. 5, we are able to estimate the parameters a_n, b_n, and c_n of (20) and (21):

$\varphi(\gamma)$	$\beta(\gamma)$
$a_1 = -0.5189$	$a_2 = -3.2938$
$b_1 = -0.2608$	$b_2 = 0.0360$
$c_1 = 0.8107$	$c_2 = 3.8715$

Finally, the number of SUs that maximize the SR capacity of CRN for a given n_{BS} and γ configuration can be suitably approximated by the following expression:

$$\begin{aligned} K^*(\gamma, n_{BS}) &= \tan[\varphi(\gamma)] \cdot n_{BS} + \beta(\gamma) \\ &= \tan(-0.5189 \cdot \gamma^{-0.2608} + 0.8107) n_{BS} - 3.2938 \cdot \gamma^{0.0360} + 3.8715 \end{aligned} \tag{22}$$

To evaluate the consistence of (22), Fig. 6 depicts surfaces of the sum-capacity obtained with ZFWF algorithm and its optimum number of SUs obtained via (22).

The last analysis aiming to completely understand *how to choose the adequate number of SUs, i.e.,* optimum number of SUs in terms of maximum achievable SR capacity for a given SINR and number of available antennas, can be checked from the surface plotting of $K^* \times n_{BS} \times$ SINR in Fig. 7. The result of this subsection consists in simulating the sum capacity optimization problem as previously explained and, for every chosen n_{BS} and SINR, finding the correspondent K^* that maximizes the SR capacity in CRNs.

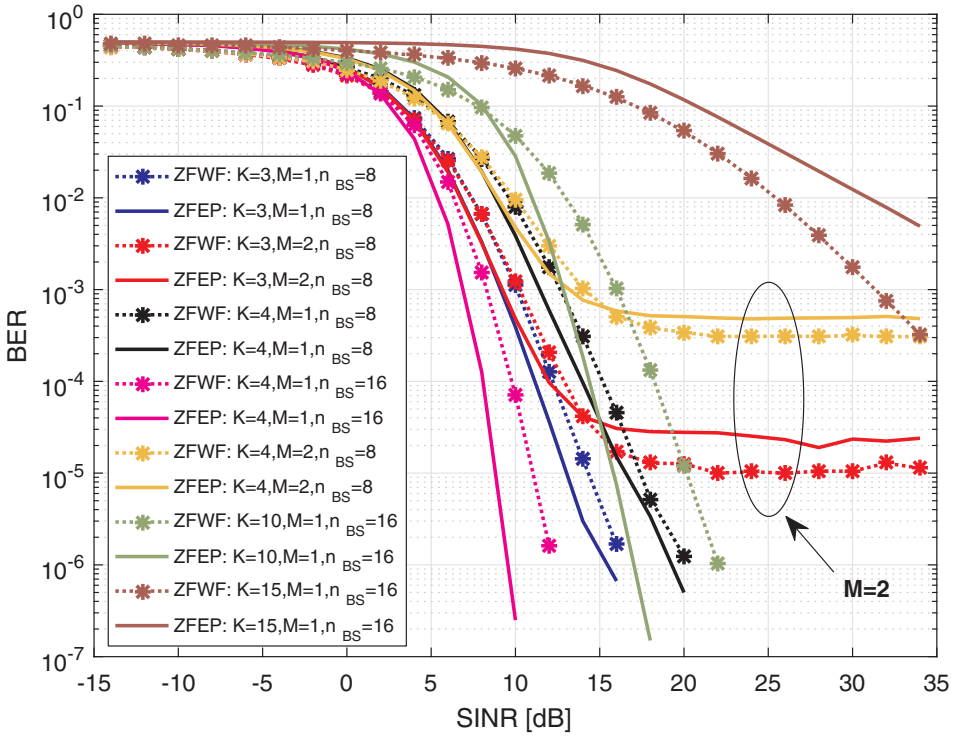

Fig. 9. BER for ZFWF and ZFEP power allocation schemes with $M = 1$ and $M = 2$ PUs.

5.3. MMSE precoder comparison

Even though ZFWF technique has proved to be efficient for capacity maximization, it is known that ZF precoding strategy usually results in high BER figures. A strategy known due to its excellent performance in terms of BER is the MMSE precoding. Other precoding techniques have been studied to enhance performance of CRN, like MMSE-based precoders [21,22], or even more recent precoding strategies, such as *bivariate probabilistic constrained programming* (BPCP) [23] and *leakage rate limiting* (LRL) precoding strategy [24].

MMSE-based precoding techniques are known to present lower BER figures if compared to many other strategies. The following results fairly compare the proposed ZF technique and a MMSE-based precoder. This simulation aims to design a precoder that minimizes the MSE for a given CRN configuration [22] and, as a consequence, presents lower bit error rates. However, techniques in [21,22] are not created to maximize capacity, and there is no optimal power allocation in this sense. Fig. 8 firstly confirms that ZFWF is more efficient in terms of sum capacity than MMSE-based strategy for CR network configurations presented in Table 2.

As expected, the water filling algorithm – which is a valid application for this scenario only if combined to ZF channel cancellation – presents significant improvements in terms of sum capacity maximization, as seen in Fig. 8. Specially if greater spatial diversity is exploited via increasing the number of antennas at SU-BS. The case of more SUs is also a form of increasing sum capacity. A secondary network with $K = 10$ and $K = 15$ SUs has been evaluated. However, increase in number of SUs also affects the BS's power limit. Additionally, more SUs in the same network end up reducing the null space in which the ZF precoding matrix must lie on, which may difficult the solution and, as SINR increases, inter user interference is also prone to increase as well.

The greater difference from ZF to MMSE-based techniques is the capacity enhancement when water filing power allocation is applied, which is valid only if combined to ZF interference cancellation; indeed, there is not much improvement to be done in MMSE-based precoders in terms of SR gain. This difference is seen in both scenario configurations of Fig. 8, once both ZFEP and MMSE-based curves present almost the same results, while ZFWF shows much greater capacity.

5.4. Bit error rate comparison

The proposed ZFWF beamforming technique is a quasi-optimal solution; also, ZF is known not to completely cancel interference is some cases. As a consequence, given the increase in capacity, some detection error may appear and BER figure-of-merit is an interesting choice to analyze the performance of a transmission system. Fig. 9 presents results of BER for several system configurations. Note that, even though ZFWF was designed to optimize capacity, it also minimally affects BER, once ZFWF has slightly smaller BER for all cases. Also, increase in number of SUs or n_{BS} affects BER performance. As expected, a higher SU spatial diversity reflects in greater BER values, as seen from the overall separation between the case with $K = 15$ users and $n_{BS} = 16$ from all other curves.

A BER floor is seen in curves with more than one PU. This is due to the fact that PUs consist of a strong interference to secondary transmissions, and this in an unavoidable matter. Once PUs have priority in any CR transmission, if one or more PUs wish to start transmitting over a certain frequency, SUs just have to learn how to deal with it. In order to do so, SUs must limit its transmission power and try to filter out PUs's signals. As a consequence, the extra power needed to keep low BER levels has to be controlled and BER floors unavoidably appear. However, active interference cancellation techniques can be used if lower BER values are required for networks with more than one PU.

6. Final remarks

This article was firstly intended to present a consistent mathematical demonstration of convexity analysis for the SR maximization problem of broadcast (DL) underlay MISO cognitive networks. We have applied the ZFWF as a sub-optimal solution to maximize the SUs' capacity while minimally interfering on primary transmissions. Our numerical results firstly compared and widely corroborated the superiority of the proposed beamforming technique regarding the ZF

combined to the equal power allocation approach. Even though the precoding was designed to maximize sum capacity, numerical results demonstrated that both power allocation strategies, when applied to some CR-MISO scenario, result in similar performance; however, results are more expressive when greater spatial diversity is employed. Under higher spatial diversity scenarios, the interference plays such an important role in CRNs capacity and BER performance; indeed, even with optimal power allocation techniques, the capacity is very limited by the interference term in SINR expression. Numerical results for bit error rate have evidenced that, for this case, sum capacity optimization implies in BER performance loss.

Comparison ZFWF, ZFWP and MMSE precoding techniques showed that, power allocation alone brings some benefits to overall network capacity, but BER is still strongly affected, depending on the system SU and PU configuration. BER performance results for all simulated cases indicated that, apart from highlighting which technique presents better results, an expressive BER floor is seen when more than one PU is present (increasing and unavoidable interference). This fact is explained not only by the power limit constraint imposed to the sum capacity optimization problem but also by the increase in interference caused by PUs, once this is an unavoidable matter.

The comparison of ZF and MMSE-based precoding techniques has confirmed that a great advantage is obtained when ZF interference cancellation is applied: the possibility of dealing with independent channels and, consequently, application of water filing power allocation to achieve much greater SR for a given secondary network configuration.

An important result unveiled in this article is the linear dependence between K and n_{BS} to achieve maximum SR for SUs in a MU-MISO network. The approximation here suggested has a rooted MSE equals to 0.29, which gives us a fair estimation of the optimal number of SUs for a given architecture of CR-BS. Also, an extended dependency between K^* and SINR was established. Our numerical results allowed us to propose an exponential approximation of φ and β to achieve an expression relating K^*,n_{BS} and SINR. This result offers a simple and effective procedure to find the optimal number of SUs that can be allocated to a certain cognitive radio network.

Acknowledgement

This work was supported in part by the National Council for Scientific and Technological Development (CNPq) of Brazil under Grant 304066/2015-0.

Appendix A. Supplementary material

Supplementary data associated with this article can be found, in the online version, at http://dx.doi.org/10.1016/j.aeue.2017.12.021.

References

[1] Force SPT. Comments of the telecommunications industry association. Washington (DC): Federal Communications Commission; November 2002. ET Docket 02-135.
[2] Datla D, Wyglinski AM, Minden GJ. A spectrum surveying framework for dynamic spectrum access networks. IEEE Trans Veh Technol 2009;58(8):4158–68.
[3] Commission FC. Notice of proposed rule making and order. Washington (DC): FCC; December 2003. ET Docket 03-322.
[4] Mitola J, Maguire GQ. Cognitive radio: making software radios more personal. IEEE Pers Commun 1999;6(4):13–8.
[5] Ahmed Khattab MBA, Perkins Dmitri. Cognitive radio networks: from theory to practice. 1st ed. Analog circuits and signal processing New York: Springer-Verlag; 2013.
[6] Zhang R, Liang YC. Exploiting multi-antennas for opportunistic spectrum sharing in cognitive radio networks. IEEE J Sel Top Signal Process 2008;2(1):88–102.
[7] Zhang L, Xin Y, Liang Yc. Weighted sum rate optimization for cognitive radio mimo broadcast channels. IEEE Trans Wireless Commun 2009;8(6):2950–9.
[8] Zheng L, Tan CW. Maximizing sum rates in cognitive radio networks: convex relaxation and global optimization algorithms. IEEE J Sel Areas Commun 2014;32(3):667–80.
[9] Nguyen VD, Tran LN, Duong TQ, Shin OS, Farrell R. An efficient precoder design for multiuser mimo cognitive radio networks with interference constraints. IEEE Trans Veh Technol 2017;66(5):3991–4004.
[10] He Y, Yin H, Zhao N. Multiuser-diversity-based interference alignment in cognitive radio networks. AEU – Int J Electron Commun 2016;70(5):617–28 Available: <http://www.sciencedirect.com/science/article/pii/S1434841116300346> .
[11] Turki I, Kammoun I, Siala M. Beamforming design and sum rate maximization for the downlink of underlay cognitive radio networks. In: 2015 International wireless communications and mobile computing conference (IWCMC); Aug 2015. p. 178–83.
[12] Zhang L, Xin Y, Liang YC. Weighted sum rate optimization for cognitive radio mimo broadcast channels. IEEE Trans Wireless Commun 2009;8(6):2950–9.
[13] Kim SJ, Giannakis GB. Optimal resource allocation for mimo ad hoc cognitive radio networks. IEEE Trans Inf Theory 2011;57(5):3117–31.
[14] Biglieri E, Goldshimith AJ, Greenstein LJ. Principles of cognitive radio. Cambridge (UK): Cambridge University Press; 2012.
[15] Nguyen HV, Nguyen V-D, Kim HM, Shin O-S. A convex optimization for sum rate maximization in a mimo cognitive radio network. In: 2016 Eighth international conference on ubiquitous and future networks (ICUFN); July 2016. p. 495–7.
[16] He YY, Dey S. Sum rate maximization for cognitive miso broadcast channels: beamforming design and large systems analysis. IEEE Trans Wireless Commun 2014;13(5):2383–401.
[17] Gallo L, Negro F, Ghauri I, Slock DTM. Weighted sum rate maximization in the underlay cognitive miso interference channel. In: 2011 IEEE 22nd international symposium on personal, indoor and mobile radio communications; Sept 2011, p. 661–5.
[18] Stephen Boyd LV. Convex optimization. Cambridge University Press; 2004.
[19] Bhatia R. Positive definite matrices. 1st ed. Princeton series in applied mathematics Princeton University Press; 2007.
[20] Balaban P, Jeruchim MC, Shanmugan KS. Simulation of communication systems. 3rd ed. Technology & engineering Springer; 2012.
[21] Lee KJ, Lee I. MMSE based block diagonalization for cognitive radio mimo broadcast channels. IEEE Trans Wireless Commun 2011;10(10):3139–44.
[22] Zhou J, Thompson J. Linear precoding for the downlink of multiple input single output coexisting wireless systems. IET Commun 2008;2(6):742–52.
[23] Law KL, Masouros C, Pesavento M. Transmit precoding for interference exploitation in the underlay cognitive radio Z-channel. IEEE Trans Signal Process 2017;65(14).
[24] Al-Ali MH, Ho KC. Robust transmit precoding for underlay mimo cognitive radio with interference leakage rate limit. In: 2016 IEEE international conference on acoustics, speech and signal processing (ICASSP); March 2016. p. 3001–5.

A.4 Linear Minimum Mean Squared Error channel estimator derivation

Consider a SISO transmission where N pilot symbols are transmitted. The received signal is $\mathbf{y} \in \mathbb{C}^{N\times 1}$. The LMMSE estimator $\hat{h} = \mathbf{c}^H\mathbf{y}$, whith $\mathbf{c} \in \mathbb{C}^{1\times N}$, is a weighted linear combination of received signals and the vector $\mathbf{c}$ is such that minimizes the mean squared error $\epsilon = \mathbb{E}\left\{\left(\hat{h}-h\right)^2\right\}$.

The MSE is written as:

$$\begin{aligned}
\epsilon &= \mathbb{E}\left\{\left(\hat{h}-h\right)^2\right\} = \mathbb{E}\left\{\left(\mathbf{c}^H\mathbf{y}-h\right)^2\right\} \\
&= \mathbb{E}\left\{\left(\mathbf{c}^H\mathbf{y}-h\right)\left(\mathbf{c}^H\mathbf{y}-h\right)\right\} = \mathbb{E}\left\{\left(\mathbf{c}^H\mathbf{y}-h\right)\left(\mathbf{c}^H\mathbf{y}-h\right)^H\right\} \\
&= \mathbb{E}\left\{\left(\mathbf{c}^H\mathbf{y}-h\right)\left(\mathbf{y}^H\mathbf{c}-h\right)\right\} = \mathbb{E}\left\{\mathbf{c}^H\mathbf{y}\mathbf{y}^H\mathbf{c} - \mathbf{c}^H\mathbf{y}h - h\mathbf{y}^H\mathbf{c} + h^2\right\} \\
&= \mathbb{E}\left\{\mathbf{c}^H\mathbf{y}\mathbf{y}^H\mathbf{c} - 2\mathbf{c}^H\mathbf{y}h + h^2\right\} = \mathbb{E}\left\{\mathbf{c}^H\mathbf{y}\mathbf{y}^H\mathbf{c}\right\} - 2\mathbf{c}^H\mathbb{E}\left\{\mathbf{y}h\right\} + \mathbb{E}\left\{h^2\right\} \\
&= \mathbf{c}^H\mathbb{E}\left\{\mathbf{y}\mathbf{y}^H\right\}\mathbf{c} - 2\mathbf{c}^H\mathbb{E}\left\{\mathbf{y}h\right\} + \mathbb{E}\left\{h^2\right\} \\
&= \mathbf{c}^H\mathbf{R}_{\mathrm{yy}}\mathbf{c} - 2\mathbf{c}\mathbf{R}_{\mathrm{yh}} + \mathbf{R}_{\mathrm{hh}} = \mathbf{c}^H\mathrm{yy}\mathbf{c} - 2\mathbf{c}\mathbf{R}_{\mathrm{yh}} + \sigma_h^2
\end{aligned}$$

The vector $\mathbf{c}$ that minimizes the MSE is found when setting $\dfrac{\partial\epsilon}{\partial\mathbf{c}}$ to zero:

$$\begin{aligned}
\frac{\partial\epsilon}{\partial\mathbf{c}} &= \frac{\partial}{\partial\mathbf{c}}\left(\mathbf{c}^H\mathbf{R}_{\mathrm{yy}}\mathbf{c} - 2\mathbf{c}^H\mathbf{R}_{\mathrm{yh}} + \mathbf{R}_{\mathrm{hh}}\right) = 0 \\
&= 2\mathbf{R}_{\mathrm{yy}}\mathbf{c} - 2\mathbf{R}_{\mathrm{yh}} + \mathbf{R}_{\mathrm{hh}} = 0 \\
&\therefore \mathbf{c} = \mathbf{R}_{\mathrm{yy}}^{-1}\mathbf{R}_{\mathrm{yh}}
\end{aligned}$$

Hence, the LMMSE for a SISO scenario is finally written as:

$$\begin{aligned}
\hat{h} &= \mathbf{c}^H\mathbf{y} = \left(\mathbf{R}_{\mathrm{yy}}^{-1}\mathbf{R}_{\mathrm{yh}}\right)^H\mathbf{y} \\
&= \mathbf{R}_{\mathrm{yh}}^H\left(\mathbf{R}_{\mathrm{yy}}^{-1}\right)^H\mathbf{y} \\
&= \mathbf{R}_{\mathrm{hy}}\mathbf{R}_{\mathrm{yy}}^{-1}\mathbf{y}
\end{aligned}$$

References

ABOURIZK, S. M.; HALPIN, D. W.; WILSON, J. R. Fitting beta distributions based on sample data. *Journal of Construction Engineering and Management*, v. 120, n. 2, p. 288–305, Jan 1994.

AKYILDIZ, I. F.; LEE, W.-Y.; VURAN, M. C.; MOHANTY, S. Next generation/dynamic spectrum access/cognitive radio wireless networks: A survey. *Computer Networks*, v. 50, n. 13, p. 2127 – 2159, 2006. ISSN 1389-1286.

AKYILDIZ, I. F.; WANG, X.; WANG, W. Wireless mesh networks: a survey. *Computer Networks*, v. 47, n. 4, p. 445 – 487, 2005. ISSN 1389-1286.

AL-ALI, M. H.; HO, K. C. Robust transmit precoding for underlay mimo cognitive radio with interference leakage rate limit. In: *2016 IEEE International Conference on Acoustics, Speech and Signal Processing (ICASSP)*. [S.l.: s.n.], 2016. p. 3001–3005.

BAI, T.; HEATH, R. W. Asymptotic coverage and rate in massive mimo networks. In: *2014 IEEE Global Conference on Signal and Information Processing (GlobalSIP)*. [S.l.: s.n.], 2014. p. 602–606.

BEN-TAL, A.; GHAOUI, L. E.; NEMIROVSKI, A. *Robust Optimization*. [S.l.]: Princeton University Press, 2009. ISBN 9780691143682.

BEYER, H.-G.; SENDHOFF, B. Robust optimization: A comprehensive survey. *Computer Methods in Applied Mechanics and Engineering*, v. 196, n. 33, p. 3190–3218, 2007. ISSN 0045-7825.

BHARGAVI, D.; MURTHY, C. Performance comparison of energy, matched-filter and cyclostationarity-based spectrum sensing. In: *Signal Processing Advances in Wireless Communications (SPAWC), 2010 IEEE Eleventh International Workshop on*. [S.l.: s.n.], 2010. p. 1–5. ISSN 1948-3244.

BIGLIERI, E.; GOLDSIMITH, A. J.; GREENSTEIN, L. J. *Principles of Cognitive Radio*. Cambridge, UK.: Cambridge University Press, 2012.

BIGLIERI, E.; GOLDSMITH, A.; GREENSTEIN, L.; MANDAYAM, N.; POOR, H. V. *Principles of Cognitive Radio*. 1. ed. [S.l.]: Cambridge University Press, 2013. ISBN 978-1-107-02875-3.

BIGUESH, M.; GERSHMAN, A. B. Downlink channel estimation in cellular systems with antenna arrays at base stations using channel probing with feedback. *EURASIP Journal on Advances in Signal Processing*, v. 2004, n. 9, p. 963649, Aug 2004. ISSN 1687-6180. Disponível em: <https://doi.org/10.1155/S1110865704403023>.

BING, B. *Emerging Technologies in Wireless LANs: Theory, Design, and Deployment*. [S.l.]: Cambridge University Press, 2008. (Cambridge Concise Histories). ISBN 9780521895842,0521895847.

CARDOSO, L.; DEBBAH, M.; LASAULCE, S.; KOBAYASHI, M.; PALICOT, J. Spectrum sensing in cognitive radio networks. In: *Cognitive Radio Networks*. Florida, US.: CRC Press, 2010.

CLAUDINO, L.; ABRAO, T. Efficient zf-wf strategy for sum-rate maximization of mu-miso cognitive radio networks. *AEU - International Journal of Electronics and Communications*, 2017. ISSN 1434-8411. Disponível em: <https://www.sciencedirect.com/science/article/pii/S143484111731912X>.

COSTA, N.; HAYKIN, S. *Multiple-Input, Multiple-Output Channel Models: Theory and Practice*. [S.l.]: John Willey and Sons Inc., New York, 2010. ISBN 978-0-470-39983-5.

DANIEL P. PALOMAR, Y. J. *MIMO Transceiver Design via Majorization Theory (Foundations and Trends in Communications and Information Theory)*. [S.l.]: Now Publishers Inc., 2007. ISBN 1601980302,9781601980304,9781601980311.

DATLA, D.; WYGLINSKI, A. M.; MINDEN, G. J. A spectrum surveying framework for dynamic spectrum access networks. *IEEE Transactions on Vehicular Technology*, v. 58, n. 8, p. 4158–4168, Oct 2009. ISSN 0018-9545.

FADLULLAH, Z. M.; FOUDA, M. M.; KATO, N.; TAKEUCHI, A.; IWASAKI, N.; NOZAKI, Y. Towards intelligent machine-to-machine communications in smart grid. *IEEE Communications Magazine*, v. 49, n. 4, p. 60–65, April 2011. ISSN 0163-6804.

FARIN, G.; HANSFORD, D. *Practical Linear Algebra: a Geometry Toolbox*. [S.l.]: Prentice Hall, 2004. ISBN 978-1-56881-234-2.

FCC, F. C. C. *Notice of Proposed Rule Making and Order*. [S.l.], December 2003.

FCC, S. P. T. F. *Comments of the Telecommunications Industry Association*. [S.l.], November 2002.

GEETHU, S.; NARAYANAN, G. A novel selection based hybrid spectrum sensing technique for cognitive radios. In: *Power, Control and Embedded Systems (ICPCES), 2012 2nd International Conference on*. [S.l.: s.n.], 2012. p. 1–6.

HASSIBI, B.; HOCHWALD, B. M. How much training is needed in multiple-antenna wireless links? *IEEE Transactions on Information Theory*, v. 49, n. 4, p. 951–963, April 2003. ISSN 0018-9448.

HERNANDES, A. G.; KOBAYASHI, R. T.; ABRAO, T. Introduction to cognitive radio newtorks and applications. In: _____. [S.l.]: CRC Press, 2016. cap. 4, p. 46–81.

HUANG, L.; XIAO, Y.; SO, H. C.; FANG, J. Accurate performance analysis of hadamard ratio test for robust spectrum sensing. *Wireless Communications, IEEE Transactions on*, v. 14, n. 2, p. 750–758, Feb 2015. ISSN 1536-1276.

JOHNSON, N. L.; KOTZ, S.; BALAKRISHNAN, N. *Continuous Univariate Distributions*. [S.l.]: Wiley-Interscience, 1995. ISBN 0-471-58494-0.

KALL, P.; WALLACE, S. W. *Stochastic Programming*. [S.l.]: John Willey and Sons Inc., New York, 1994.

KAY, S. M. *Fundamentals of Statistical Signal Processing, Volume I: Estimation Theory*. [S.l.]: Prentice Hall, 1993. ISBN 0133457117,9780133457117.

KHATAMI, S. H.; MOHAMEDPOUR, K.; ANDARGOLI, S. M. H. Power allocation for cognitive radio mimo-ofdm broadcast channels based on block-diagonalization beamforming. In: *2017 Iranian Conference on Electrical Engineering (ICEE)*. [S.l.: s.n.], 2017. p. 1878–1883.

KHATTAB DMITRI PERKINS, M. B. a. A. *Cognitive Radio Networks: From Theory to Practice*. 1. ed. [S.l.]: Springer-Verlag New York, 2013. (Analog Circuits and Signal Processing). ISBN 978-1-4614-4032-1,978-1-4614-4033-8.

KOBAYASHI, R. T.; ABRAO, T. Theoretical error for asynchronous multi-user large-scale mimo channel estimation. *IET Communications*, v. 11, n. 1, p. 17–24, 2017. ISSN 1751-8628.

LAW, K. L.; MASOUROS, C.; PESAVENTO, M. Transmit precoding for interference exploitation in the underlay cognitive radio z-channel. *IEEE Transactions on Signal Processing*, PP, n. 99, p. 1–1, 2017. ISSN 1053-587X.

LEE, K. J.; LEE, I. Mmse based block diagonalization for cognitive radio mimo broadcast channels. *IEEE Transactions on Wireless Communications*, v. 10, n. 10, p. 3139–3144, October 2011. ISSN 1536-1276.

LI, T.; MANDAYAM, N. B.; REZNIK, A. A framework for resource allocation in a cognitive digital home. In: *Global Telecommunications Conference (GLOBECOM 2010), 2010 IEEE*. [S.l.: s.n.], 2010. p. 1–5. ISSN 1930-529X.

MARIANI, A.; GIORGETTI, A.; CHIANI, M. Test of independence for cooperative spectrum sensing with uncalibrated receivers. In: *Global Communications Conference (GLOBECOM), 2012 IEEE*. [S.l.: s.n.], 2012. p. 1374–1379. ISSN 1930-529X.

MARZETTA, T. L.; HOCHWALD, B. M. Capacity of a mobile multiple-antenna communication link in rayleigh flat fading. *IEEE Transactions on Information Theory*, v. 45, n. 1, p. 139–157, Jan 1999. ISSN 0018-9448.

MCDONOUGH; N., R.; WHALEN; D., A. *Detection of Signals in Noise (2nd Edition)*. [S.l.]: Elsevier, 1995. ISBN 978-0-12-744852-7.

MCHENRY, D. M. M.; LANE-ROBERTS, G. *New York City Spectrum Occupancy Measurements Sep. 2004*. [S.l.], 2004.

MITOLA, J.; MAGUIRE, G. Q. Cognitive radio: making software radios more personal. *IEEE Personal Communications*, v. 6, n. 4, p. 13–18, August 1999. ISSN 1070-9916.

QIU, R. C.; HU, Z.; LI, H.; WICKS, M. C. *Cognitive Radio Communications and Networking: Principles and Practice*. 1. ed. [S.l.]: John Wiley and Sons, 2012. ISBN 9780470972090.

RAMAN, C.; YATES, R. D.; MANDAYAM, N. B. Scheduling variable rate links via a spectrum server. In: *First IEEE International Symposium on New Frontiers in Dynamic Spectrum Access Networks, 2005. DySPAN 2005.* [S.l.: s.n.], 2005. p. 110–118.

SAHAI, S. M. M. A.; TANDRA, R. *Spectrum Sensing: Fundamental Limits.* [S.l.], 2009. Available at `http://www.eecs.berkeley.edu/~sahai/Papers/SensingChapter.pdf`.

SAYRAC HRISHIKESH VENKATARAMAN, G.-M. M. B. *Cognitive Radio and its Application for Next Generation Cellular and Wireless Networks.* 1. ed. [S.l.]: Springer Netherlands, 2012. (Lecture Notes in Electrical Engineering 116). ISBN 978-94-007-1826-5,978-94-007-1827-2.

SCHUBERT, M.; BOCHE, H. Solution of the multiuser downlink beamforming problem with individual sinr constraints. *IEEE Transactions on Vehicular Technology*, v. 53, n. 1, p. 18–28, Jan 2004. ISSN 0018-9545.

TANDRA, R.; SAHAI, A. Snr walls for feature detectors. In: *New Frontiers in Dynamic Spectrum Access Networks, 2007. DySPAN 2007. 2nd IEEE International Symposium on.* [S.l.: s.n.], 2007. p. 559–570.

TANDRA, R.; SAHAI, A. *SNR walls for signal detection 1.* 2008.

TOUTOUNCHIAN, M. A.; VAUGHAN, R. Beamforming for mimo cognitive radio with single primary and multiple secondary users. In: *2016 IEEE Canadian Conference on Electrical and Computer Engineering (CCECE).* [S.l.: s.n.], 2016. p. 1–5.

TSE, D.; VISWANATH, P. *Fundamentals of Wireless Communication.* [S.l.]: Cambridge University Press, 2005. ISBN 9780511125980,0511125984,9780521845274,0521845270.

TUGNAIT, J. On multiple antenna spectrum sensing under noise variance uncertainty and flat fading. *Signal Processing, IEEE Transactions on*, v. 60, n. 4, p. 1823–1832, April 2012. ISSN 1053-587X.

VILLARDI, G. P.; ABREU, G. T. F. de; HARADA, H. Tv white space technology: Interference in portable cognitive emergency network. *IEEE Vehicular Technology Magazine*, v. 7, n. 2, p. 47–53, June 2012. ISSN 1556-6072.

WIESEL, A.; ELDAR, Y. C.; SHAMAI, S. Linear precoding via conic optimization for fixed mimo receivers. *IEEE Transactions on Signal Processing*, v. 54, n. 1, p. 161–176, Jan 2006. ISSN 1053-587X.

XU, Y.; ZHAO, X.; LIANG, Y. C. Robust power control and beamforming in cognitive radio networks: A survey. *IEEE Communications Surveys Tutorials*, v. 17, n. 4, p. 1834–1857, Fourthquarter 2015. ISSN 1553-877X.

ZENG, Y.; LIANG, Y.-C. Spectrum-sensing algorithms for cognitive radio based on statistical covariances. *Vehicular Technology, IEEE Transactions on*, v. 58, n. 4, p. 1804–1815, May 2009. ISSN 0018-9545.

ZHOU, J.; THOMPSON, J. Linear precoding for the downlink of multiple input single output coexisting wireless systems. *IET Communications*, v. 2, n. 6, p. 742–752, July 2008. ISSN 1751-8628.